ADAPTIVE CONTROL OVER EXTENDED TARGETS

J.E. Pearson, S. Hansen, and T.R. O'Meara

Hughes Research Laboratories
3011 Malibu Canyon Road
Malibu, CA 90265

September 1976

N60921–76–C–0050
Interim Technical Report
For Period 27 September 1975 Through 27 April 1976

Approved for public release; distribution unlimited

Sponsored By
NAVAL SURFACE WEAPONS CENTER
White Oak Laboratory
Silver Spring, MD 20910

UNCLASSIFIED

SECURITY CLASSIFICATION OF THIS PAGE (When Data Entered)

REPORT DOCUMENTATION PAGE		READ INSTRUCTIONS BEFORE COMPLETING FORM
1. REPORT NUMBER	2. GOVT ACCESSION NO.	3. RECIPIENT'S CATALOG NUMBER
4. TITLE (and Subtitle) ADAPTIVE CONTROL OVER EXTENDED TARGETS,		5. TYPE OF REPORT & PERIOD COVERED Interim Technical Report 27 Sept 1975-27 April 1976 6. PERFORMING ORG. REPORT NUMBER
7. AUTHOR(s) James E. Pearson, Sigfried Hansen, and Thomas R. O'Meara		8. CONTRACT OR GRANT NUMBER(s) N60921-76-C-0050
9. PERFORMING ORGANIZATION NAME AND ADDRESS Hughes Research Laboratories 3011 Malibu Canyon Road Malibu, CA 90265		10. PROGRAM ELEMENT, PROJECT, TASK AREA & WORK UNIT NUMBERS ARPA Order No. 3016
11. CONTROLLING OFFICE NAME AND ADDRESS NAVAL SURFACE WEAPONS CENTER, WOL White Oak, Silver Spring, MD 20910 Attn: WR42		12. REPORT DATE September 1976 13. NUMBER OF PAGES 79
14. MONITORING AGENCY NAME & ADDRESS (if different from Controlling Office)		15. SECURITY CLASS. (of this report) Unclassified 15a. DECLASSIFICATION DOWNGRADING SCHEDULE

16. DISTRIBUTION STATEMENT (of this Report)

Approved for public release; distribution unlimited.

17. DISTRIBUTION STATEMENT (of the abstract entered in Block 20, if different from Report)

18. SUPPLEMENTARY NOTES

19. KEY WORDS (Continue on reverse side if necessary and identify by block number)

Coherent Optical Adaptive Techniques (COAT), Adaptive Optics, Turbulence Compensation, Target Effects

20. ABSTRACT (Continue on reverse side if necessary and identify by block number)

Three types of adaptive optical systems are described that are being experimentally investigated. Each system is designed to be applied to high-power laser systems, to be insensitive to target effects, and to be effective in turbulence compensation. Two of the systems are multidither coherent optical adaptive techniques (COAT) and employ an imaging receiver. The imaging receivers employ "image-plane aperture censoring techniques" or "IMPACT" to enhance glint →next page

DD FORM 1 JAN 73 1473 EDITION OF 1 NOV 65 IS OBSOLETE

UNCLASSIFIED

SECURITY CLASSIFICATION OF THIS PAGE (When Data Entered)

172 600 LB

cont.

discrimination and, in some cases, to allow convergence on featureless target surfaces. The third system uses noncoherent light returned from the target to obtain phase corrections for a transmitted laser beam. Such systems, which may or may not use multidither techniques, are called "TRIM-COAT" because they combine transmitting and imaging COAT concepts.

The one system studied to date uses an annular uncompensated receiver aperture and is known as "Annular-Aperture IMPACT." This system operates like a conventional outgoing-wave multidither COAT system in strong turbulence, requiring a well-defined target highlight for good convergence. In low turbulence (on the return path), however, the system has demonstrated its ability to converge a laser beam on a weak glint in the presence of a stronger one and to converge the beam on a featureless target.

The remaining two systems to be studied are described, along with Annular Aperture IMPACT, in this report. They will be experimentally evaluated during the second half of the contract period. Studies on offset pointing and isoplanatic effects will also be pursued in the second contract period.

TABLE OF CONTENTS

LIST OF ILLUSTRATIONS

LIST OF ILLUSTRATIONS (Continued)

LIST OF ILLUSTRATIONS (Continued)

SUMMARY

The principal goal of this program is to demonstrate coherent optical adaptive technique (COAT) phase control concepts that can be applied to high-power laser systems, that are insensitive to target dynamics and target surface effects, and that are effective in turbulence compensation. This goal has been demonstrated with a number of COAT systems to be discussed in this report.

The work reported here was carried out during the second part of this program. It is an experimental evaluation of three COAT systems that differ primarily in their receiver configurations. The interim report,[1] reflecting work carried out during the first part of this program, contains a complete description of the three COAT systems. These descriptions will be summarized in Section 1. The interim report also contains a detailed discussion of the problems produced by isoplanatism and target effects, as well as an evaluation of the advantages and disadvantages of these systems when applied to high power lasers. These discussions will not be repeated here.

The three systems studied all employ an 18-channel multidither COAT system to provide real-time phase control signals to a deformable mirror. Two of the systems employ an imaging receiver which works off of the coherent light return from the target. A field stop is used at the receiver to limit the field of view. This image plane aperture censoring technique (IMPACT) permits enhanced glint discrimination capabilities and also enables these systems to converge on completely featureless targets. The third system uses non-coherent light return from the target to correct the target image; these phase corrections are then impressed upon the transmitted high-power laser beam to ensure convergence upon the target. Such systems, which may or may not use multidither techniques are called "TRIM-COAT" because they combine transmitting and imaging COAT concepts.

Four of the five possible fundamental modes of operation of these three systems were demonstrated and evaluated experimentally. The fifth mode of operation could not be evaluated due to low signal-to-noise

ratios in the target return. Their turbulence compensation performance was evaluated using natural turbulence on a 120-m rooftop propagation range. All three systems operating with single glints exhibited 60% convergence in strong turbulence ($C_N^2 \cong 2 \times 10^{-14}$ $cm^{-2/3}$). The performance of all three systems as a function of signal return and control channel signal-to-noise ratio was essentially identical whether operating with glint or featureless targets. Low-turbulence convergence levels of 90% or greater, convergence times of 2 msec or less, and peak beam irradiance fluctuations of < 10% were obtained for $S/N \geq 20$.

The effectiveness of the IMPACT stop was evaluated with multi-glint targets, where the glints were in relative translation or rotation. Intruder glints up to 20 dB stronger than the reference glint were successfully locked out at spacings of two beam diameters in strong turbulence. IMPACT was also shown to be highly effective in preventing glint hopping when the reference glint was partially destroyed.

Additional computer studies of isoplanatic effects on offset pointing and extended target referencing were originally envisioned for this part of the program (they were not a part of the Statement of Work). Due to time and financial limitations, however, they were not extended beyond the point already summarized in the interim report.

SECTION 1

INTRODUCTION

A. PROGRAM OBJECTIVES

The major goal of this program is to demonstrate and evaluate COAT phase control concepts with three attributes: They must be applicable to high-power laser systems, they must be insensitive to target dynamics and surface effects; they must be effective in turbulence compensation. To attain this goal, the program focuses on the following three tasks or objectives:

1. Demonstrate several COAT systems experimentally. These must be systems that can effectively correct for turbulence distortions with complex semidiffuse targets. They must also be insensitive to glint and target dynamics.

2. Analyze and compare the performance of these COAT systems and assess their applicability to high-power laser operations.

3. Using computer simulation, evaluate the isoplanatic patch size on the offset pointing and extended target referencing.

A discussion of the problems produced by isoplanatism and target effects appeared in the Interim Technical Report.[1] The interested reader is referred to the report for an introduction to these issues.

The Interim Report also included a complete description of the three COAT systems to be investigated in this study and an evaluation of their advantages and disadvantages when applied to highpower lasers. The following outline of each system's receiver geometry and salient operating characteristics is included as a brief review.

B. COAT SYSTEMS TO BE EVALUATED

1. Annular Aperture IMPACT (Image Plane Aperture Censoring Technique)

Annular aperture IMPACT is an outgoing-wave system that uses an annular receiver mirror to image the target plane. The image is formed from high-power laser light reflected off of the target. The annular mirror picks off the target return signal before it reaches the deformable mirror (see Figure 1). Thus the return wave is not corrected, and under strong turbulence conditions the target image can be degraded. A field stop (the IMPACT aperture) at the image plane is used to limit the detector's field of view.

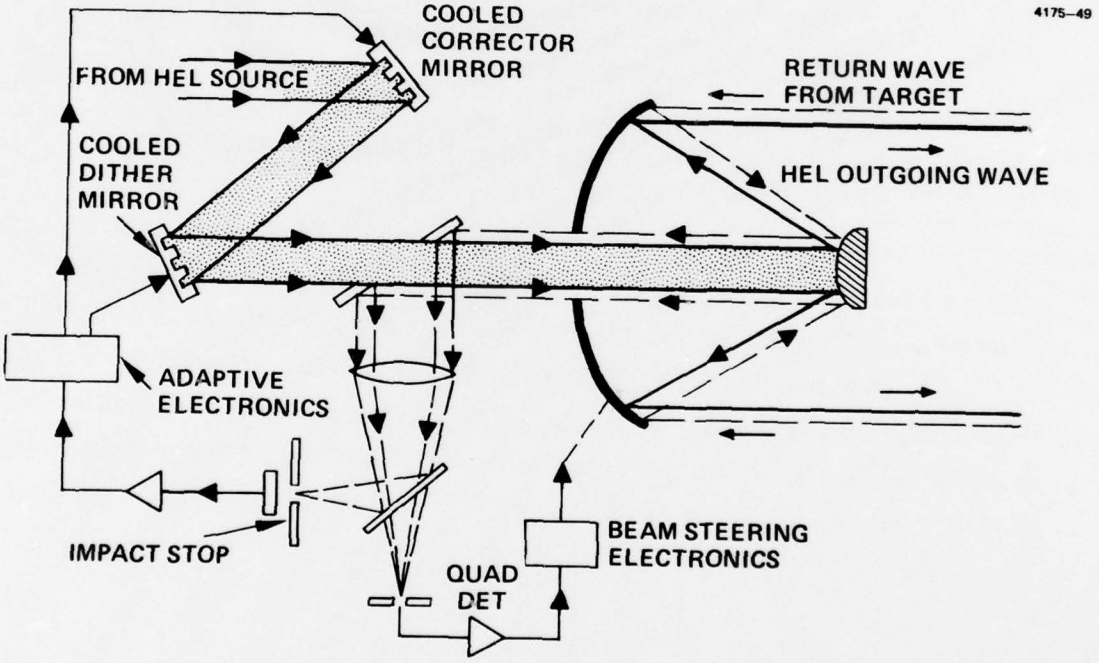

Figure 1. Annular aperture IMPACT system applied to high power laser.

While operating in the glint mode, the IMPACT stop is made larger than the diffraction-limited glint image. The system then works much like a standard outgoing-wave multidither system, but the IMPACT stop permits rejection of the returns from nearby glints which might otherwise cause the COAT system to initially converge on an unwanted glint, or to break lock once convergence has been obtained.

While operating in the featureless target mode, the IMPACT stop is made smaller than the image of the diffraction-limited laser beam incident on the target. The COAT servo maximization of light through the IMPACT stop then produces a diffraction-limited beam at the target. If the target is completely diffuse and featureless no tilt-error information is generated and thus an auxiliary tracking method is also required. This is shown as a quadrant detector in Figure 1, although other methods are applicable (see Interim Report[1]).

Proper operation in both modes requires a good image. Since the image degrades with increasing turbulence, one would expect the glint discrimination capabilities and featureless target convergence to degrade also.

2. Shared Aperture IMPACT

Shared-aperture IMPACT is an outgoing-wave — return-wave system. It also employs reflected laser light for target imaging, with the receiver sharing the transmitting optics used by the high-power laser. This system uses a beamsplitter to pick off the return signal after it reflects off of the deformable mirror (see Figure 2). The return path is thereby corrected and the target image is not degraded by the effects of turbulence.

The IMPACT stop permits glint mode and featureless target mode operation much as in the case of the annular aperture system. An auxiliary tracking control is also required here for featureless target operation. Due to the image-correcting action of the deformable mirror, one would expect the performance of the shared aperture system to degrade less quickly with increasing turbulence than the annular aperture system.

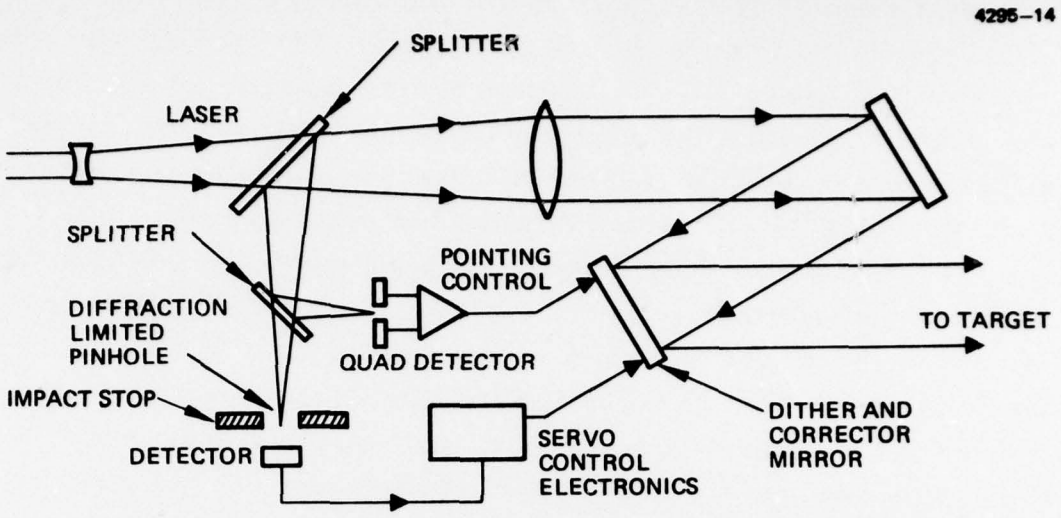

Figure 2. Schematic of basic shared aperture IMPACT system.

3. TRIM-COAT

TRIM-COAT is a pure return-wave system. It uses broad-band, non-coherent light returns from the target to correct the phase of the transmitted laser. The receiver configuration employs a beam splitter to pick off the broad-band return signal after it reflects off of the deformable mirror (see Figure 3). The COAT servo electronics is used to correct the broad-band target image. Since the high-power laser also reflects off of the image-correcting mirror, the proper conjugate phase information is imparted to the beam which causes it to converge on the target.

The use of advanced detector systems (see Interim Report) using multiple detectors as the receiver will enable the TRIM-COAT system to operate with nearly featureless targets (limited by isoplanatism). However, the laboratory demonstration carried out in this study, which employs only a single pinhole and single detector (see Figure 3) requires a fairly well-defined target highlight for proper convergence.

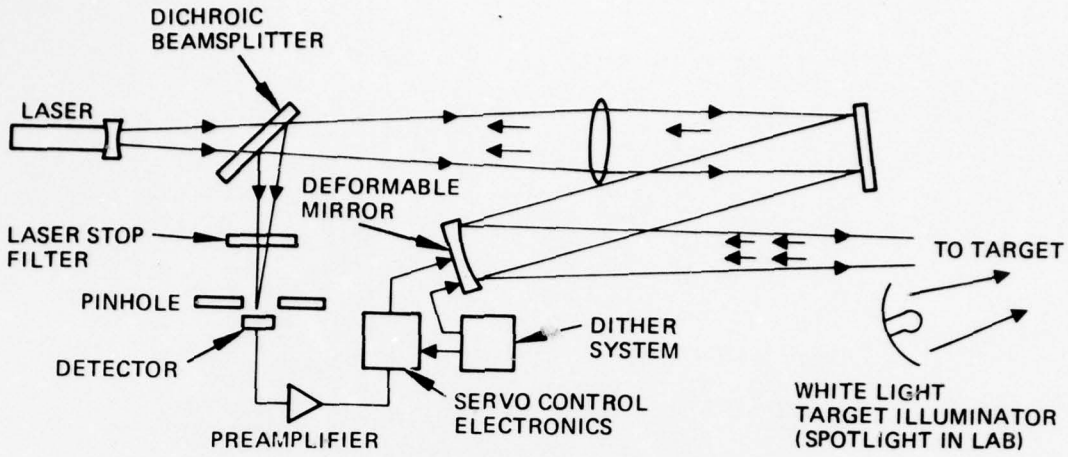

Figure 3. A localized referencing TRIM-COAT system using a single pinhole, single detector receiver. Many system variations are possible; the illustrated system is appropriate for a low power, visible wavelength laboratory demonstration.

C. ORGANIZATION OF THIS REPORT

This report contains an experimental evaluation of the above three COAT systems. Section 2 describes the experimental apparatus used in this study. Section 3 evaluates the basic system operation of the three COAT configurations using simple targets in various levels of turbulence. Section 4 evaluates the performance of the three COAT systems with complex and moving targets. Section 5 includes some recommendations for future studies. An appendix is included at the end of the report to summarize the S/N characteristics of the photomultiplier/preamp circuitry used for this study.

SECTION 2

EXPERIMENTAL APPARATUS

One of the requirements of the contract is that the contractor utilize available experimental hardware; the contract is not intended to be a hardware construction program. As a result of past and ongoing Hughes IR&D and Government contract programs, we have available at the Hughes Research Laboratories (HRL) all of the essential experimental hardware: deformable mirror, COAT servo electronics, target and target motion equipment, propagation range, and turbulence monitoring equipment. These items are discussed in this section.

A. DEFORMABLE MIRROR

Since the systems we are studying employ imaging receivers, and since one system operates on noncoherent light, it is necessary as well as convenient to use a continuous-surface, deformable mirror for the phase corrector element. The 37-actuator unit we are using is pictured in Figures 4 and 5. The mirror uses a particularly simple design[2] that provides 0.5 μm of surface motion for 400 V of drive, which is quite adequate for the visible-wavelength experiments being conducted on this program. The influence function of the central actuator is shown in Figure 6. Notice that the surface at the center of an adjacent actuator moves only 2% of the peak motion. This 2% "mechanical" coupling results in an 18% coupling[3] of the two servo channels, however.

The mirror frequency response is shown in Figure 7. Since it is usable up to about 20 kHz, the single mirror is used to apply both the dither and correction signals. Note, however, that the mirror induces a phase lag, which is compensated for by adjusting the phase of the reference signal applied to the synchronous detector in the appropriate control channel.

M11615 5353-27

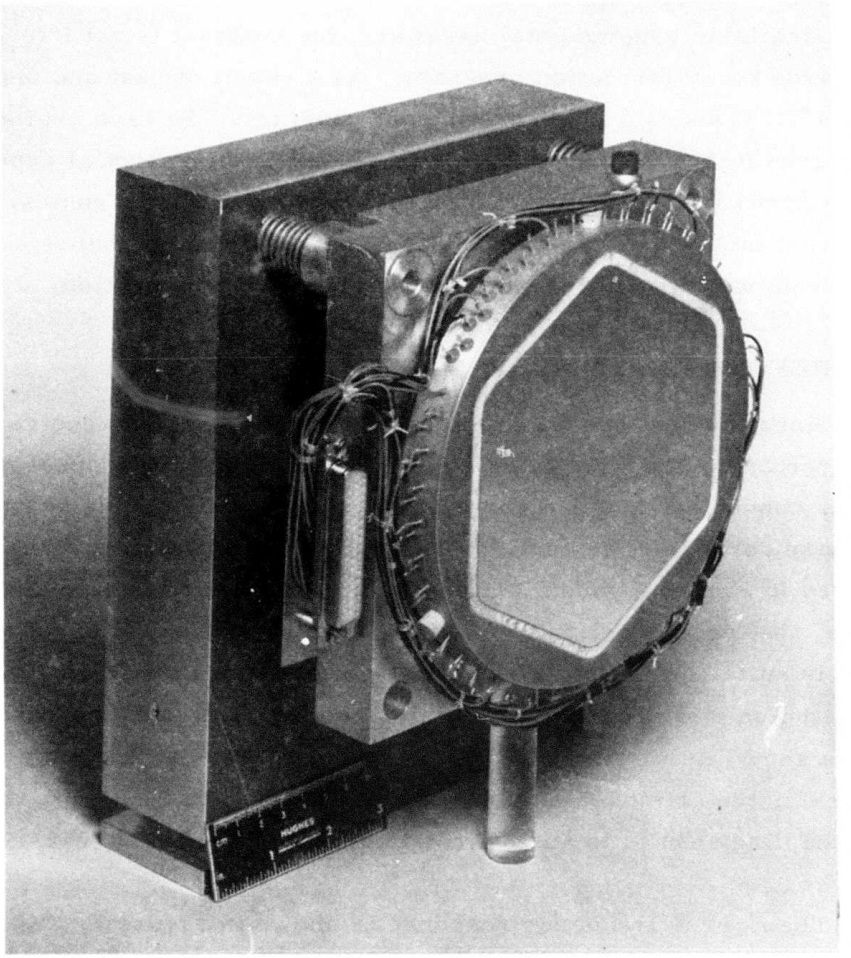

(a)

Figure 4. Photograph of deformable mirror used to apply dither and correction signals for experimental system studies.

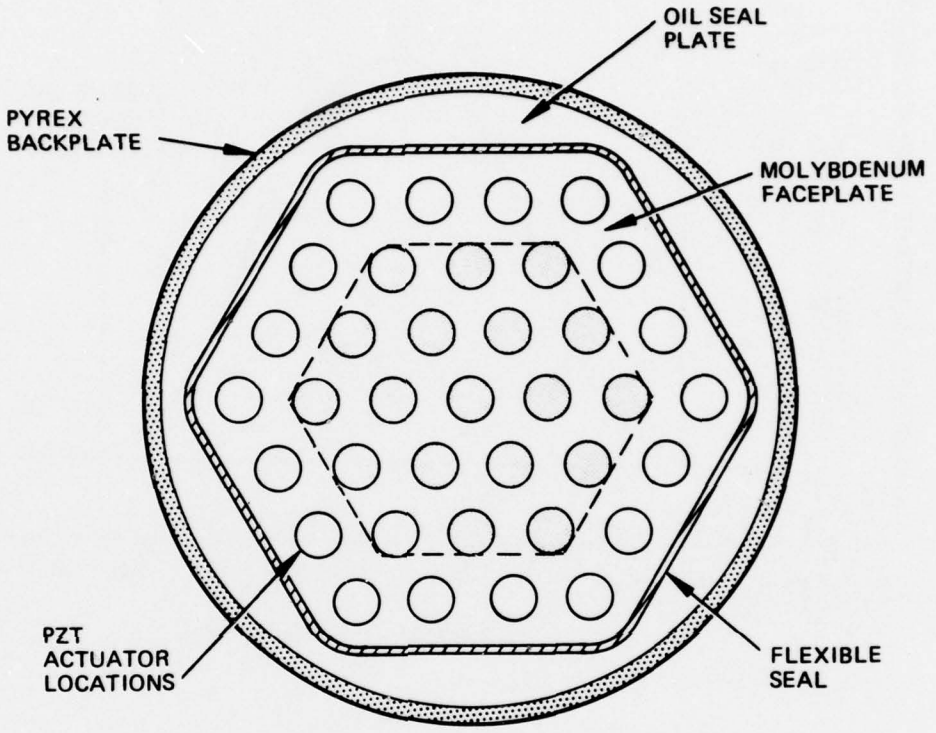

(b)

Figure 5. Schematic diagram of deformable mirror showing illumination aperture (enclosed by dotted line). The shaded actuators have a control channel drive.

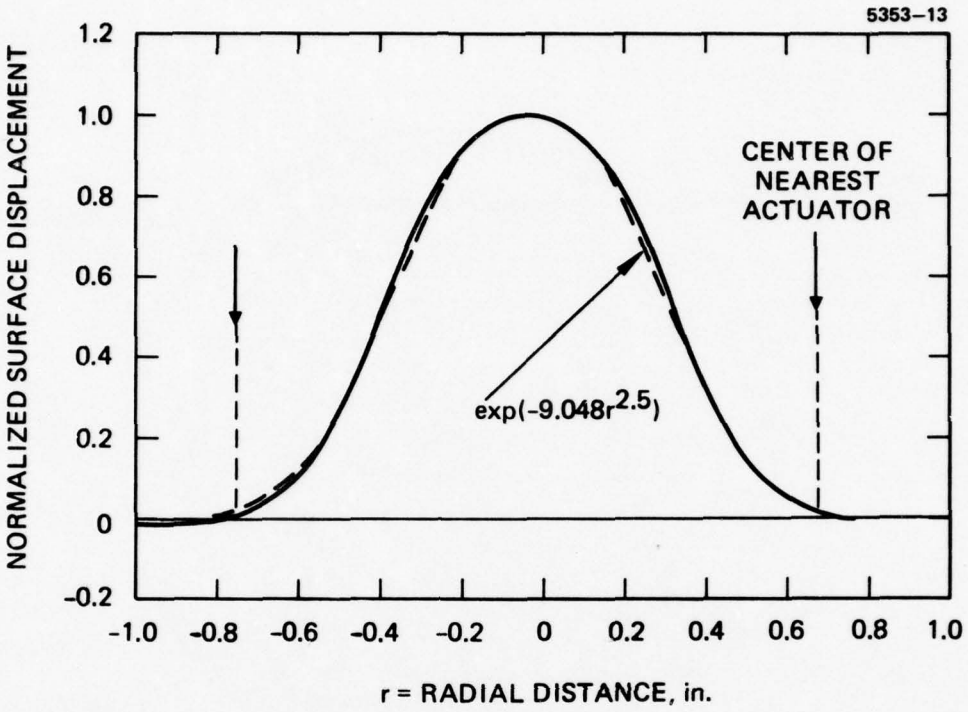

Figure 6. Influence function of central actuator in mirror shown in Figures 4 and 5.

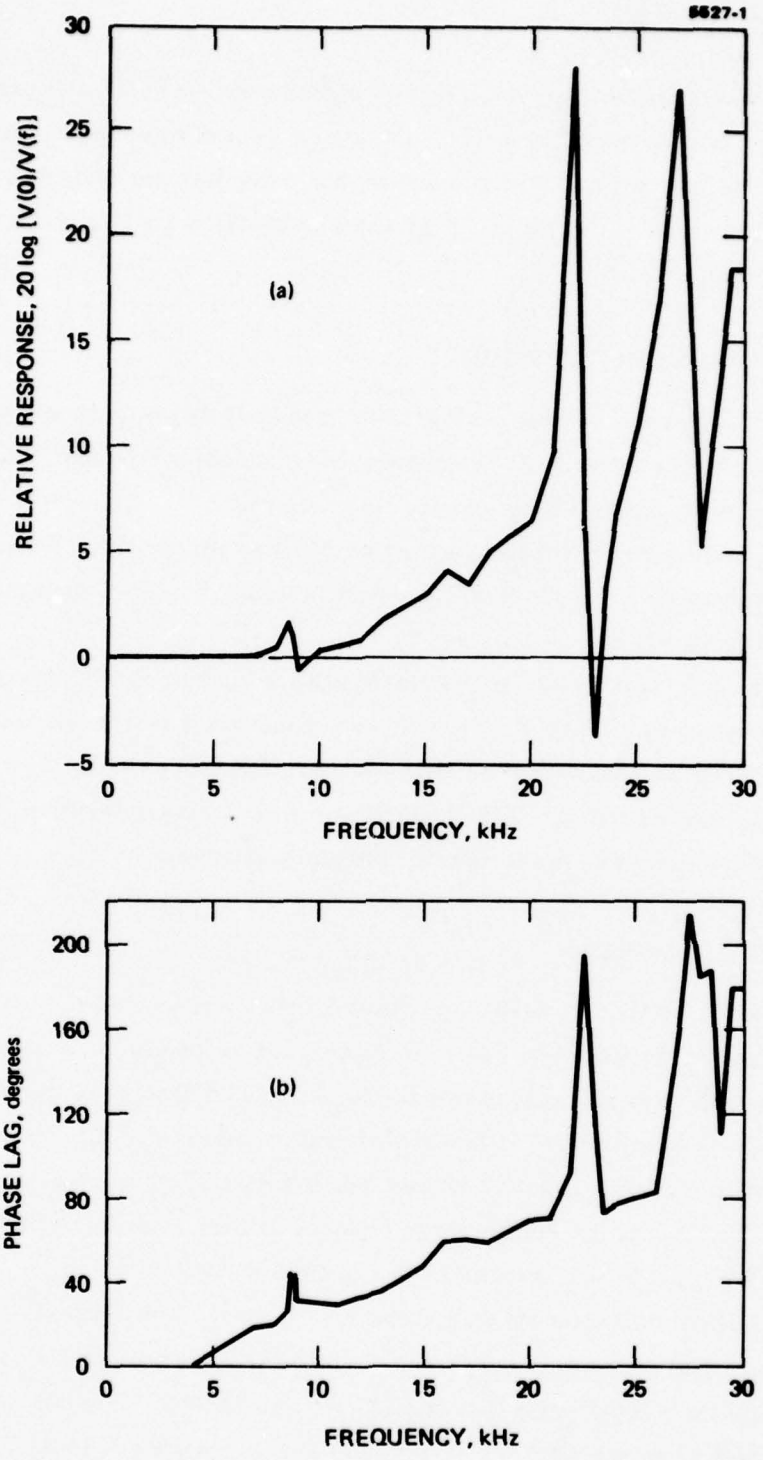

Figure 7. Frequency response characteristics of center actuator of 37-element deformable mirror. Response of other actuators is very similar. The quality V(f) in (a) is the voltage necessary to maintain a fixed surface deflection amplitude.

Since only 18 channels of control electronics are available for this program, the outer ring of 18 actuators is not used (not illuminated) and one of the actuators in the second ring has no COAT control channel applied to it. Only the 18 shaded actuators in Figure 5 are servo-controlled.

B. CONTROL ELECTRONICS

A block diagram of the multidither control system is shown in Figure 8. In all its essential features, it is identical to the DARPA/RADC control system used on earlier programs.[3,4] The only addition is the series injection transformer used for combining the dither and control signals onto a single PZT mirror actuator. A photograph of the electronics is shown in Figure 9.

The control system with the deformable mirror exhibits a convergence time of 1.5 to 2.0 msec as illustrated in the traces in Figure 10. This is the same as the DARPA/RADC system and is the design goal of the system. The corresponding system bandwidth is 400 to 500 Hz, quite adequate for turbulence compensation.

C. OPTICAL SYSTEM

The COAT optical system is shown in schematic and picture forms in Figures 11 and 12. A 1-W argon laser beam is expanded, by a 7x microscope objective located in the spatial filter and by lens ℓ_4, to fill the 9.5-cm aperture of the deformable mirror. The beam is then reduced to 2.0 cm diameter and recollimated by lenses ℓ_4 and ℓ_0. The 2.0-cm diameter is required for scaling this experiment to a 3.8-μm, 4-km range equivalent (see Section 2.D).

The photomultiplier (PMT) detector may be positioned in one of several locations, depending upon which COAT system is to be evaluated. For TRIM-COAT and Shared-Aperture IMPACT studies, the PMT is placed at position (1). For Annular Aperture IMPACT studies it is located at position (2). The TRIM-COAT configuration is identical to the Shared-Aperture IMPACT, with the addition of a 4880 Å laser-reject

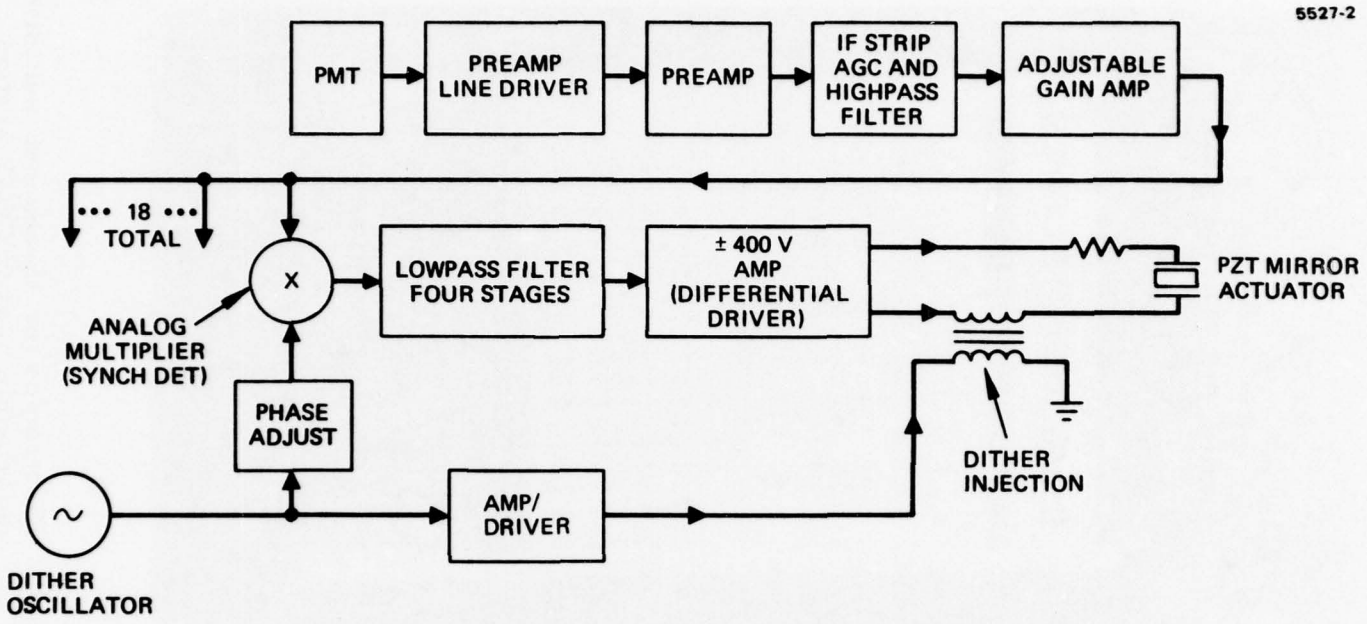

Figure 8. Block diagram of multidither control system used for IMPACT and TRIM-COAT systems studies.

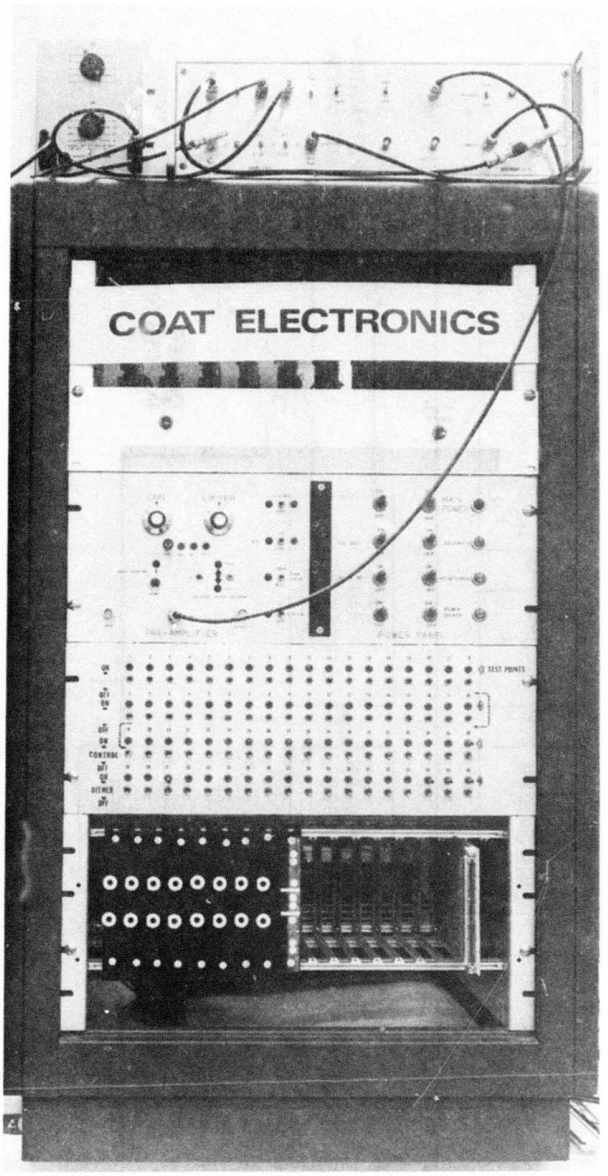

Figure 9. Electronics for 18-channel multidither deformable mirror COAT system.

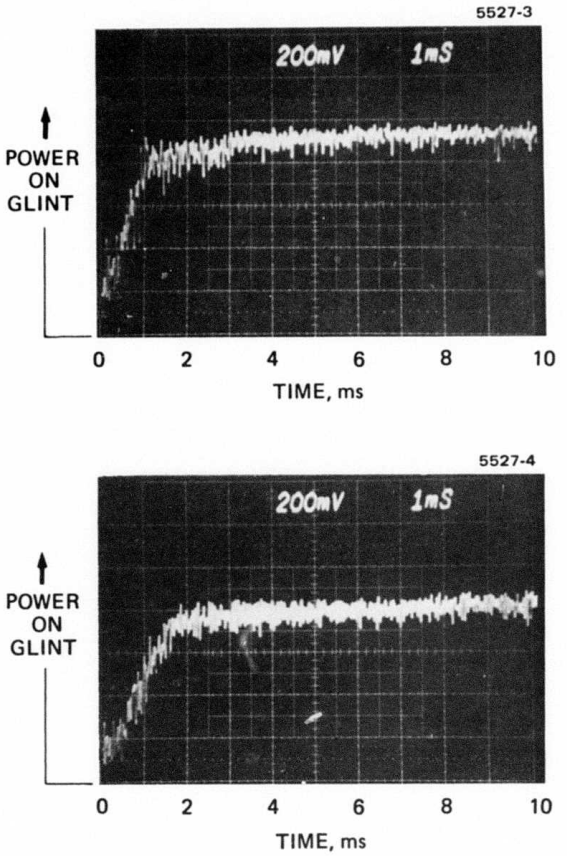

Figure 10. Two examples of 18-channel COAT system convergence with the deformable mirror. The scope sweep starts when the servo loop is closed. The time scale is 1 msec per major division in both pictures.

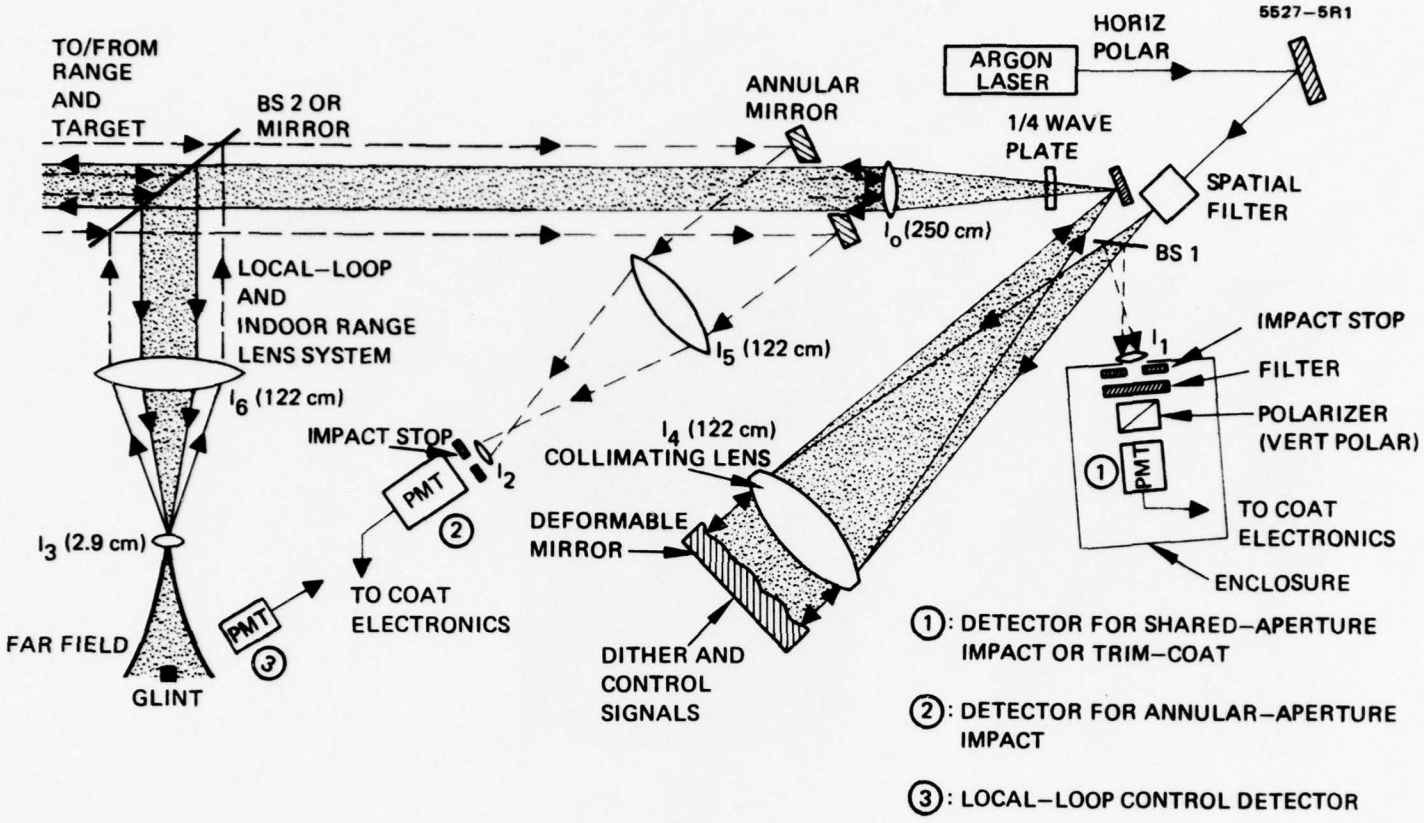

Figure 11. Optical arrangement for the various COAT system studies.

M11735

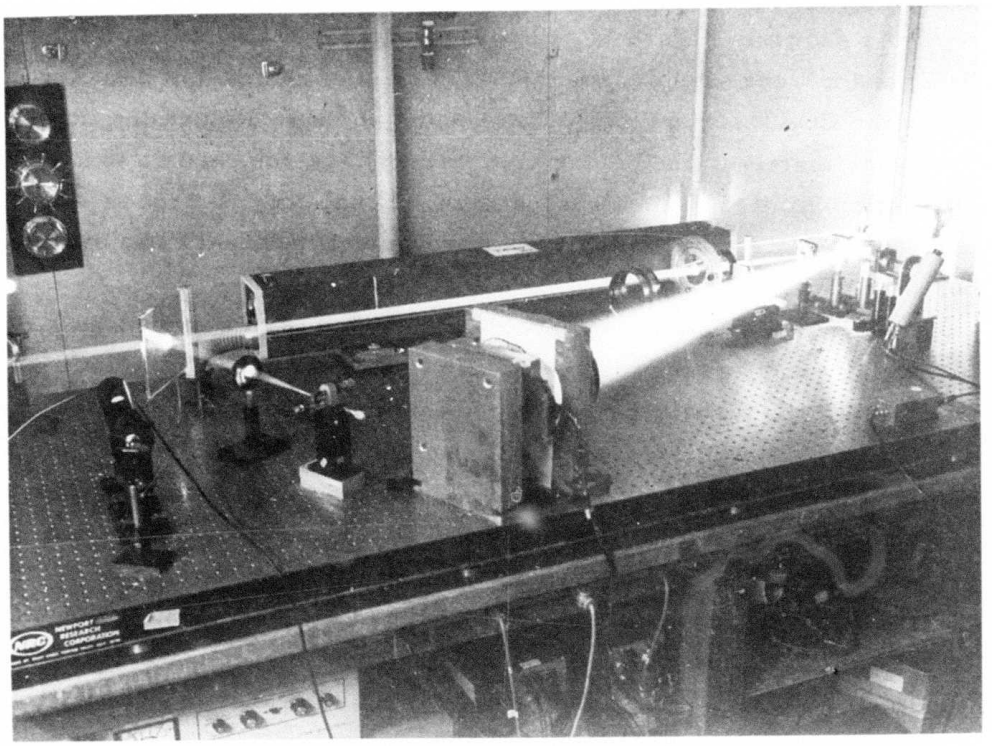

Figure 12. Photograph of optical system used for COAT studies.

filter in front of the PMT. A quarter-wave plate is inserted in the output beam for use with the Shared-Aperture IMPACT system. This plate, plus a polarizer in front of the PMT that is crossed with the laser polarization, acts to discriminate against backscatter from the optics. An enclosure is also placed around the PMT at position (1) to prevent stray light from entering the detector.

As shown in Figure 11, the system also contains a beam splitter (BS2) and a "local-loop" detector. When the output of this detector is fed to the COAT servo electronics, residual phase distortions in the optics (primarily in the deformable mirror) are removed so that a near diffraction-limited beam is propagated. Local-loop control usually resulted in factor of 1.5 to 2.0 improvement in Strehl ratio over that obtained with COAT off.

Much of the low-turbulence data reported in this study was obtained by propagating the laser beam inside the laboratory rather than across the turbulence range. In this case, beamsplitter BS2 was replaced by a flat mirror and additional mirrors were placed at the output of lens ℓ_3 to direct the beam around the turbulence-range periscope to the target. For these indoor measurements the distance between ℓ_3 and the target (=2.9 m) was chosen to produce a diffraction-limited beam diameter equal to that obtained by propagation across the range (7 mm). This was done so that the same targets and target-monitoring arrangement could be used in both the indoor and outdoor studies.

When using the indoor range setup, lenses ℓ_3 and ℓ_6 become part of the receiver optics. Their diameters were chosen to be large enough so that they would not be the limiting elements in determining the entrance pupil of the system. For both the indoor and range studies the entrance pupil was determined either by the o.d. of the annular mirror (7.1 cm with annular aperture IMPACT) or of the deformable mirror mask (2.0 cm with TRIM-COAT and shared-aperture IMPACT). For the indoor measurements, the quarter-wave plate was positioned at the output of lens ℓ_3.

The target geometry and beam monitoring equipment are shown schematically in Figure 13. A small portion of the laser beam that is converged on the target is split off by an uncoated glass plate. The plate is ground so that there is a 30^{o} wedge between surfaces. Two beams, propagating at slightly different angles, are thus produced. These two beams are spatially separated by a lens and a flat mirror located near the lens' focal point. One beam is sent to a silicon photodiode detector, the other to a milk-glass plate where it is monitored by a black-and-white TV camera.

The iris in front of the silicon photodiode is small compared to the beam diameter; it is positioned so that the detector views only the central maximum of the beam. The photodiode is connected to a chart recorder and oscilloscope. Peak target irradiance, beam convergence time, and beam stability are read out on these instruments.

The black-and-white TV camera is coupled to a VP-8 image analyzer which uses the video signal to generate two display outputs. One display is a color TV monitor, with each color corresponding to a different intensity level. The boundaries between colors are thus isointensity contours. The second display is a 3-D beam profile that is viewed on an oscilloscope.

D. PROPAGATION RANGE

Since isoplanatic effects play such an important role in the operation of imaging systems, we felt that the use of an extended, turbulent propagation path was essential to achieving the goals of the contract. We thus utilize an outdoor, rooftop propagation range at HRL, which is connected to the laboratory by a periscope, as shown in Figure 14. A folded path is used so that both the laser transceiver and the target are located in the laboratory. The rooftop path is 100 m and the total periscope path length is roughly 20 m. Atmospherically-induced isoplanatic effects are thus always a part of our experiments and no turbulence scale-size scaling is necessary such as that required with isolated phase screens.

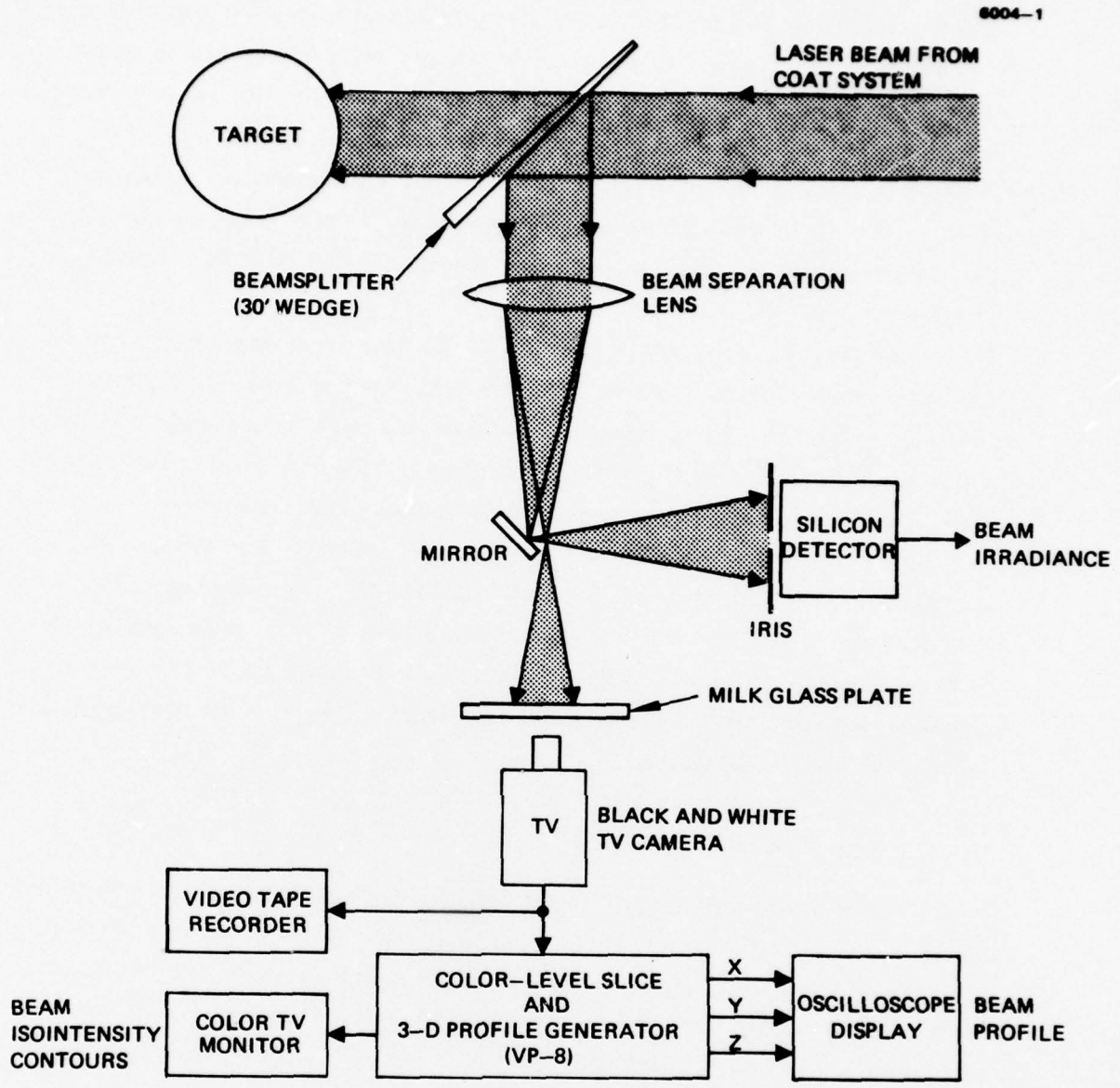

Figure 13. Target geometry and beam monitoring.

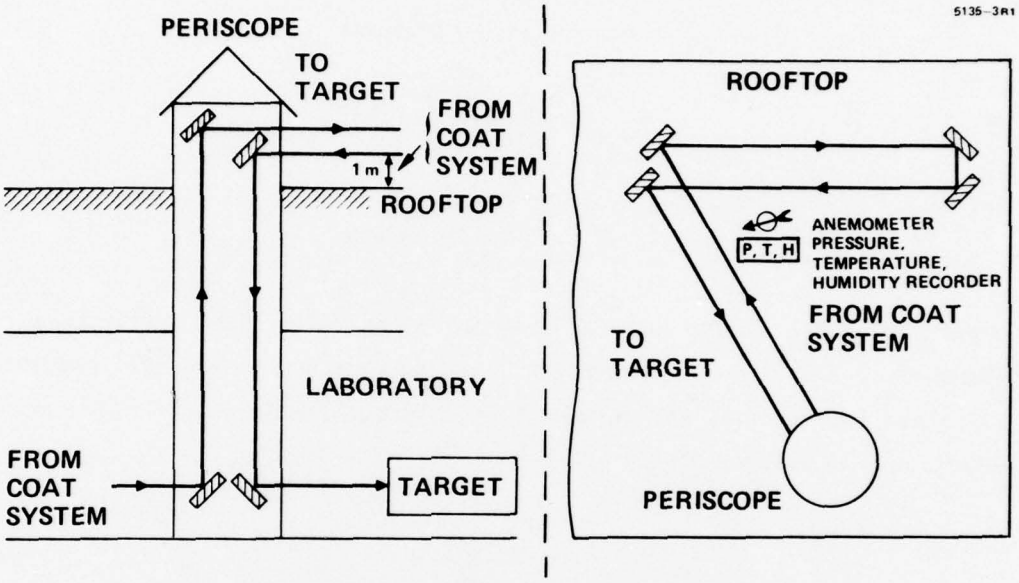

Figure 14. Rooftop propagation range, 120 m long, at the Hughes Research Laboratories.

It is necessary, however, to scale the optical fresnel number, α_F, and the turbulence strength as measured by the parameter α_S. In addition, the target dimensions should be scaled so that the number of diffraction-limited resolution elements, N, across a characteristic dimension, T, is constant. These three requirements are stated mathematically as

$$\alpha_F = \frac{kD_T^2}{Z} = \text{constant} \tag{1}$$

$$\alpha_S = C_N^2 k^{7/6} Z^{11/6} = \text{constant} \tag{2}$$

$$N = T/S = \text{constant} \tag{3}$$

where $k = 2\pi/\lambda$ is the optical wavenumber, D_T is the transmitter diameter, Z is the target range, and C_N^2 is the atmospheric structure constant (turbulence strength). The diffraction-limited focal-spot size, S, is found from

$$S = \frac{1.22\lambda Z}{D_T} \quad . \tag{4}$$

The requirement in Eq. (2) is equivalent to holding constant the ratio r_o/S, where r_o is Fried's coherence length as defined by

$$r_o = 1.68\left(k^2 C_N^2 z\right)^{-3/5} \text{ (plane wave)} \quad . \tag{5}$$

The results of performing the scaling exercise to obtain D_T, T, and C_N^2 for our visible-wavelength experiments are shown in Table 1. As can be seen, at the short wavelength and range, very small values of r_o are found for strong turbulence.

TABLE 1. SCALING OF IR TO VISIBLE EXPERIMENT FOR TWO DIFFERENT CASES

Parameter	λ = 3.8 μm, Z = 4 km				λ = 0.488 μm, Z = 120 m			
D_T, transmitter diameter, cm	32		64		2		4	
T, target dimension, cm	100		100		6.1		6.1	
S, focal spot size, cm	5.3		2.7		0.32		0.16	
α_F, fresnel number	42		169		42		169	
N = T/S	19		38		19		38	
C_N^2, $M^{-2/3}$	10^{-16}	10^{-14}	10^{-16}	10^{-14}	5.9×10^{-15}	5.9×10^{-13}	5.9×10^{-15}	5.9×10^{-13}
$r_o = \left[0.42\ k^2 C_N^2 Z\right]^{-3/5}$, cm	159	10	159	10	9.6	0.61	9.6	0.61
r_o/S	30	1.9	60	3.8	30	1.9	60	3.8

T1993

E. TURBULENCE MONITOR

The atmospheric structure constant (C_N^2) is monitored during all outdoor range experiments by means of an optical scintillometer.[5] The device consists of a He-Ne laser, a silicon photodiode with a restricted field of view, and an electronics signal processing package. The He-Ne laser is propagated over the turbulence range directly adjacent to the argon beam and illuminates the silicon photodiode. The turbulence encountered along the beam path causes the He-Ne laser beam to scintillate, and these fluctuations are sensed by the photodiode. The electronics package generates an output voltage which is proportional to the root mean square of the log of the fluctuations. C_N^2 is proportional to the square of this output voltage, with the constant of proportionality being determined by the geometry of the system and known properties of the electronics.[5, 6, 7] Measurements obtained with the scintillometer have shown fair agreement with microthermometer measurements of C_N^2, (Ref. 5) and the turbulence data reported in this study are believed to be accurate to within 50%.

SECTION 3

BASIC OPERATION OF THE THREE COAT SYSTEMS

A. INTRODUCTION

In this section we evaluate the performance of the three COAT systems in various levels of turbulence using simple targets. Four out of the possible five modes of operation described in Section 1 are investigated: (1) Annular Aperture IMPACT, glint operation; (2) Annular Aperture IMPACT, featureless target operation; (3) Shared Aperture IMPACT, glint operation; and (4) TRIM-COAT. Strehl ratio, convergence time, and beam stability are determined as a function of target return signal level and signal-to-noise ratio. The performance of these systems is compared one to another and also to a "standard" multi-dither COAT configuration where the receiver is located at the target. In the standard system there is no turbulent return path, therefore the performance of this configuration represents the best that can be expected with the present COAT servo electronics.

As discussed in more detail below, we were unable to obtain proper operation of the Shared Aperture IMPACT system with featureless targets. This was due primarily to poor S/N caused by small signal return from our semi-diffuse featureless targets (Scotchlite).

The experiments reported in this section fall into two categories: (1) detailed low turbulence ($C_N^2 < 10^{-17}$ $cm^{-2/3}$) studies requiring long periods (~1 hr) of reproducible conditions that were carried out inside the laboratory, and (2) quickly-executed experiments, conducted over a wide range of turbulence levels ($4 \times 10^{-17} \leq C_N^2 \leq 4 \times 10^{-14}$ $cm^{-2/3}$), that were carried out with the outdoor propagation range. The indoor experiments were not planned originally, since long periods of reproducible low turbulence are readily obtained over the outdoor range after sundown. However, variable weather conditions present in Malibu during this fall and winter made it virtually impossible to obtain extensive sets of comparative data after dark. Humid onshore winds and cool temperatures produced both dense fog and water condensation on the

range mirrors. These caused factor-of-10 variations in the transmitted beam intensity over periods of minutes, and occasionally caused complete beam attenuation. Rather than spend excessive time waiting for the weather to improve, it was decided to move the more complex low-turbulence experiments indoors.

B. BASIC LOW-TURBULENCE SYSTEMS PERFORMANCE

Measurements of peak target irradiance, convergence time, and beam stability, as well as TV display photographs of the beam profile, were obtained as a function of return signal level and S/N ratio. These data were obtained using the indoor range. Specific details of the experimental configurations are as follows:

1. Experimental Details

a. Annular Aperture IMPACT (glint operation)

A single cats-eye (lens with mirror at its focal point) was used as a glint in these experiments. It had an effective diameter of ~1 mm, considerably less than the ~7 mm diameter of the fully converged argon beam. Lens ℓ_2 (see Figure 11) was a 10x microscope objective (16 mm focal length). This produced an image of the glint ~0.15 mm in diameter at the IMPACT stop. The IMPACT stop was located 20 cm from ℓ_2 and was opened to a diameter of 2 mm (much larger than glint image size).

b. Annular Aperture IMPACT (featureless target operation

The target in this configuration was an 8- by 8-cm flat section of Schotchlite, a semi-diffuse scatterer of relatively high reflectivity. Lens ℓ_2 was again a 10x microscope objective spaced 20 cm from the IMPACT stop. The image size of the converged 7 mm diameter argon beam was ~0.75 mm at the IMPACT stop location. The IMPACT stop was chosen to be ~0.25 mm in diameter (approximately 1/3 of the image size) for these measurements. Stops up to ~1/2 of the image diameter were found to prcduce similar performance.

c. Shared Aperture IMPACT (glint operation)

The glint in this configuration was chosen to be a flat mirror with a 2 mm diameter iris in front of it. The cats-eye glint produced results similar to the above glint, but was not used here due to the smaller (~1/10) return from it, which limited the range of return signals to be studied.

Lens ℓ_1 was a 10x microscope objective and was spaced 45 cm from the IMPACT stop. This produced an image of ~0.5 mm diameter. The IMPACT stop diameter was chosen fairly small (1 mm) in order to reduce the backscatter reaching the PMT. The return from the glint was large enough so that an ND 1.5 (15 dB) neutral density filter was also placed in front of the PMT to further reduce backscatter. The ratio of dc return signal to backscatter signal was approximately 3000:1 (35 dB) for these studies.

d. TRIM-COAT

It was originally intended to employ white light or He-Ne laser illumination of a highly reflective target in these studies. However, both of these illumination schemes failed to produce a detectable signal at the PMT (i.e., signals were <1 mV at the output of the preamp/line driver). Shining strong white light sources directly into the optical system did produce easily observable signals, but the signals did not have sufficiently high S/N to ensure good system operation. For example, shining a high intensity microscope illumination lamp with a 2-mm aperture in front of it directly into ℓ_3 from the target position produced ~8 mV of signal and S/N ~12. As will be demonstrated, this is sufficient for partial convergence but allows no leeway for varying the signal levels upward to determine the point of Strehl ratio saturation.

To obtain the necessary range in signal strength, we used a He-Ne laser to simulate the TRIM-COAT target highlight. The laser was placed at the target position and directed toward ℓ_3. A 19-cm focal length lens placed directly in front of the He-Ne laser diverged the initially ~1-mm beam to a size of ~2.5 cm at ℓ_3. This served to

decrease the power received by the PMT to tolerable levels (additional filters at the PMT were required for further signal reduction) and to ensure that the 0.47 mm entrance pupil of the optical system was uniformly illuminated. For all practical purposes the He-Ne laser thus appeared to the optical system to be a 6328 Å glint that was radiating isotropically at the target plane.

A 20x (9-mm focal length) microscope objective was used for ℓ_1. This produced a ~1.3-mm diameter spot at the IMPACT stop which was 45 cm away. Several stop sizes in the range 20% to 40% of the spot size were tried with equally good results. For these measurements a 0.51-mm diameter IMPACT stop was employed (~40% of the spot size).

2. Data Obtained on Indoor Range

Figures 15 through 18 are plots of peak target irradiance as a function of dc signal return level. The curves represent the long-term average peak power in the beam with all $2N\pi$ states[2, 8, 9] removed. The transmitter optics have been defocused to give a COAT-off peak irradiance which is 10 to 15% of full beam convergence. This was done in order to give the COAT system a significant error to correct in low turbulence and to make any degradation with lowered signal returns more noticeable.

The dc signal levels were measured at the output of the preamplifier/line driver which directly follows the PMT (see Figure 8). The signal levels were varied by placing neutral density filters in front of the PMT. Also shown along the x axes of these figures are average S/N values presented to each of the control channels. This S/N is defined as the ratio of the rms dither return signal for a typical control channel to the rms noise in the 400-Hz control channel bandwidth. It is defined for the unconverged beam (COAT off). The dominant noise in our system at the signal levels studied here is PMT shot noise. Thus, the S/N ratio varies as the square root of the return signal. The S/N was not measured directly during these experiments, but was inferred from S/N versus dc signal return calibration measurements which are described in the Appendix.

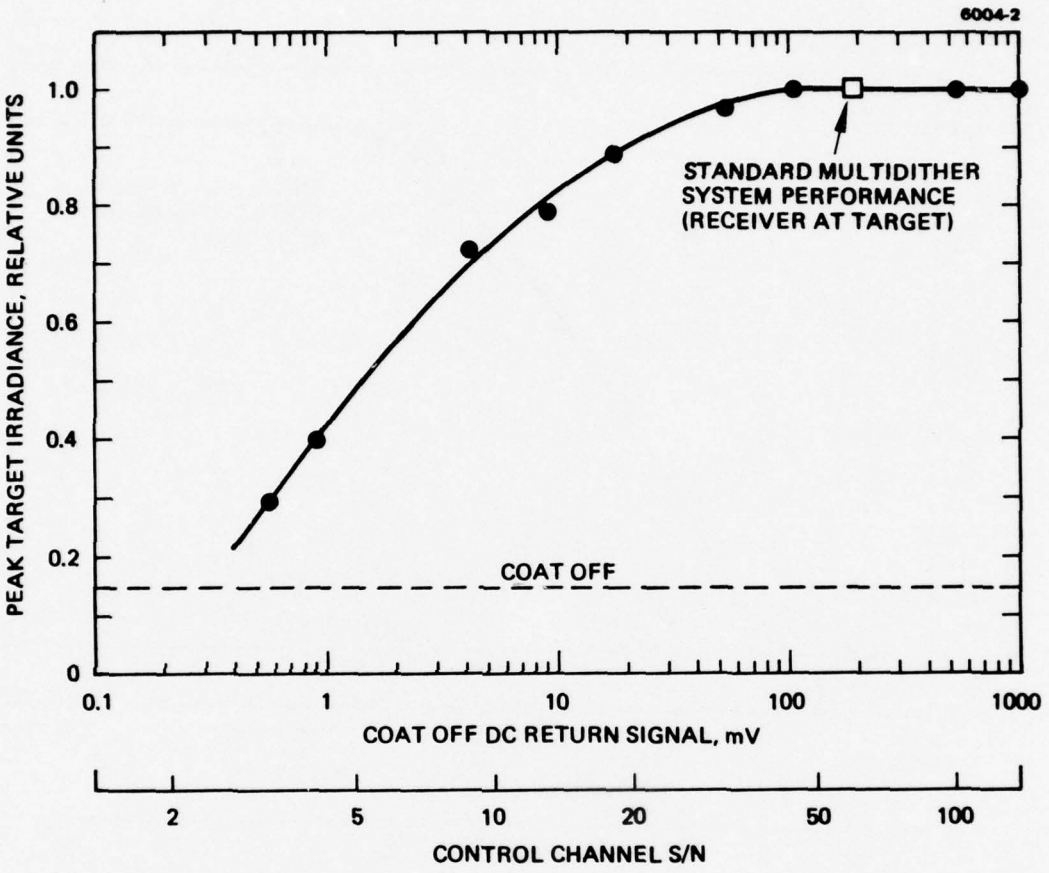

Figure 15. Glint mode operation of Annular Aperture IMPACT showing effect of signal return level upon peak target irradiance.

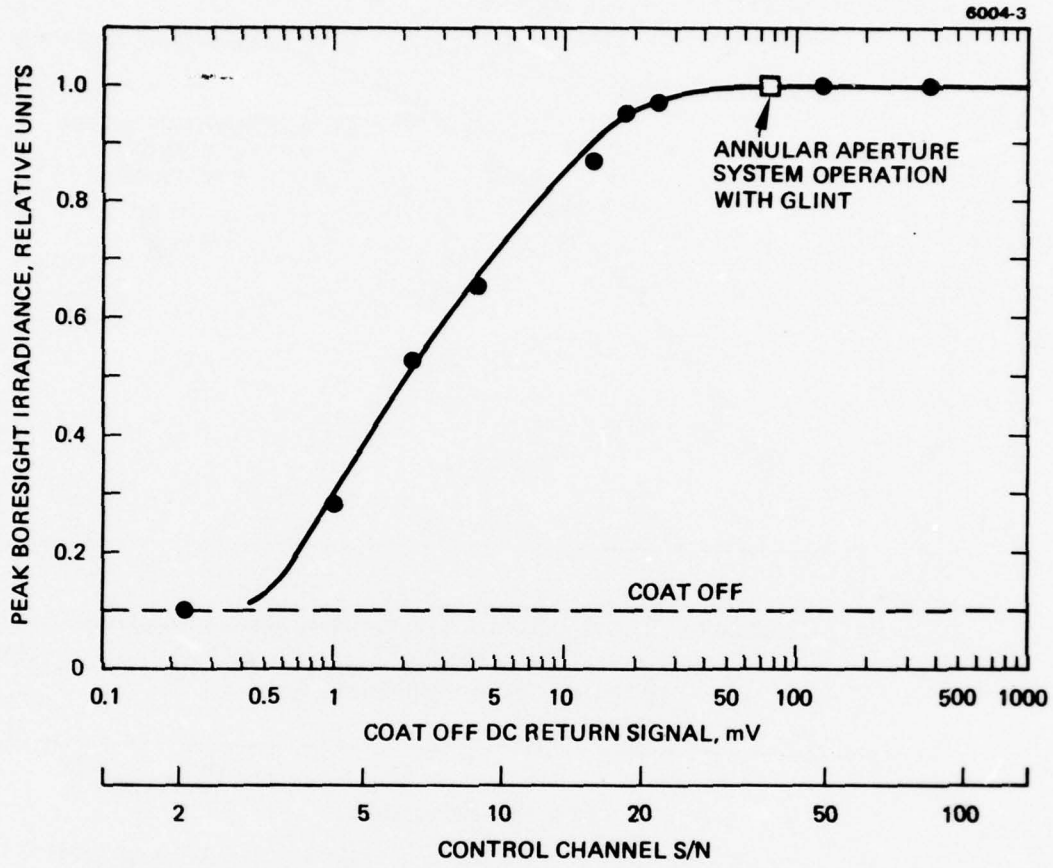

Figure 16. Featureless target operation of Annular Aperture IMPACT showing effect of signal return level upon peak boresight irradiance.

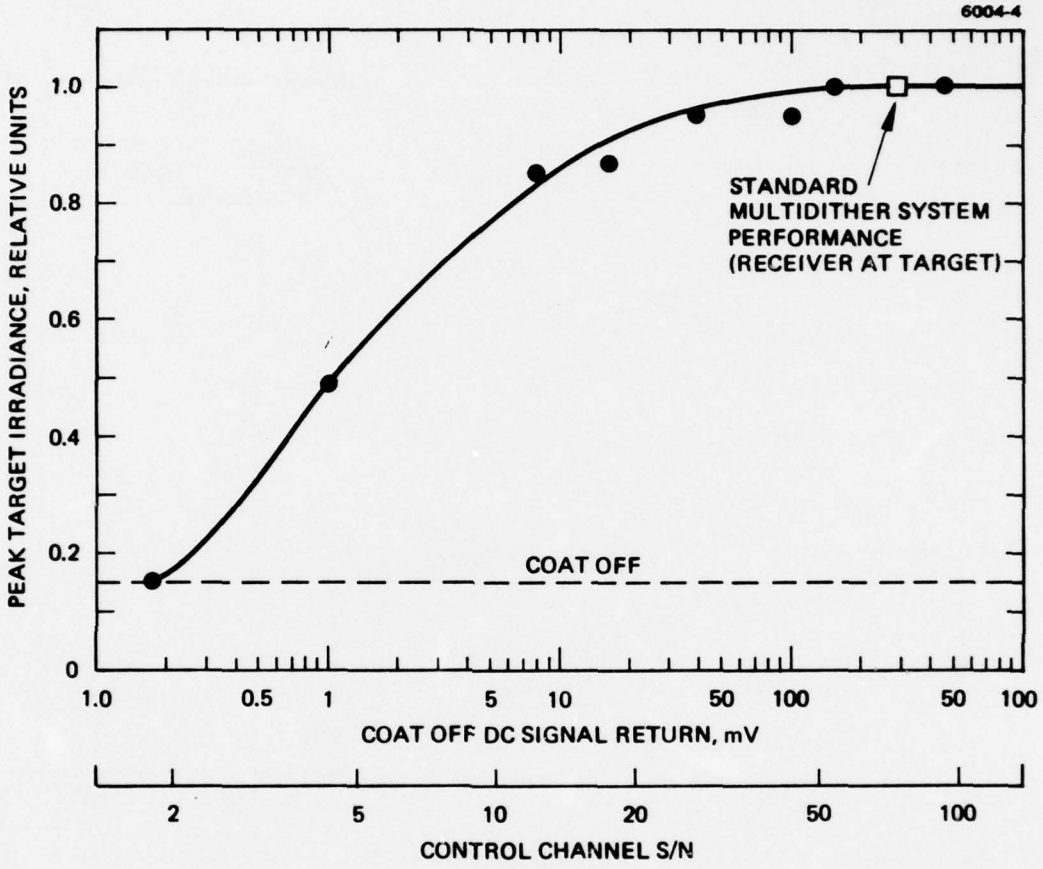

Figure 17. Peak target irradiance as a function of return signal for Shared Aperture IMPACT operating with simple glint.

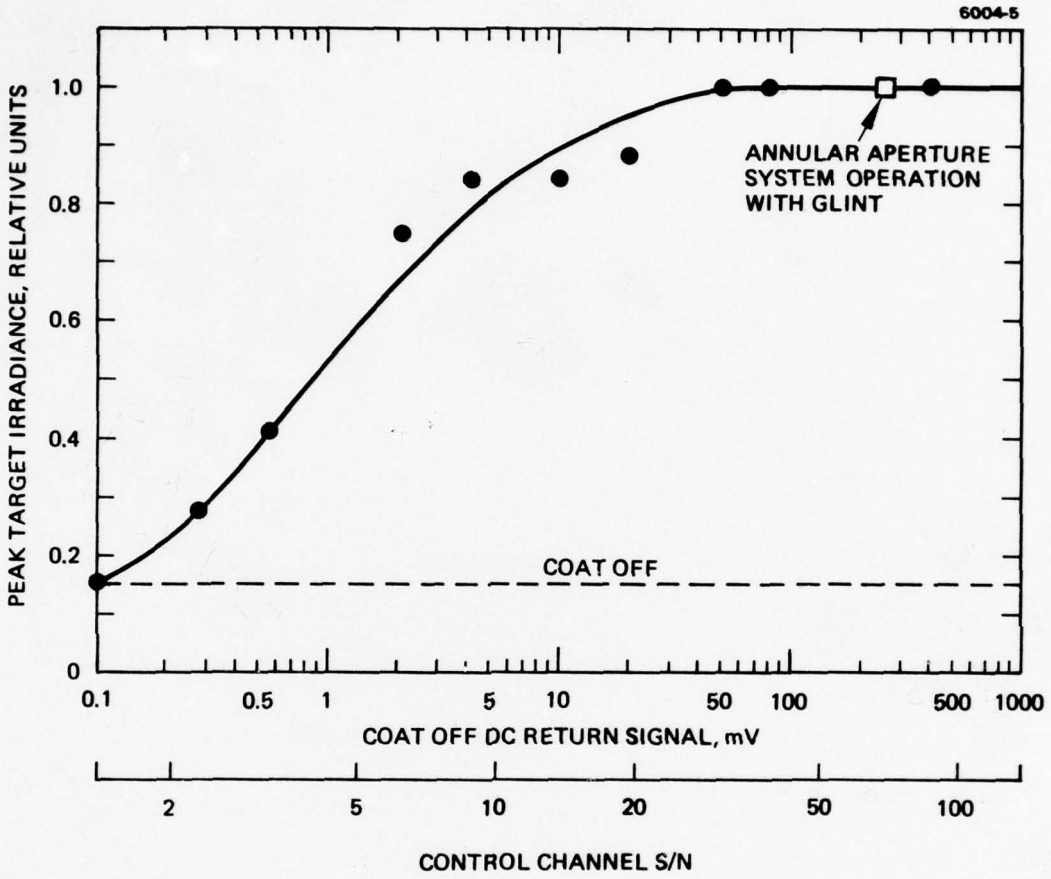

Figure 18. Peak target irradiance as a function of return signal for TRIM-COAT configuration.

Figures 15 through 18 indicate that all four configurations perform roughly the same. At COAT-off signal-return levels of several tenths of multivolts (S/N ~2-3) essentially no COAT correction occurs. Eighty percent convergence occurs at 4 to 8 mV (S/N ~8-12), 90% convergence occurs at 10 to 20 mV (S/N ~14-20), while full convergence is produced by 50 to 150 mV (S/N ~30-50).

For signals over 150 mV (S/N >50) all four configurations reach saturation and produce identical Strehl ratios. This is the same as the saturation Strehl ratio produced by the standard COAT system (receiver at target). These relationships were determined by direct side-by-side comparisons with the standard system and by comparisons between the other four configurations. System comparisons that were employed in Figures 15 through 18 to determine the peak target irradiance = 1 normalization are indicated by square data points.

To complete documentation of the system's performance at low turbulence levels we present a fairly extensive set of beam profile and oscilloscope photographs corresponding to representative locations along each of the curves shown in Figures 15 through 18. These photographs are shown in Figures 19 through 22. Each column of three photographs corresponds to a fixed signal return and S/N level. These are indicated at the bottom of each column. The photographs in the top row are beam profiles (side view) taken from the TV display. Those in the middle row show the convergence time of the beam (peak irradiance) as measured at the target by the silicon detector shown in Figure 13. The photographs in the bottom row show the stability of the peak beam irradiance over a 2-sec time interval.

The beam profiles are included primarily for qualitative comparison. Due to nonlinearities in the TV camera response, the peak heights of the profiles are not related directly to the peak irradiance measured by the silicon detector. For beam profiles of ~6 major divisions in height a factor-of-4 decrease in laser beam intensity results in a factor-of-~3 decrease in profile height. The sidelobe structure is thus enhanced somewhat in the profile photographs, and the peak beam irradiance appears to fall off with decreasing return signal strength more slowly than it actually does.

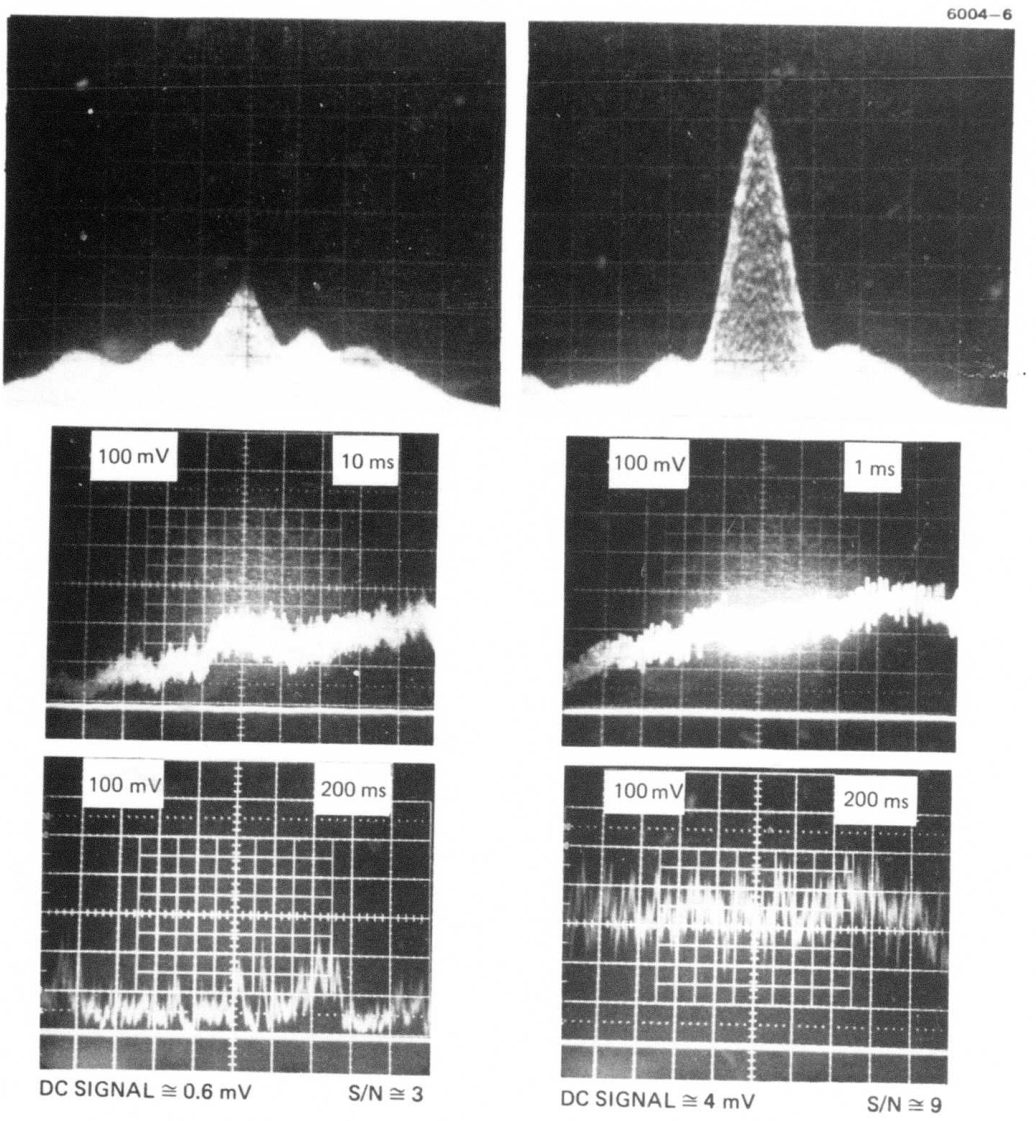

Figure 19(a). Annular Aperture IMPACT (glint mode) performance. Beam profiles (top row), convergence time (center) and beam stability (bottom) are shown.

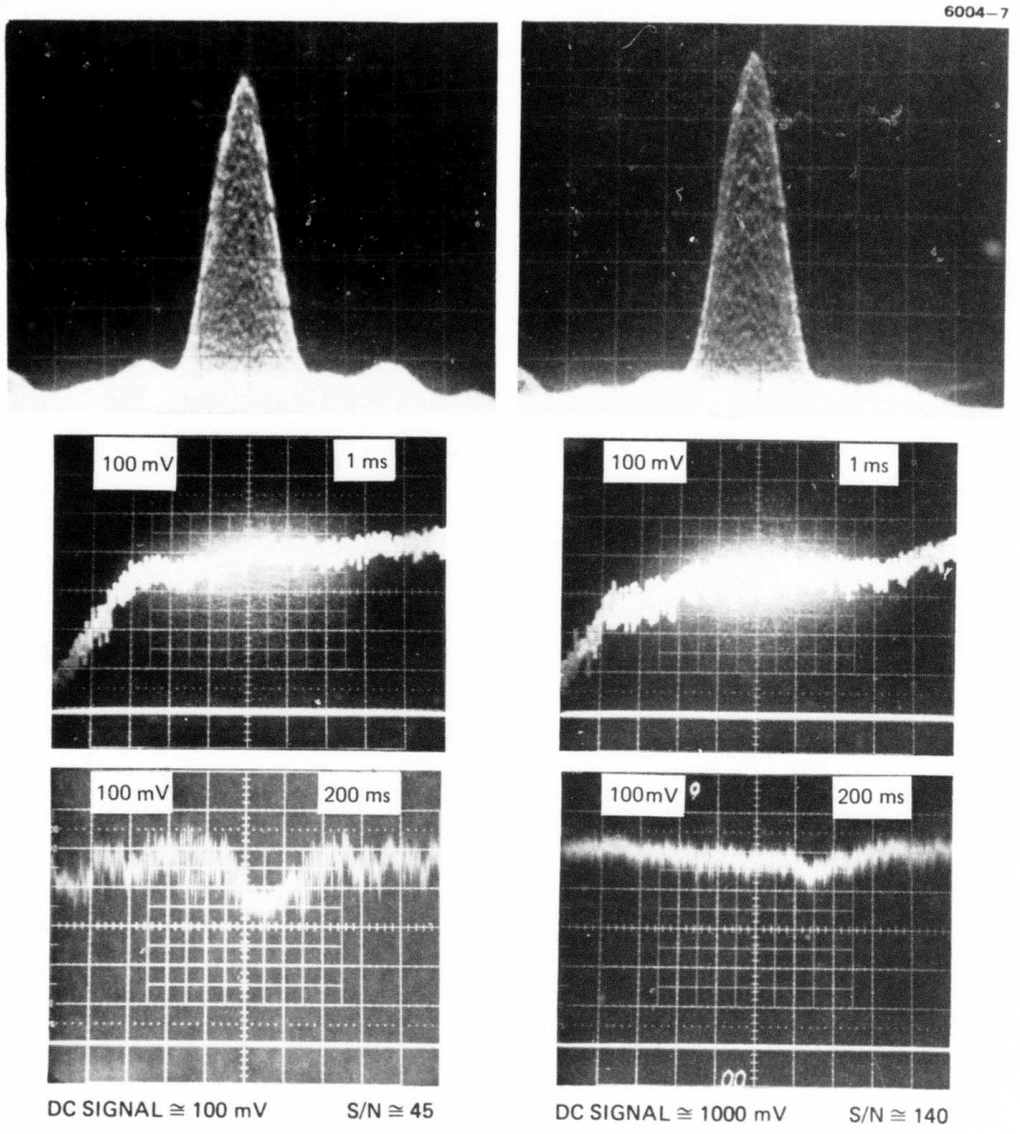

Figure 19(b). Annular Aperture IMPACT (glint mode) performance (continued).

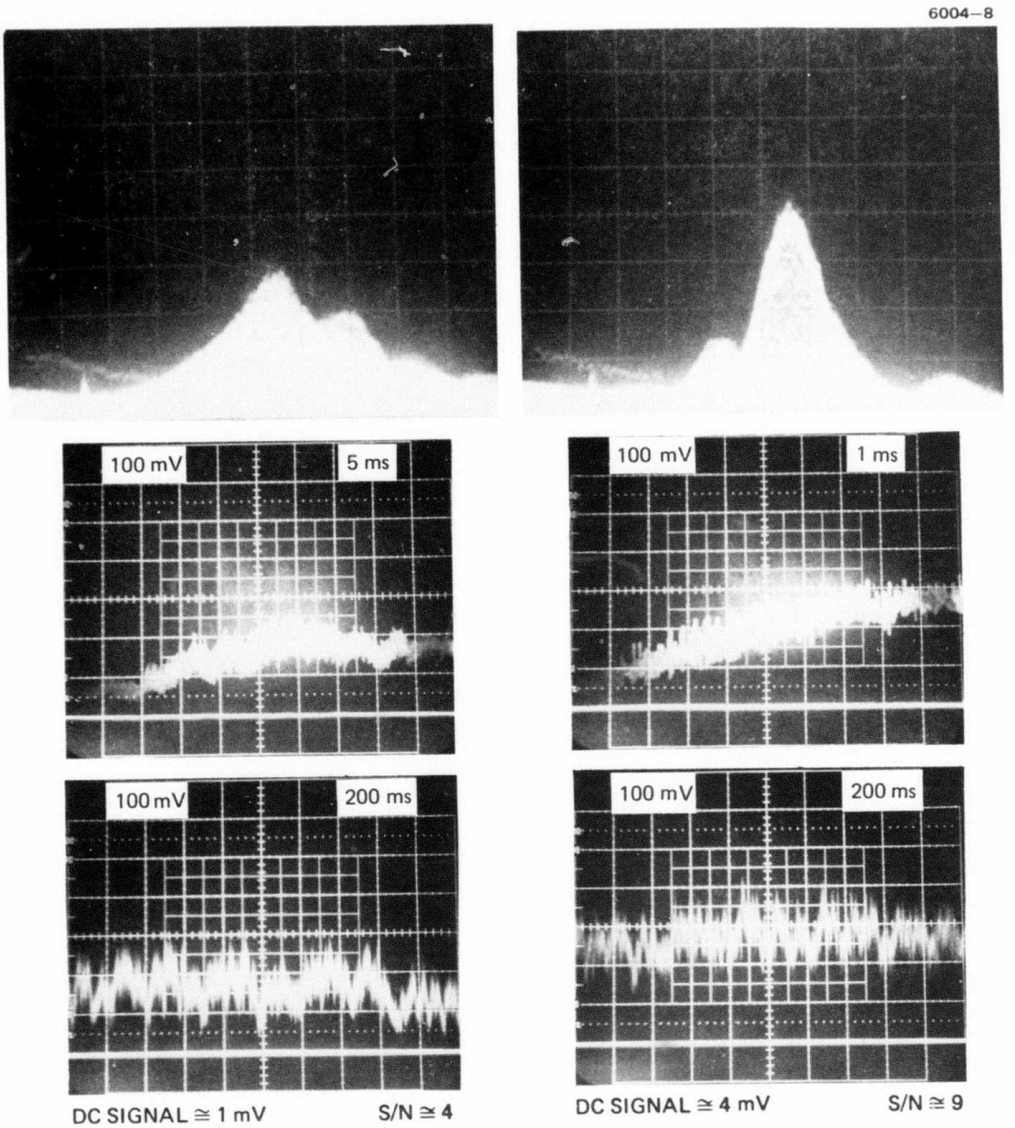

Figure 20(a). Annular Aperture IMPACT (featureless target mode) performance. Beam profiles (top row), convergence time (center) and beam stability (bottom) are shown.

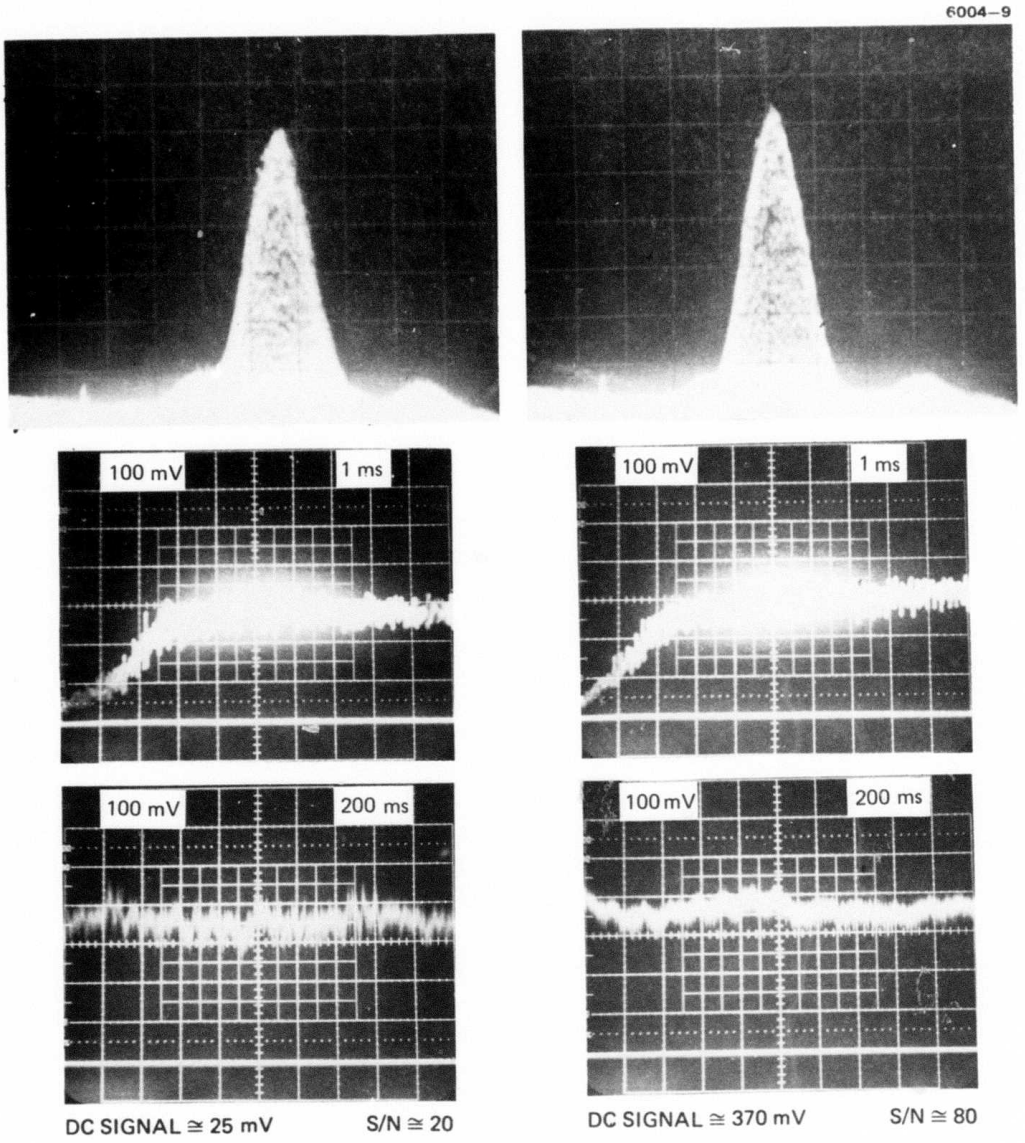

Figure 20(b). Annular Aperture IMPACT (featureless target mode) performance (continued).

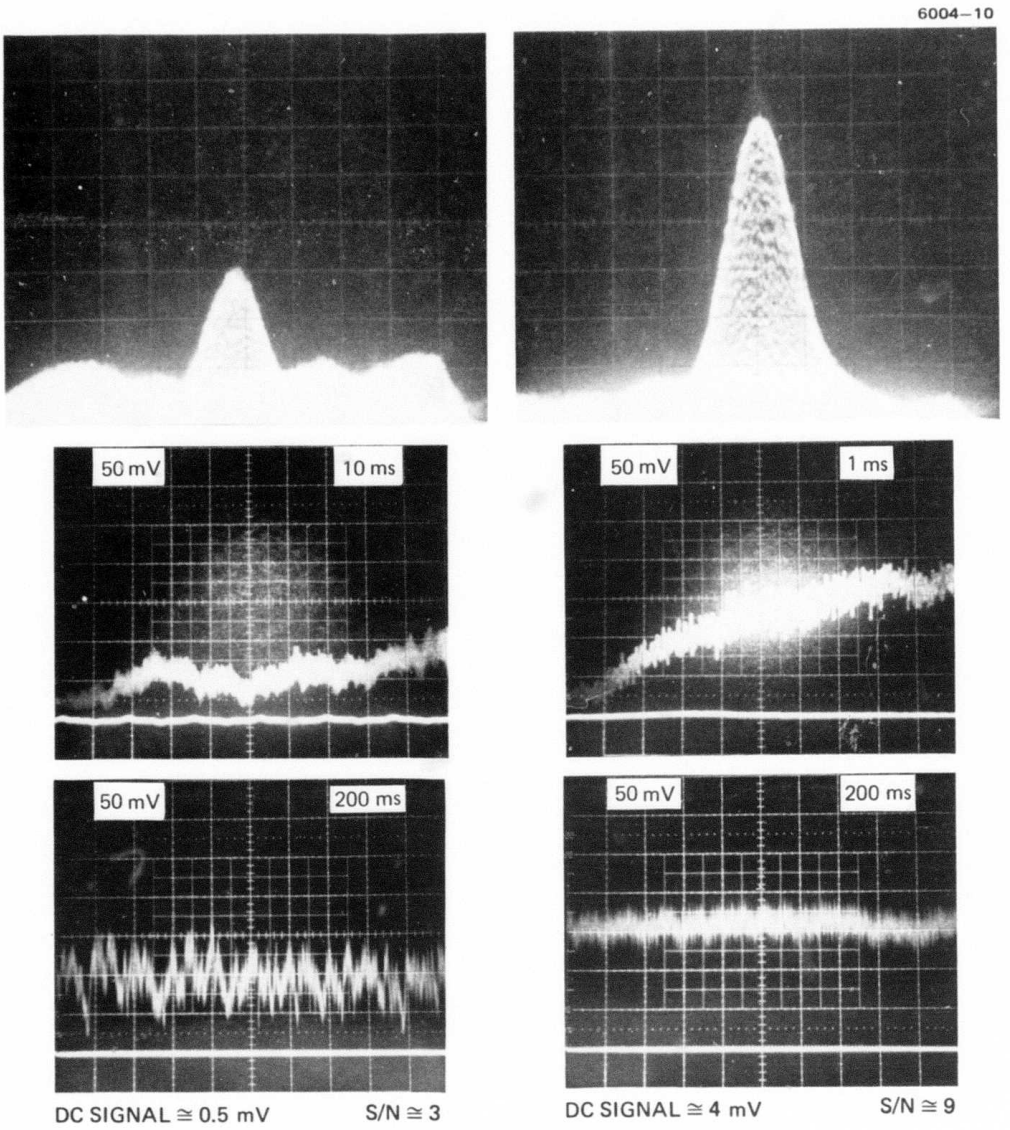

Figure 21(a). Shared Aperture IMPACT (glint mode) performance. Beam profiles (top row), convergence time (center) and beam stability (bottom) are shown.

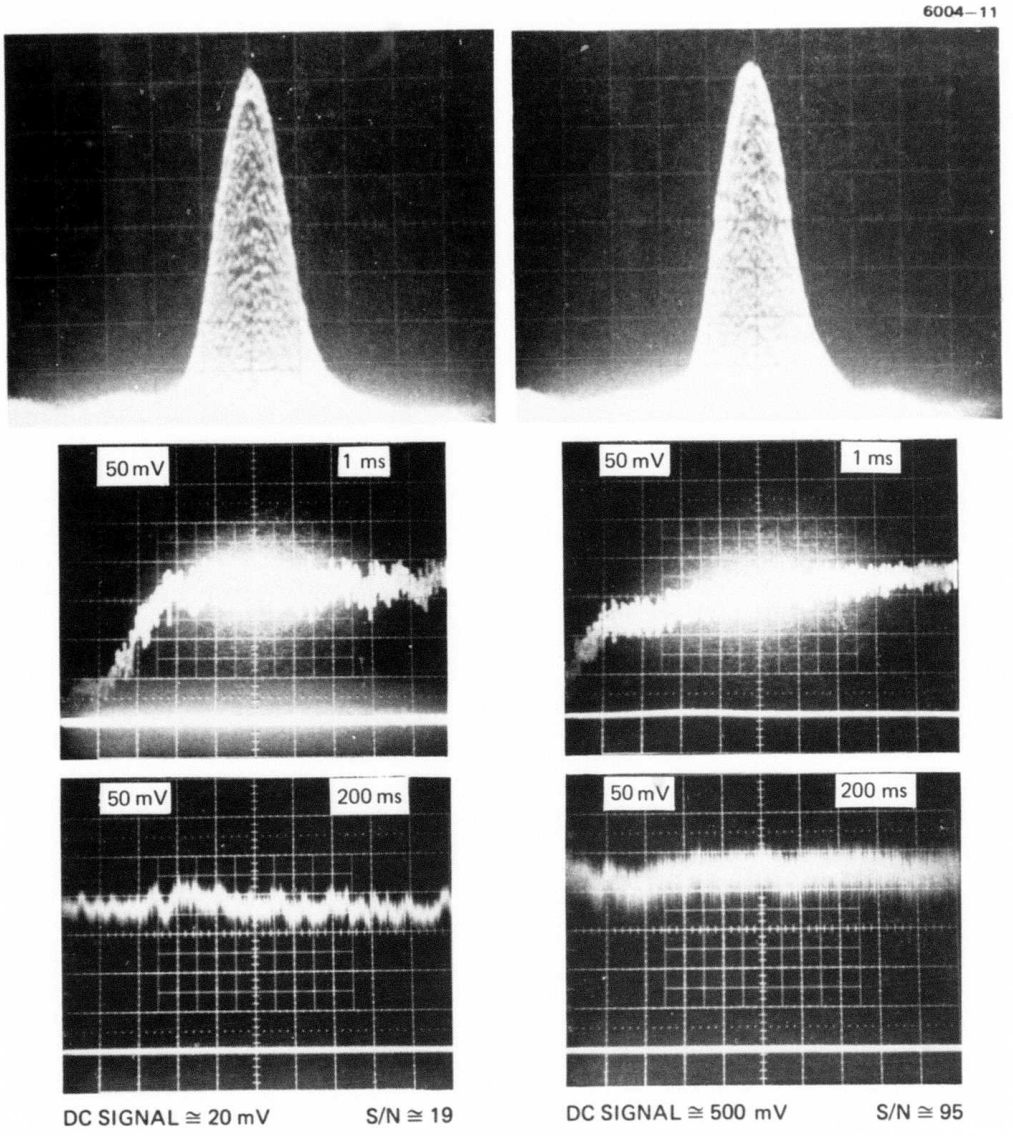

Figure 21(b). Shared Aperture IMPACT (glint mode) performance (continued).

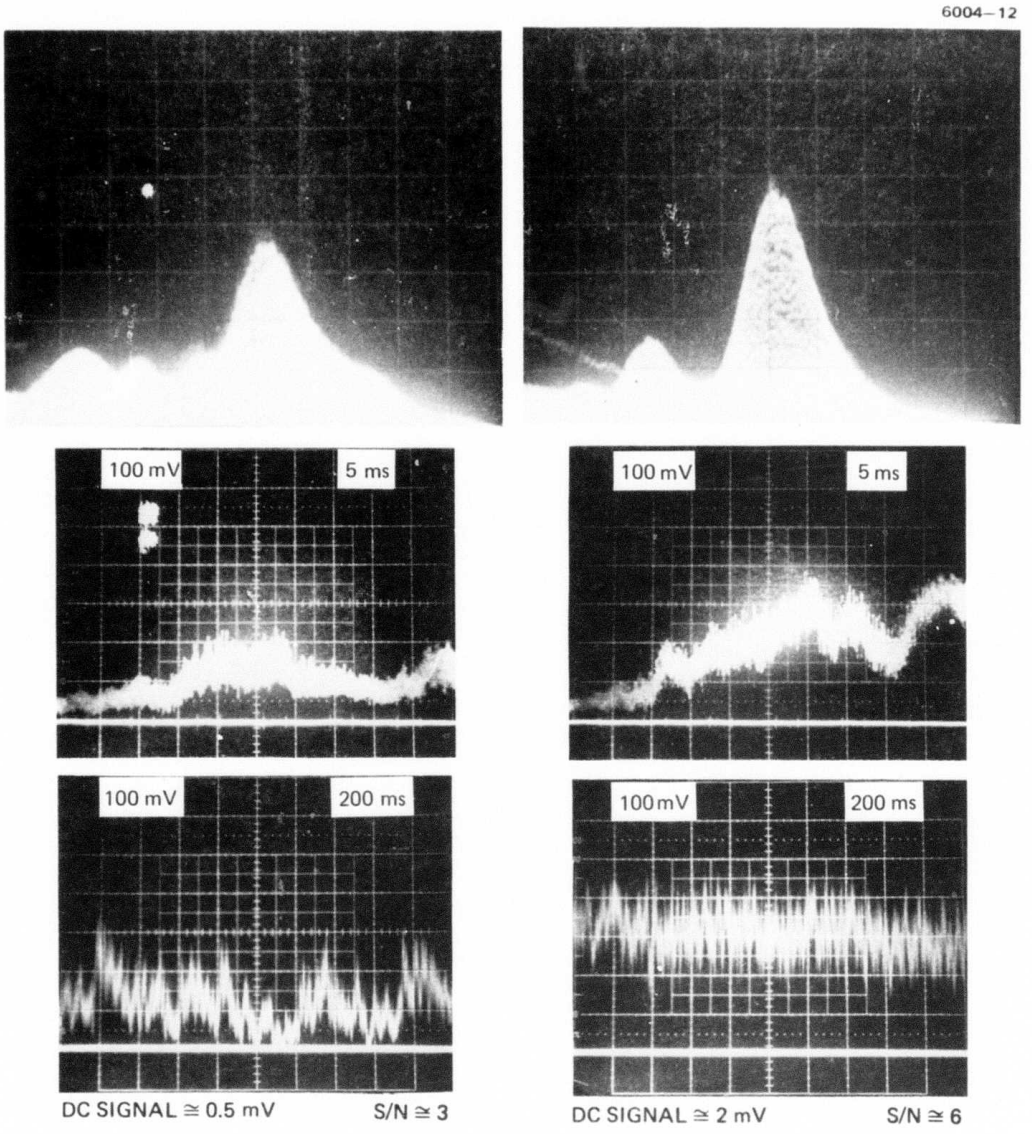

Figure 22(a). TRIM-COAT performance. Beam profiles (top row), convergence time (center), and beam stability (bottom) are shown.

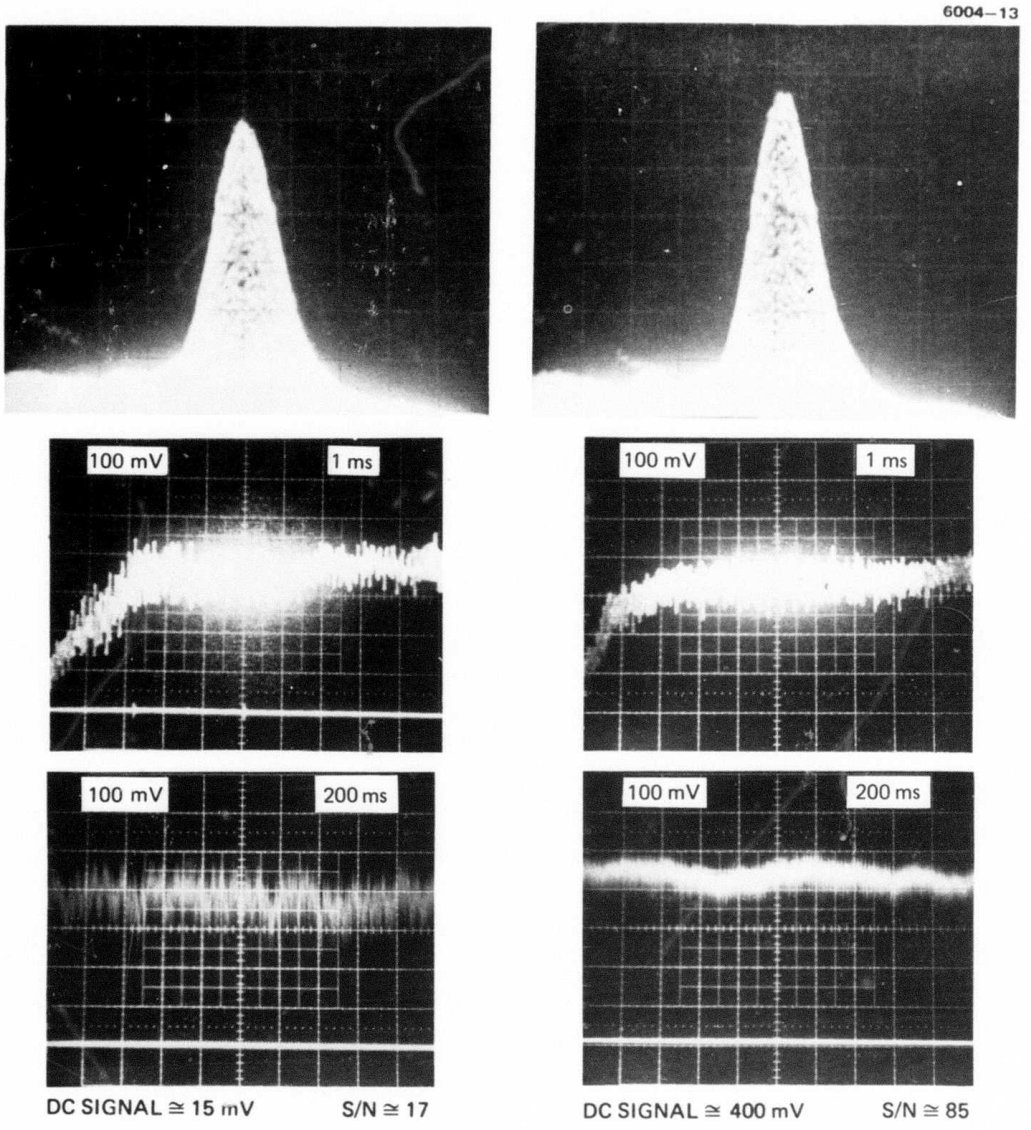

Figure 22(b). TRIM-COAT performance (continued).

The convergence time and beam stability traces are linear and may be used for quantitative comparisons. The high-frequency "noise" superimposed upon these traces is the dither modulation. The lower-frequency, overall deflections in these traces represent the actual beam variations. Minor variations in the saturation (plateau) value of peak target irradiance are evident in these photographs from one COAT system to the next. This is attributable to the data being taken on different days.

Variations of ± 10% in the maximum peak target irradiance attainable occurred from day to day. These variations were observed with the standard system also, and correlated well from system to system when side-by-side comparisons were made. They are thus not related to any fundamental difference in the COAT systems studied, but rather to the normal variations encountered in any experimental setup.

Careful inspection of Figures 19 through 22 indicates that the four COAT configurations perform quite similarly. For dc signal levels greater than ~25 mV ($S/N \gtrsim 20$), well-formed beams with only minor sidelobe structures are formed. Convergence times of ~2 msec or less are observed, and beam stability is good with fluctuations limited to less than ± 5 or 10%. The convergence-time photographs show that for this range of signal levels, the beam converges to only ~80% of its long-term average during the initial rise. This 80% level is apparently a $2N\pi$ state. Convergence to this level is nearly always observed. To remove the system from this state required an external perturbation, such as jiggling lens ℓ_o or passing an object through the beam.

At dc signal levels of 4 to 5 mV ($S/N \sim 8$-10) marked sidelobe structures have appeared. The convergence times have slowed to 3 to 5 msec and the beam fluctuations are now roughly ± 10 to 20%. At lower dc return levels of ~1 mV ($S/N \sim 4$), almost no improvement in the beam profile is noticeable with the COAT system on. The rise time has slowed to >10 msec and beam fluctuations are now of the same magnitude as the average beam intensity.

The main conclusion to be drawn from the data presented in Figures 15 through 22 is that for proper system operation, return signal levels of >25 mV (S/N >20) are required for the four COAT configurations studied. Under these conditions we obtain: (1) peak beam irradiances of >90% of the saturation value, (2) convergence times of 2 msec or less, and (3) beam irradiance fluctuations of <10% of the average value.

3. Featureless Target Operation of the Shared Aperture IMPACT System

As noted in the introduction, we were unable to demonstrate proper operation of the Shared Aperture IMPACT System in the featureless target mode. Several attempts were made throughout the study, both over the propagation range and indoors. We were never successful, primarily due to the fact that at most only 1 to 2 mV of dc signal return was ever observed. (This observation was made on the indoor range, with a Scotchlite target, 20x microscope objective for ℓ_1, 0.51 mm IMPACT stop spaced 45 cm from ℓ_1, no attenuation filter in front of the PMT, argon beam collimated.) As noted above, for proper system operation >25 mV of signal are required for the other four COAT configurations. We would expect this system to have similar behavior.

In the above configuration, about 3 to 5 mV of backscatter from the optics reached the PMT. When the COAT servo loop was closed the total signal at the PMT (return signal plus backscatter) would increase by approximately a factor of two, but no improvement in the beam quality was observed. The COAT system apparently was maximizing the backscatter through the IMPACT stop.

There are several approaches that could have been employed to increase the signal return and thus enhance the probability of demonstrating this system: (1) Find a semi-diffuse reflector that returns more light than the Scotchlite employed here; (2) use a receiver larger than the 2 cm diameter employed here; (3) use a more powerful argon laser (1 W used here). Approach (3) is made somewhat suspect by the

fact that increasing the laser power will also increase the backscatter. Use of this approach would thus also require revamping of the optical system to produce further backscatter reductions. This is a major system change and is beyond the scope of the contract. Approach (2) also requires a major system change and in addition would violate the scaling of this experiment to a 4 km, 3.8 μm scenario using our present 120 m turbulence range (see Section 2.D). Regarding approach (1), we have been looking for an improved semi-diffuse reflector but have not found one.

Further experimentation on the Shared Aperture IMPACT system operating with featureless targets was therefore abandoned. This demonstration should be tried again in the future, probably through the use of Approach (2), above.

C. BASIC SYSTEM OPERATION IN TURBULENCE

In this section we investigate the turbulence-compensating abilities of the four COAT configurations using simple targets. Peak target irradiance, convergence time and beam stability were obtained as a function of turbulence level. The outdoor range was employed for these measurements. We first present a series of representative side-by-side comparisons and then follow this with a summary plot of turbulence-compensation capabilities as a function of turbulence level.

1. Some Representative Data

The optical configurations and targets employed here are basically the same as those described previously (Sections 2.C and 3.B). Since the turbulence produced severe distortions of the laser beam, it was not necessary to defocus the transmitting optics to give the COAT system an error to correct. An approximately collimated beam was used for all measurements. The average signal return was maintained at >100 mV (S/N >40) so that each system was operating on the flat portion of the curves shown in Figures 15 through 18.

a. Annular Aperture IMPACT (glint operation)

Figure 23 shows a side-by-side comparison of this configuration and several other modes of operation in strong turbulence. The top trace shows the peak target irradiance as a function of time, the lower curve shows the simultaneously-recorded atmospheric structure constant (C_N^2). The beam irradiance detector and scintillometer circuitry were both adjusted to have a response/integration time of ~1 sec. The dashed line across the top of the irradiance trace represents the best low-turbulence ($C_N^2 \cong 4 \times 10^{-17}$ cm$^{-2/3}$) performance obtained over the outdoor range with the COAT receiver located at the target.

Four modes of operation are investigated in this series: glint operation of Annular Aperture IMPACT, the "standard" system with the receiver at the target, COAT off (beam manually steered to target), and local loop operation (beam steered manually). The standard system represents COAT operation with no return path turbulence to degrade performance. The local loop (see Section 2.C) is used to remove residual distortions in the transmitter optics so that an approximate diffraction-limited beam is sent out onto the turbulence range. The difference between the dashed line and local loop irradiance levels thus represents the degradation to an approximate diffraction-limited beam caused by the turbulence. In this case, the degradation is almost a factor of five.

The performance of the Annular Aperture (glint) system is seen to be equal to that of the standard system: peak target irradiance for both are 60 to 70% of their low turbulence values and the COAT on/local loop improvement is 2.5.

The average C_N^2 during the run was 2×10^{-14} cm$^{-2/3}$ (strong turbulence) and varied by typically ±50% over periods of ~10 sec, although larger variations are evident near the end of the run. The smaller excursions in the lower trace are due primarily to the statistical nature of turbulence and the 1-sec integration time employed here. However, the larger, longer-term fluctuations correlate well with changes in wind velocity over the roof. An increase in wind

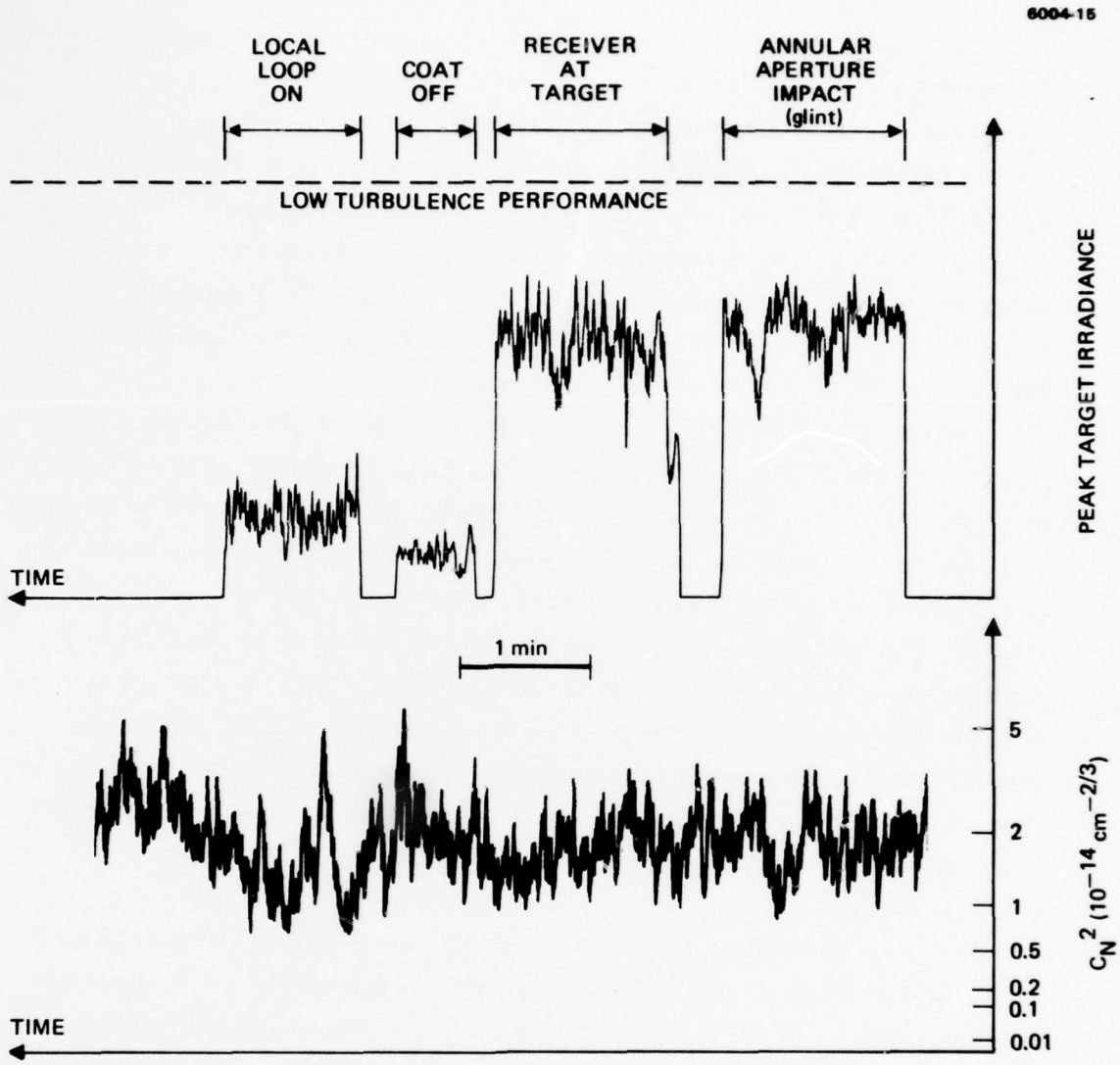

Figure 23. Performance of Annular Aperture IMPACT (glint mode) in high turbulence.

velocity produces lower turbulence and vice-versa. This is apparently due to the turbulent air which rises from the roof surface being blown out of the path of the beam before it can rise to the 1-m height of the optics. Wind velocity during this run ranged from 0 to 5 mph.

Figure 24 shows photographs of the beam stability and convergence times for the Annular Aperture (glint) system in strong turbulence ($C_N^2 \cong 1.0 \times 10^{-14}$ cm$^{-2/3}$). During the 1-sec interval shown in the top photograph, the peak target irradiance varied by $\sim \pm 50\%$ about the mean. Two examples of the system convergence time are shown in the lower photographs: in one the beam converges to nearly the average level ($\sim$12 V in these photographs) in the usual time of $\sim$2 msec, in the other the beam converges to a $2N\pi$ state initially, then finally after $\sim$5 msec converges to approximately the average value. Convergence to $2N\pi$ states was usually observed. Full or nearly full convergence was seen only $\sim 10\%$ of the time.

b. Shared Aperture IMPACT (glint operation)

Figure 25 shows side-by-side comparative performances of the Shared Aperture, Standard and COAT OFF modes of operation. The average C_N^2 is 1×10^{-14} cm$^{-2/3}$. Initially the Shared Aperture system is seen to produce correction to about the 60% level. Upon switching to the receiver-at-target mode the level drops to 40 to 50%. At this point one might conclude that the Shared Aperture system works better than the receiver-at-target configuration (an unlikely event). However, upon switching back and forth repeatedly between the two systems, we see that the two optical configurations actually perform about the same. It is the overall ability of COAT to correct the turbulence which is varying.

The approximately $\pm 25\%$ variations observed here for a given COAT system to correct a given level of turbulence were observed for all the systems studied at one time or another. Its cause is not yet understood. It may be something as simple as a transient defect in the COAT electronics (such as a transient phase error in the dither or receiver electronics), or it may be a fundamental problem (such as a

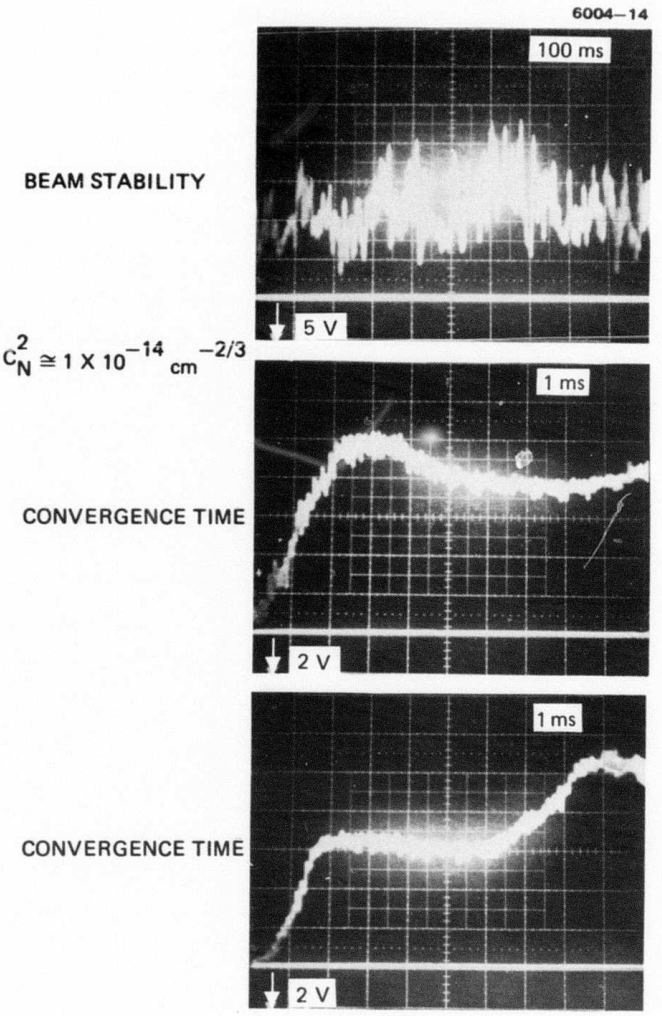

Figure 24. Beam stability and convergence time of Annular Aperture IMPACT (glint mode).

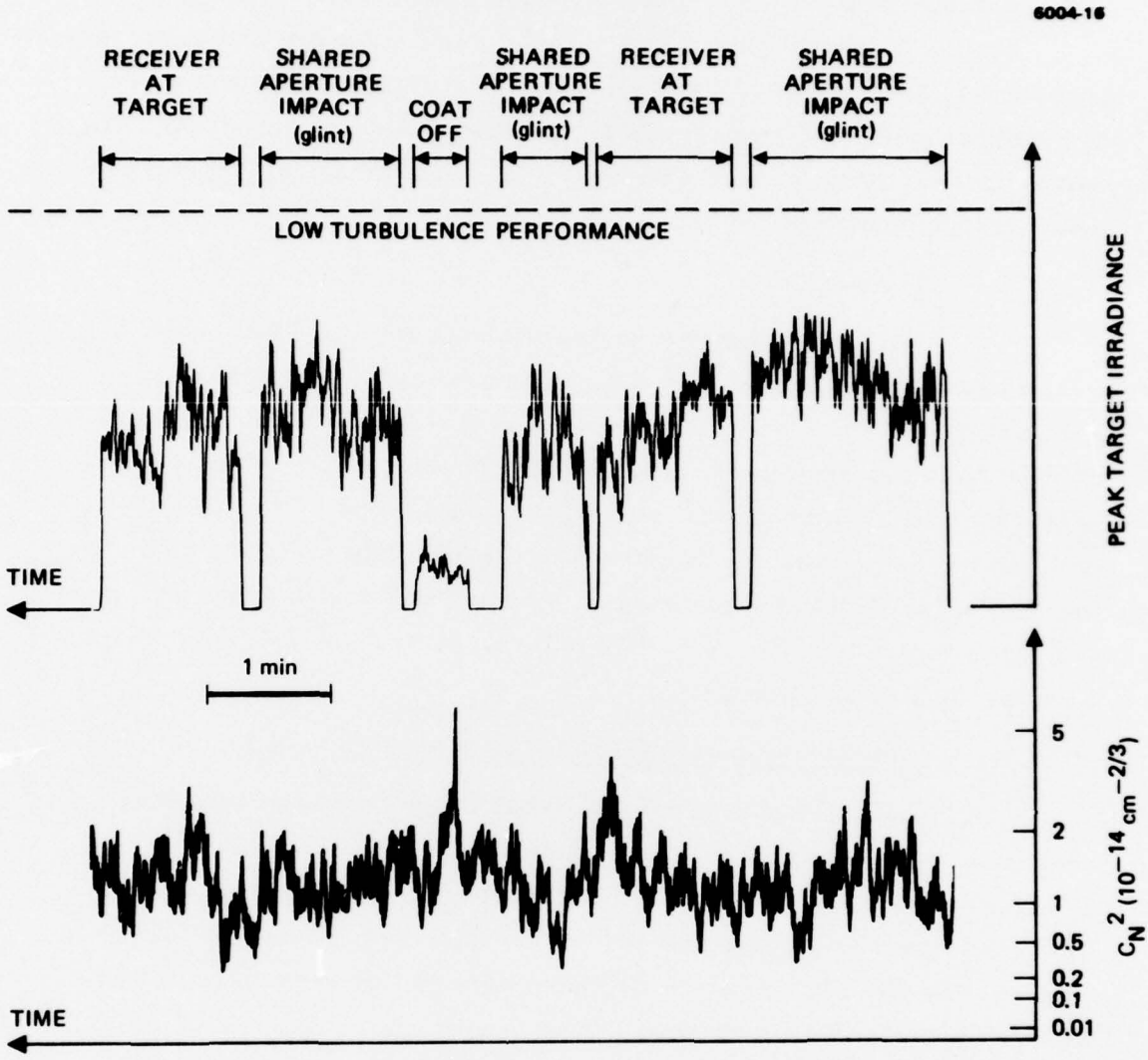

Figure 25. Performance of Shared Aperture IMPACT (glint mode) in high turbulence.

subtle change in the rate at which C_N^2 fluctuates inducing the system to lock up in 2Nπ states). The problem requires further investigation.

Figure 26 shows photographs of the beam stability and convergence times. C_N^2 here is about 2×10^{-14} $cm^{-2/3}$. Beam fluctuations are again about ± 50%. Convergence times are 2 msec as expected. The same statements regarding 2Nπ states found in the Annular Aperture description apply here also.

c. TRIM-COAT

For completeness we include data for the TRIM-COAT system in Figures 27 and 28. The performance of this system is essentially the same as glint operation of the Annular Aperture and Shared Aperture configurations. Figure 27 shows that TRIM-COAT produces ~60% convergence with $C_N^2 \cong 2 \times 10^{-14}$ $cm^{-2/3}$, thereby performing as well as the receiver-at-target mode. Figure 28 shows that the beam fluctuations are again approximately ± 50% and that convergence times are ~2 msec. As before, convergence to 2Nπ states occurs ~90% of the time.

d. Annular Aperture IMPACT (featureless target)

As discussed previously in Section 1, featureless target operation with the Annular Aperture IMPACT system requires an auxiliary tilt control for maximum performance in turbulence. The COAT system used in the study does not have provisions for this, and as a result, the performance reported here is not as good as in the previously described systems.

Figure 29 compares the featureless target performance of Annular Aperture IMPACT with the standard configuration in intermediate turbulence levels ($C_N^2 \cong 5 \times 10^{-16}$ $cm^{-2/3}$). The peak boresight irradiance is only about 40% of the maximum possible, about half of that obtained with the receiver at the target, and about twice that obtained with COAT OFF. The local loop was removed for these runs in order to eliminate backscatter from beamsplitter BS2 (see Figure 11); therefore a direct local-loop comparison is not possible. However, on runs with the other systems, the local-loop improvement

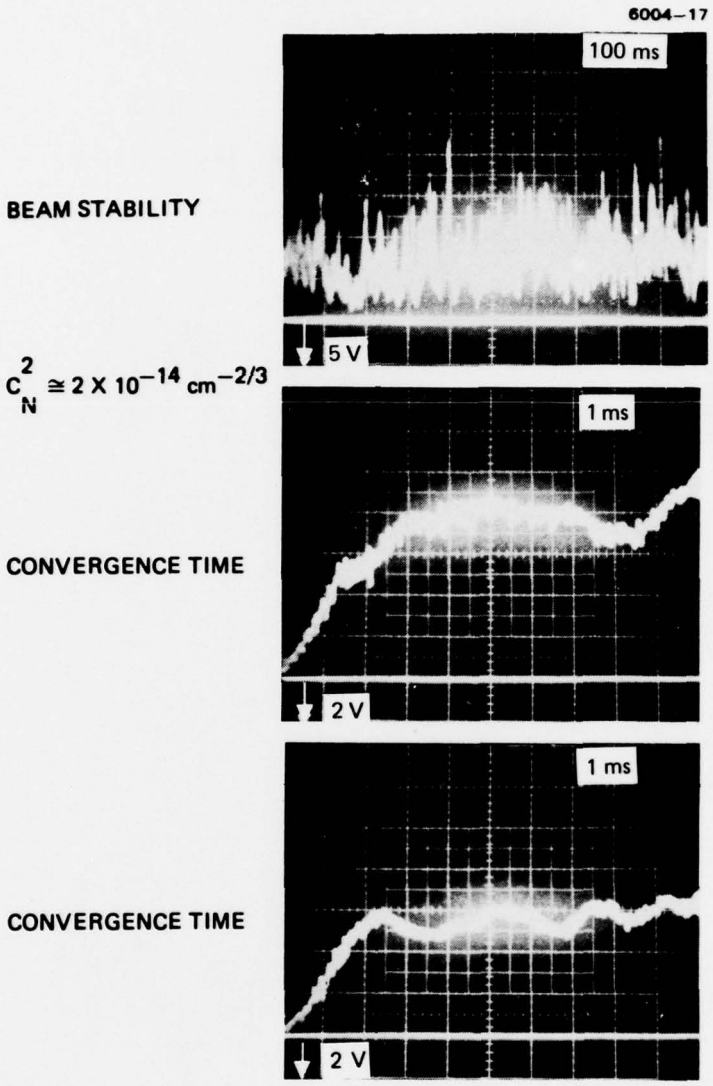

Figure 26. Beam stability and convergence time of Shared Aperture IMPACT (glint mode).

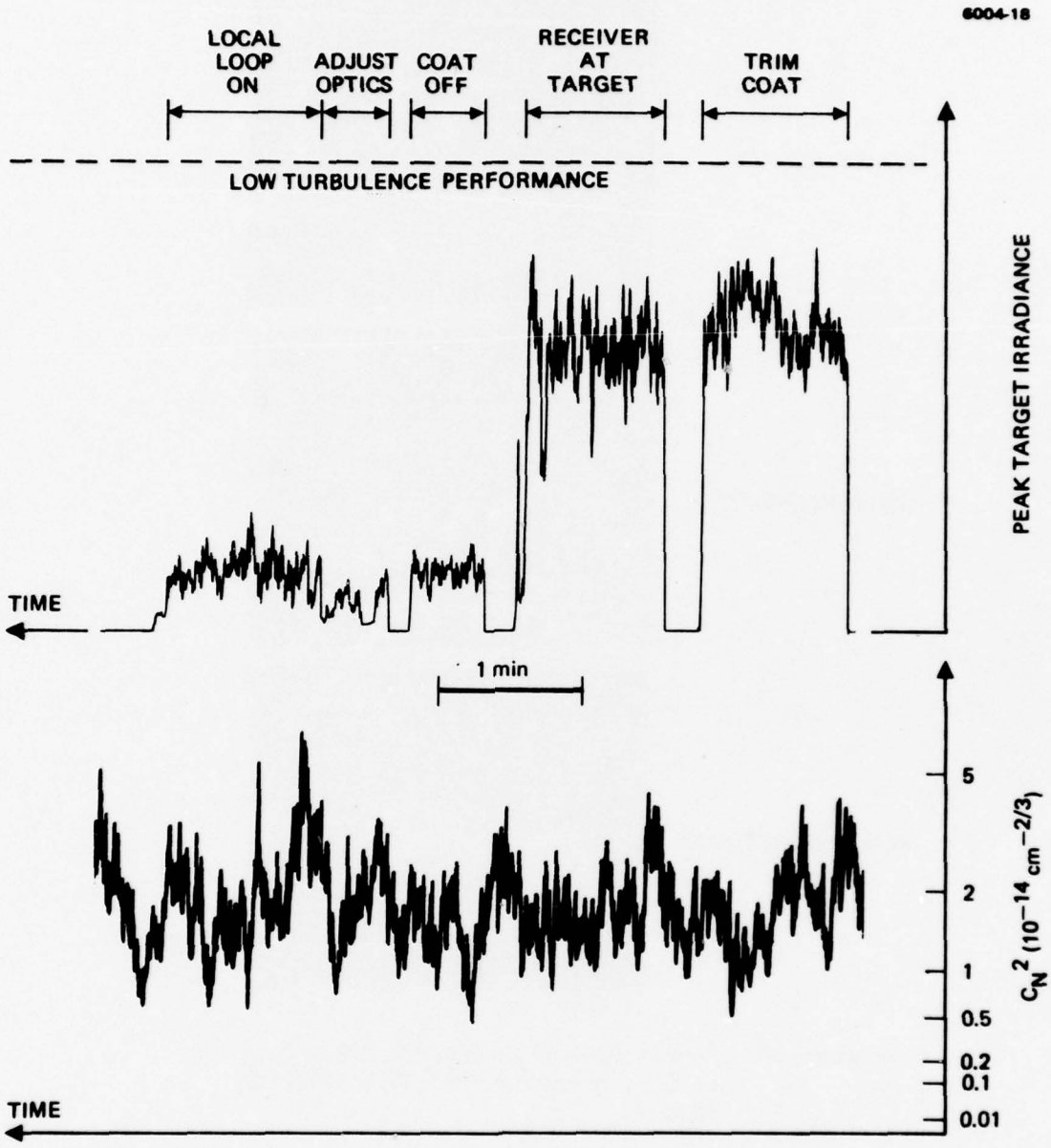

Figure 27. Performance of TRIM-COAT in high turbulence.

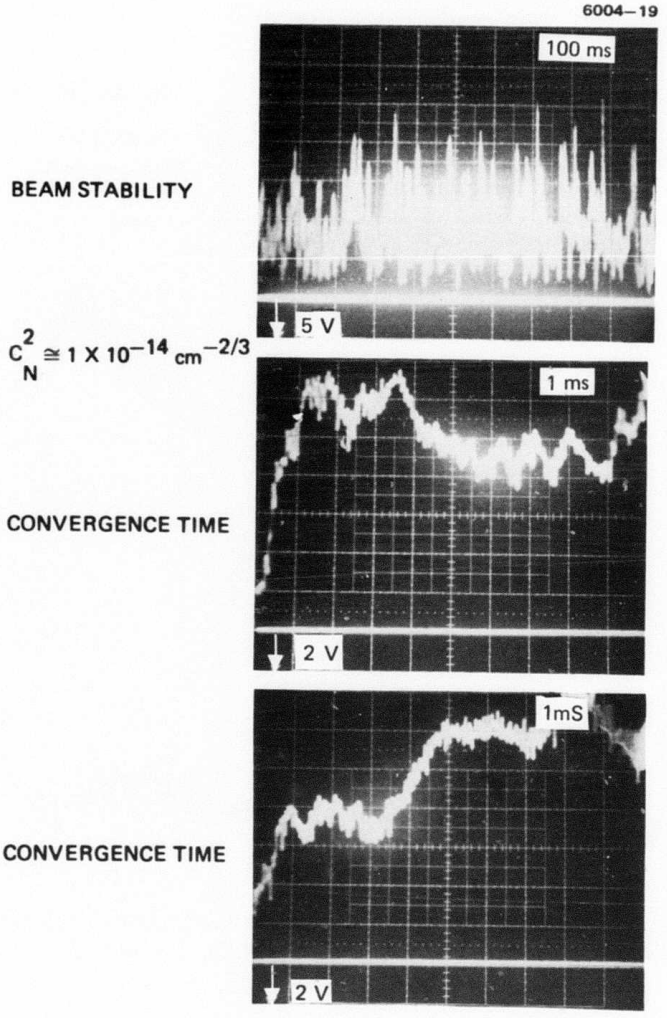

Figure 28. Beam stability and convergence time of TRIM-COAT.

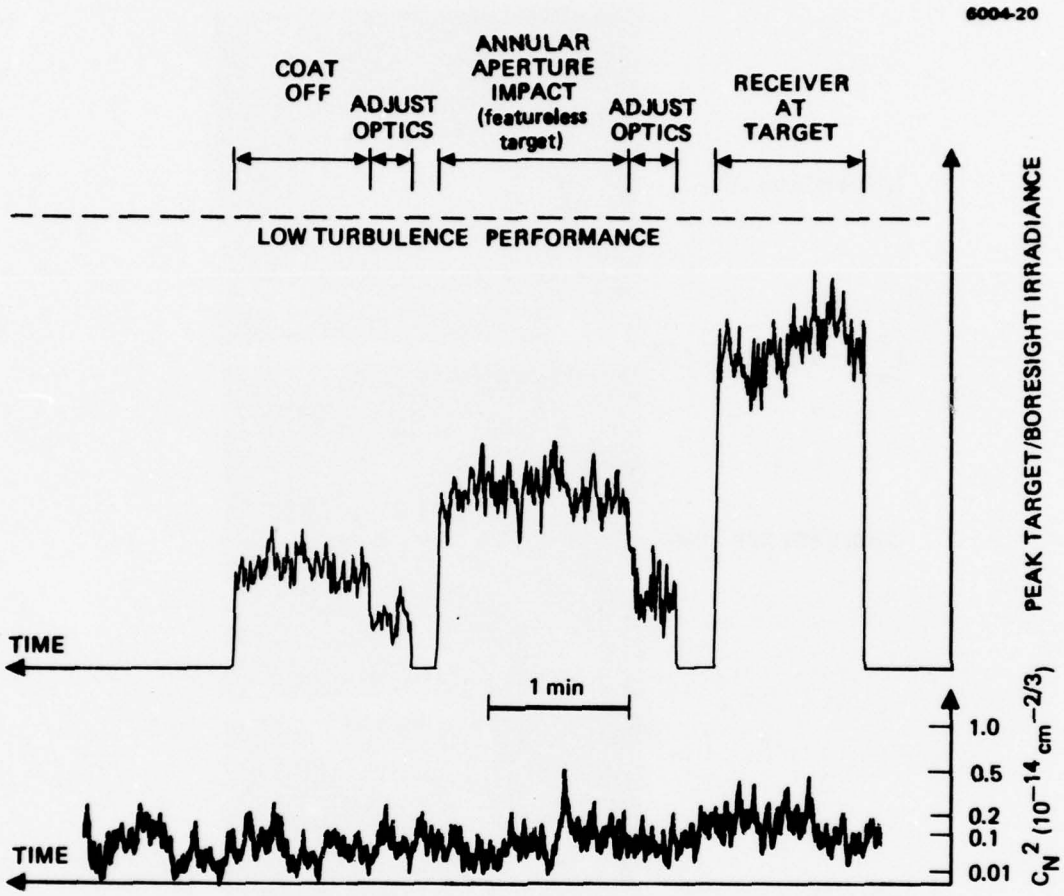

Figure 29. Performance of Annular Aperture IMPACT (featureless target mode) in intermediate level turbulence.

at the target was usually 50 to 100% over the COAT OFF condition, so that the featureless target performance shown here is probably roughly comparable to the local-loop performance.

Still photographs of the beam profiles obtained with the featureless target configuration and the standard system are shown in Figure 30. Here $C_N^2 \cong 1.0 \times 10^{-15}$ cm$^{-2/3}$. Both beams were photographed near their maximum peak irradiance excursions. For both beams the peak irradiance varied by roughly ± 20%. The beam produced by the standard system is locked onto a glint located at the transmitter boresight. It was observed to have essentially no tilt (side to side) motion. The featureless target beam is seen from Figure 30 to have a peak irradiance of roughly 75% of the standard beam. Although its average side-to-side position was the transmitter boresight, errors induced by the turbulent return path caused the beam to tilt from side to side by roughly ± 1/2 beam radius. A tilt error of about 1/2 beam radius is shown in Figure 30.

From these observations it is fairly clear that if these tilt errors could have been removed by an auxiliary tilt control, the boresight irradiance of the featureless target beam would have been roughly 75% of that obtained with the receiver at the target. Compensation of the return path (as in the Shared Aperture IMPACT system) would presumably make the convergence level even higher. Evaluation of both the Annular Aperture and Shared Aperture systems with an auxiliary tilt control is an important project for future study.

Figure 31 shows beam stability and convergence time data for this system at intermediate turbulence levels ($C_N^2 \cong 2 \times 10^{-15}$ cm$^{-2/3}$). Beam fluctuations are roughly ± 25%. Convergence times are again ~2 msec as expected. Partial convergence to $2N\pi$ states is observed at roughly the same frequency (~90% of the time) as in the other systems studied.

6004–21

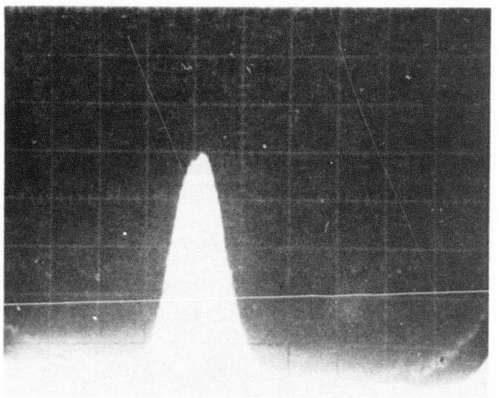

RECEIVER AT THE TARGET (GLINT OPERATION)

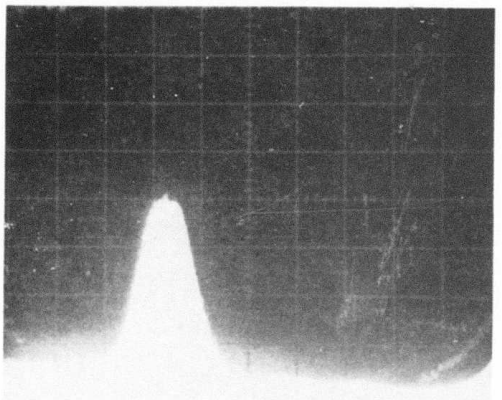

ANNULAR APERTURE IMPACT (FEATURELESS TARGET OPERATION)

$$C_N^2 \cong 1 \times 10^{-15}\ \mathrm{cm}^{-2/3}$$

Figure 30. Comparison of beam profiles obtained with Annular Aperture IMPACT (featureless target mode) and the standard system with the receiver located at the target.

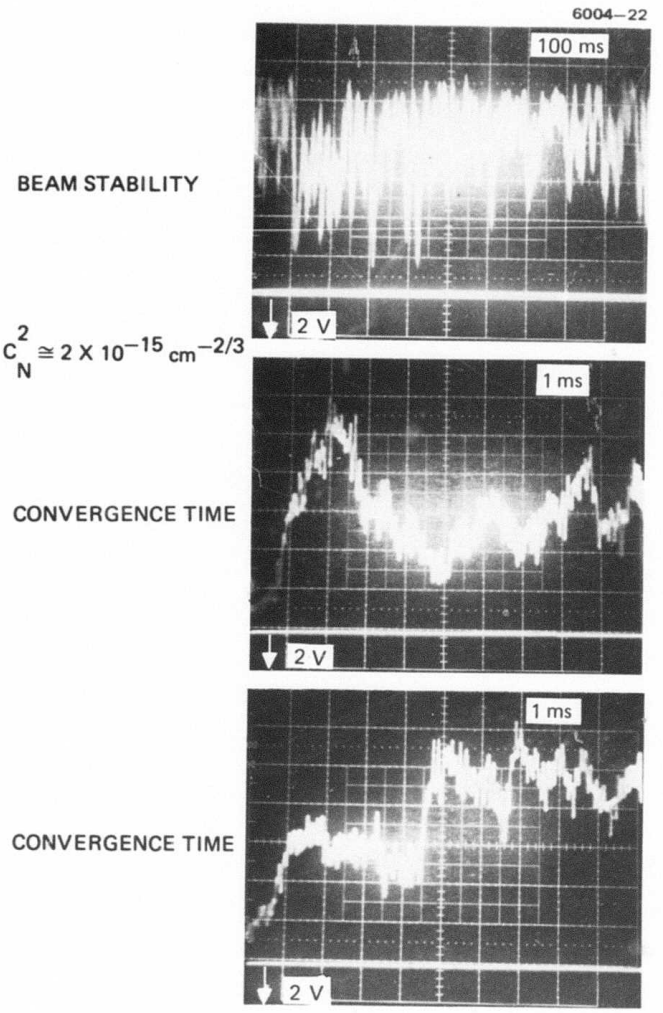

Figure 31. Beam stability and convergence time of Annular Aperture IMPACT (featureless target mode).

2. Summary of Turbulence Performance with Simple Targets

Figure 32 is a plot of peak target irradiance as a function of C_N^2. Data for the three COAT systems (four modes of operation) as well as for the standard (receiver-at-target) system, local loop and COAT off modes are shown. Data points for the laboratory measurements are also plotted in their approximate location (C_N^2 estimated). The two straight lines in the figure indicate two groups of data points that behave roughly the same. The units for C_N^2 shown in the figure are $cm^{-2/3}$. To convert to $m^{-2/3}$ multiply by 22. To scale to the 4-km, 3.8-μm scenarios described in Section 2.D, divide C_N^2 by 59.

Annular Aperture IMPACT (glint operation), Shared Aperture IMPACT (glint operation) and TRIM-COAT are observed to perform equally well over the range $10^{-18} \lesssim C_N^2 \lesssim 4 \times 10^{-14}$ $cm^{-2/3}$. Their performance is equal to that of having the receiver located at the target. This is not unexpected since with single glints the image quality of the glint is not important. With no other glint on the target, the process of maximization of the total light return signal must converge the beam on the glint whether the return path is corrected or not. Approximately full convergence is maintained up to $C_N^2 \cong 5 \times 10^{-17}$. Thereafter the convergence level gradually degrades to about 60% of maximum at $C_N^2 \cong 2 \times 10^{-14}$ $cm^{-2/3}$ (strong turbulence). This is about a factor-of-three improvement over the simple propagation of a diffraction-limited beam across the range (local loop mode), and about a factor-of-six improvement over having the COAT system completely off. The 60% convergence levels obtained here in high turbulence with a deformable mirror are the same as those obtained with the RADC phasor matrix with tracking controls.[10]

Figure 32 shows that, over most of the range of C_N^2 studied, the performance of Annular Aperture IMPACT operating with featureless targets is not as good as that of the other systems. While the same peak boresight irradiance was obtained in the laboratory ($C_N^2 < 10^{-17}$ $cm^{-2/3}$), at $C_N^2 \cong 5 \times 10^{-17}$ the irradiance has fallen to 70%, and at $C_N^2 \cong 2 \times 10^{-14}$ $cm^{-2/3}$ the irradiance is little better than that obtained with the local loop in operation.

This relatively poor performance is due primarily to the lack of an auxiliary tracking control in the present optical system. As noted in the previous section there is evidence that this modification would improve the peak boresight irradiance by a factor of ~1.4 at $C_N^2 \cong 5 \times 10^{-16}$ $cm^{-2/3}$, thereby giving ~75% of the peak irradiance produced by the other systems. The use of the Shared Aperture system, which has a corrected return path, would presumably do even better.

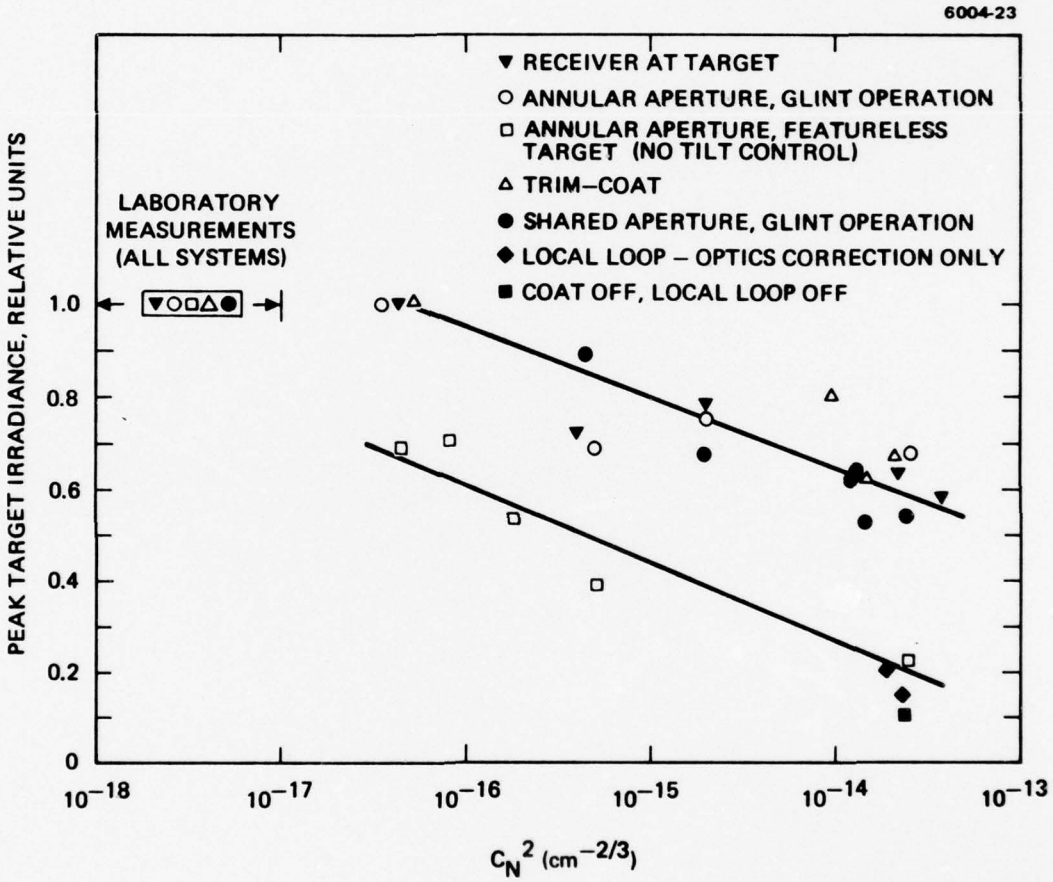

Figure 32. Convergence of the various COAT systems as a function of turbulence level.

SECTION 4

INVESTIGATION OF TARGET EFFECTS

A. INTRODUCTION

In this section we investigate the sensitivity of each of the COAT systems to glint and target dynamics. We present glint destruction and glint "pop-up" demonstrations which show the effectiveness of the IMPACT stop at locking out an intruder glint when the intruder-to-reference-glint strength ratio changes. The radius of effective guarding action for the IMPACT stop is mapped out as a function of intruder-to-reference-glint strength ratio, and the degradation of guarding action with turbulence is determined. Convergence on a rotating multi-glint target and also on the near-edge highlight of a rotating sphere are studied. The effects of glint size and the glint return signal to background return signal contrast ratio are also investigated.

B. GLINT DISCRIMINATION

1. Glint Destruction and Glint "Pop-Up" Demonstrations

An important feature for COAT systems to exhibit is an intensitivity for glint hopping when the glints on a complex target vary in strength or position. In this section we present visual demonstrations of the insensitivity of Annular Aperture IMPACT and Shared Aperture IMPACT to the partial destruction of the reference glint, and the insensitivity of TRIM-COAT to the sudden appearance of an intruder glint.

These experiments were carried out inside the laboratory using the apparatus described in Section 2.C. Higher-power microscope objectives were used for lenses ℓ_1 and ℓ_2 (see Figure 11) than were employed for this work in Section 3, in order to increase the image sizes at the PMT. This permitted the use of variable-diameter irises as IMPACT stops. Annular Aperture IMPACT and Shared Aperture IMPACT used 40 x (5mm focal length) microscope objectives for ℓ_2 and ℓ_1 respectively. These produced images 50% of the target size, respectively, when objective-to-IMPACT stop distances were 20 cm and 45 cm, respectively.

TRIM-COAT employed a 20 X (9mm focal length) microscope objective for ℓ_1 which was spaced 45 cm from a 0.25-mm pinhole. The images were ~ 25% of the target size. Cats-eye glints were used for the two IMPACT systems, and two defocused He-Ne lasers were used as glints in the TRIM-COAT experiments. In order to give the COAT system an error to correct in these indoor experiments, the transmitter optics were defocused to reduce the COAT-off peak irradiance to ~15% of its converged value. The experiments were carried out with return signal levels > 50 mV (S/N > 30) to ensure full beam convergence.

a. Annular Aperture IMPACT System

Figure 33 shows a target acquisition and glint destruction simulation using the Annular Aperture IMPACT system. The transmitter boresight is initially steered midway between two glints which are spaced 1.5 beam radii apart. (One beam radius = 3.5 mm; the fully converged beam diameter (at the base) is 7 mm.) The reference glint (R) is initially 2.5 times stronger than the intruder glint (I). The IMPACT stop diameter (D) is initially set at 3.4 beam diameters (fully open). The following sequence of events then takes place (refer to numbered photos in Figure 33):

(1) With the IMPACT stop fully open, the COAT servo loop is closed. Since R/I = 2.5, the COAT system partially converges on the reference glint.

(2) The transmitter boresight is pointed at R and $2N\pi$ lock-ups are removed.

(3) The IMPACT stop is closed to D = 1.0 beam diameter. Target acquisition is now complete, with the IMPACT stop obscuring the return from the intruder glint.

(4) The reference glint is now partially destroyed. The return signal from R is decreased by a factor of 30 by quickly placing a neutral-density filter in front of it. The intruder glint is now 12 times stronger than the reference. Nevertheless, the system continues to maintain its lock on R with essentially no decrease in Strehl ratio.

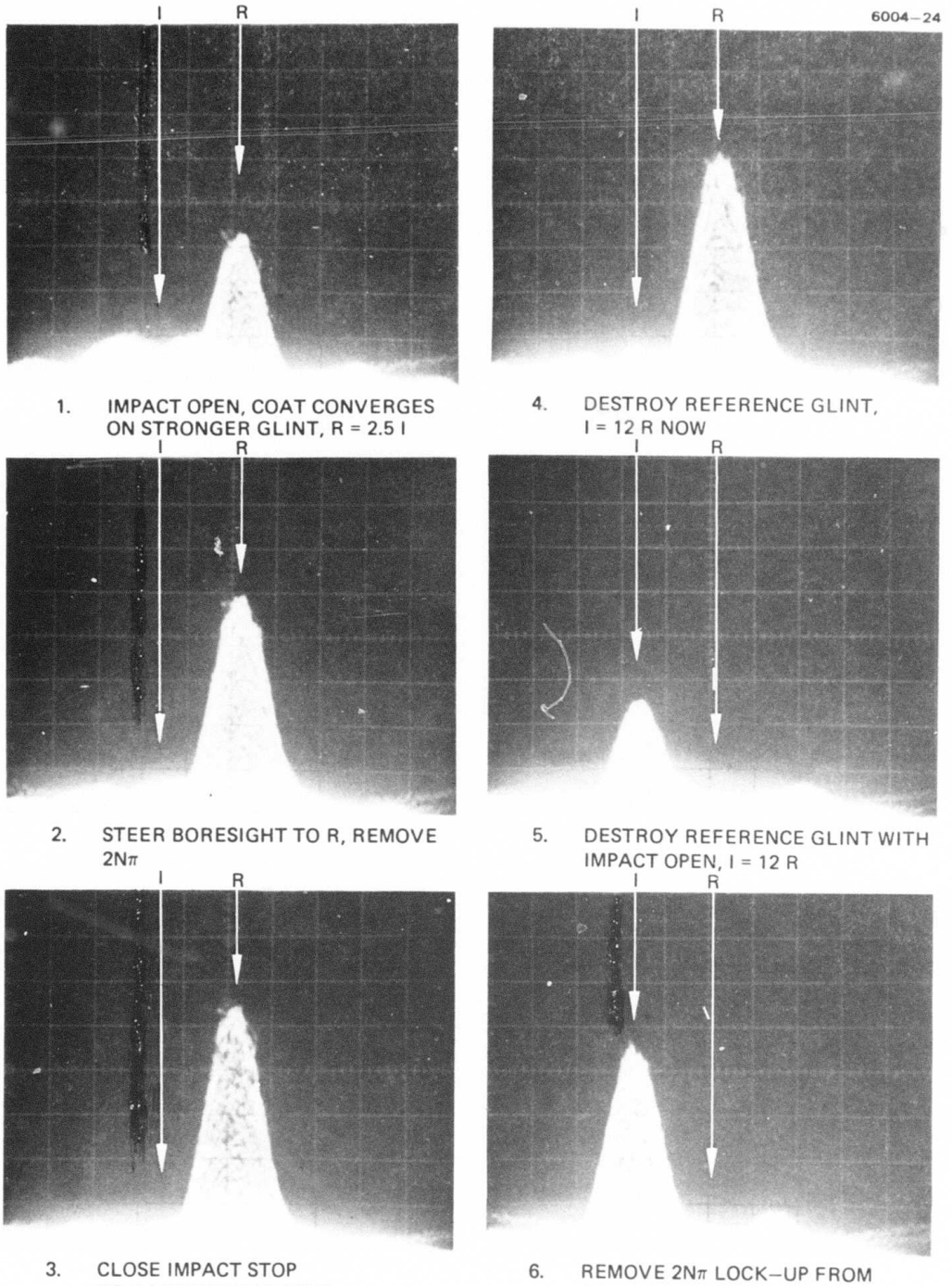

Figure 33. Annular Aperture IMPACT used to prevent glint hopping when reference glint is partially destroyed. Positions of reference and intruder designated by R and I.

(5) The same sequence as in (1), (2) and (4) is repeated, but with the IMPACT stop fully open. Upon destruction of the reference glint, the beam hops over to the intruder. It is locked-up in a low-lying $2N\pi$ state.

(6) With the boresight still on R, the $2N\pi$ lock-up is removed.

b. Shared Aperture IMPACT system

A similar target acquisition and glint destruction scenario is shown in Figure 34 using the Shared Aperture IMPACT system. Here the reference and intruder glints are spaced 3 beam radii apart and initially $R/I = 2.0$. Referring to the numbered photos in Figure 34, the following sequence is enacted:

(1) With the boresight pointed midway between the two glints, the COAT servo look is closed, producing partial convergence on the stronger reference glint.

(2) The boresight is tilted towards R, and $2N\pi$ lock-ups are removed.

(3) The IMPACT stop is closed to $D = 0.5$ beam diameter. Target acquisition is now complete, with the IMPACT stop obscuring the return from the intruder glint.

(4) The reference glint is partially destroyed by placing a filter in front of R which decreases the signal return from it by a factor of 23. The intruder glint is now ~ 12 times stronger than the reference. Some degradation in Strehl ratio is evident, but for the most part lock-on is maintained.

(5) The events of (1), (2) and (4) are again repeated as before, but the IMPACT stop is left fully open. When the reference is destroyed, the beam jumps over to the intruder glint. The beam is locked-up in a low lying $2N\pi$ state.

(6) Here the boresight has been pointed at the intruder glint and $2N\pi$ lock-ups have been removed.

c. TRIM-COAT System

The TRIM-COAT system is particularly interesting from the viewpoint that the laser beam may be offset from the reference glint/highlight and thus avoid the problems of glint destruction which were

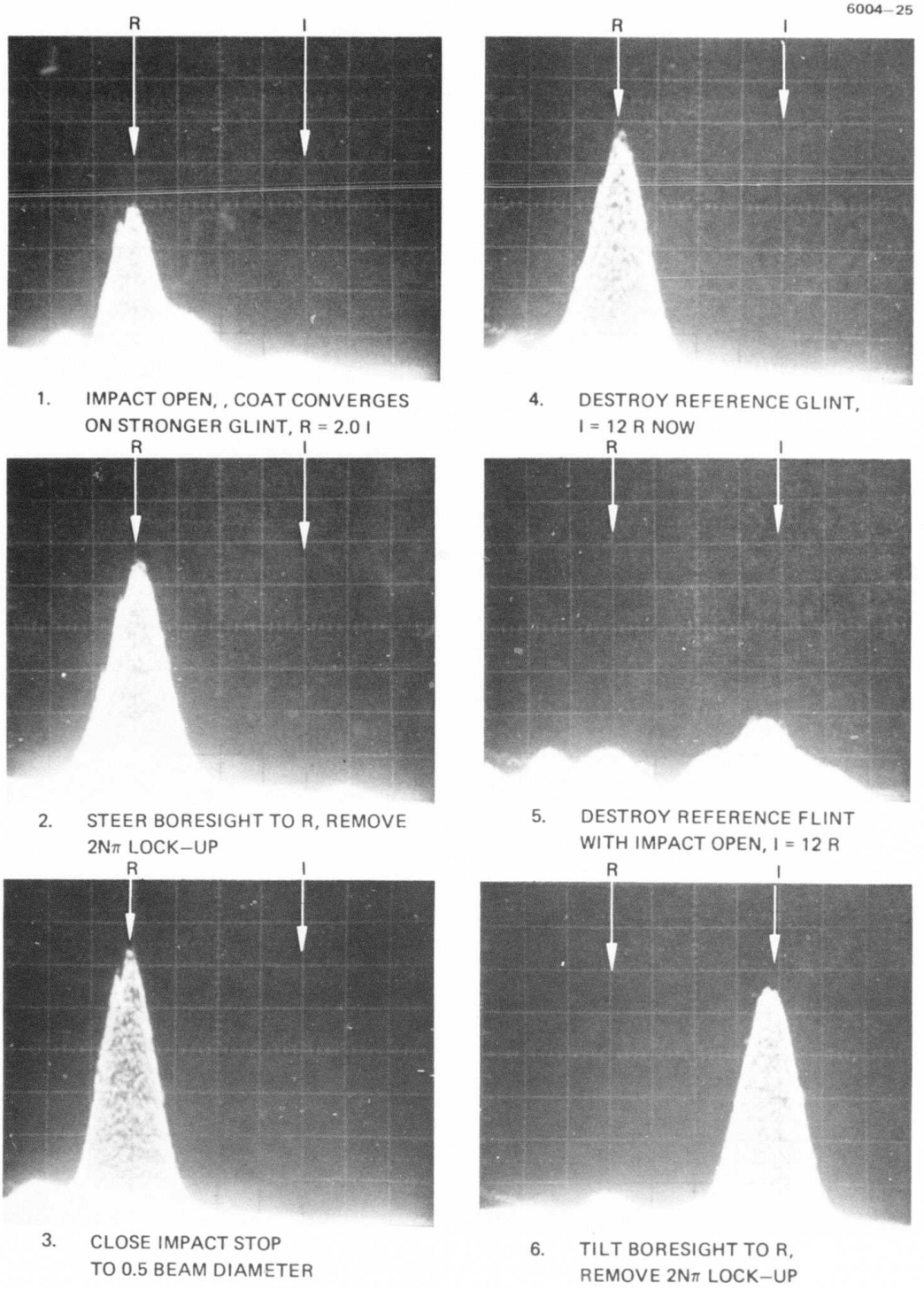

Figure 34. Shared Aperture IMPACT used to prevent glint hopping when reference glint is partially destroyed.

simulated above. However, the question still remains of how the system reacts to an intruder glint appearing suddenly in the vicinity of the reference. Such a situation can easily arise, for example, with a rotating target.

Although the ideal TRIM-COAT system will employ a more complex receiver than the single pinhole detector used here, a simple glint "pop-up" demonstration will illustrate that the TRIM-COAT concept does have glint discrimination capabilities. Figure 35 shows the simple glint "pop-up" scenario. Two glints are spaced 3 beam radii apart and adjusted to hve the ratio I/R = 5. The sequence of events is:

(1) The intruder glint (I) is initially blocked. Photo shows the COAT off beam and the positions of the two glints.

(2) The COAT servo loop has been closed, producing convergence on the reference glint. The $2N\pi$ lock-ups have been removed.

(3) The intruder glint, which is 5 times stronger than the reference, has been exposed. No noticeable degradation in Strehl ratio has occurred.

(4) The transmitter and receiver optics have been steered toward the intruder with the reference still exposed. Upon removal of $2N\pi$ lock-ups, full convergence is now obtained on the intruder glint. The beam is offset slightly to the left of the intruder.

The above demonstrations indicate that all these systems are insensitive to glint reflectivity changes on multiple glint targets. They were presented primarily as a basic illustration of the workings and importance of the IMPACT stop, and as a means of visualizing what actually happens to the beam during glint and IMPACT stop changes.

2. Radius of Effective Guarding Action

In this section we determine the effect of IMPACT stop size upon the glint discrimination performance of the Annular Aperture IMPACT and Shared Aperture IMPACT systems. Experiments were performed both indoors and over the turbulence range using essentially the same equipment employed in the preceding section. The intruder glint was mounted on a translation stage so that it could be moved easily relative

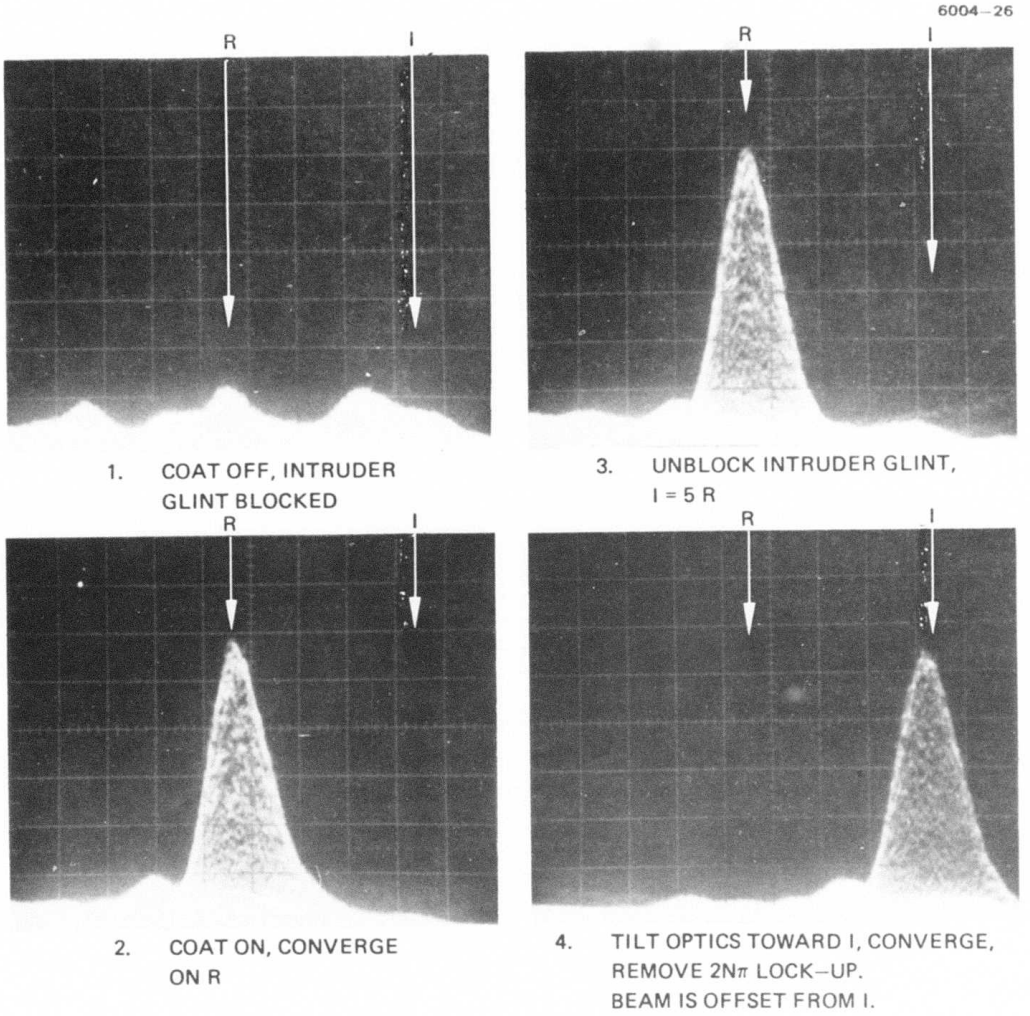

Figure 35. Demonstration of TRIM-COAT's insensitivity to glint hopping when stronger glint suddenly appears next to reference positions of reference and intruder designated by R and I.

to the stationary reference glint. Neutral density filters of various strength were placed in front of the reference glint to vary the intruder-to-reference (I/R) glint strength ratio.

The data indicate that both systems can be made quite insensitive to glint dynamics with the proper choice of IMPACT stop diameter. The major differences observered here between the two occur primarily because of the higher resolution of the Annular Aperture system (a secondary result of our experimental set-up) and because of the corrected return path in the Shared Aperture system (a fundamental difference).

For a given I/R ratio and IMPACT stop size the radius of guarding action was determined in the following way. With the intruder ~10 beam radii from the reference, the COAT system was converged on the reference and all $2N\pi$ lockups were removed. For indoor measurements the transmitter optics were defocused as before to give the system an error to correct. This also made interference from the intruder more easily detectable. For the outdoor turbulence measurements an approximately-collimated beam was employed. The intruder glint was then translated uniformly at ~1 beam radius/sec toward the reference. The beam profile was observed on the TV display, and when noticeable (~10%) degradation in Strehl ratio occurred the intruder motion was halted. The distance between the intruder and reference was taken as the radius of guarding action. This radius represents the point at which glint hopping starts to occur for a given IMPACT stop size and I/R ratio.

It was also determined that if the intruder was backed up ~1-2 mm (0.3-0.6 beam radius) from the guarding action radius the system would fully converge on the reference from the COAT off state. Thus by adding this amount to the guarding radius, the curves to be presented may be used to estimate how well the systems will converge on a weak glint in the presence of a stronger one.

The data for the Annular Aperture IMPACT system are shown in Figure 36. In this figure we plot I/R as a function of guarding radius (R_G) for various size IMPACT stop radii (R_I). Both are expressed in terms of converged-beam radii (1 beam radius = 3.5 mm at the target).

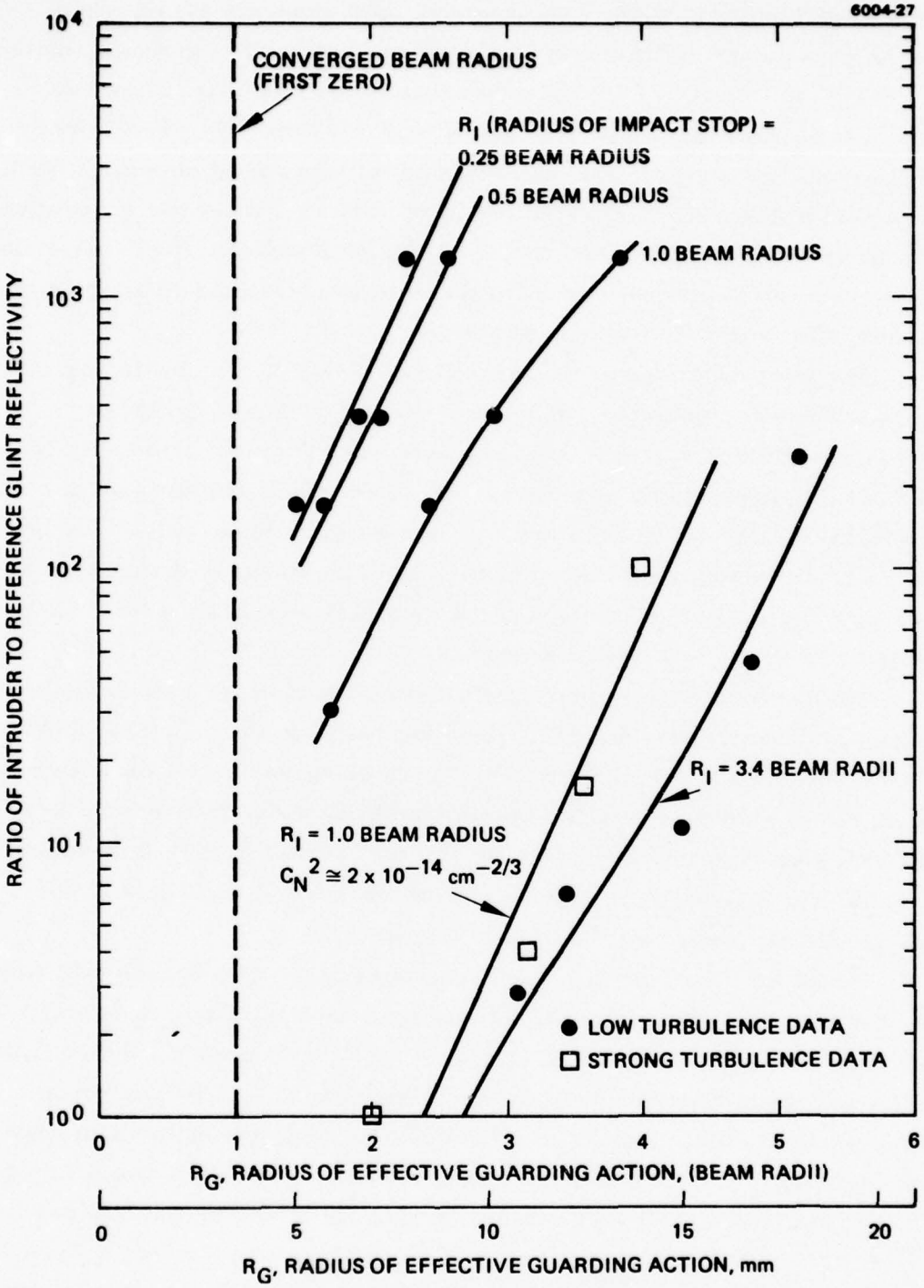

Figure 36. Glint discrimination capabilities of Annular Aperture IMPACT.

R_G is also shown in units of millimeters on a separate scale. The square data points represent measurements obtained in strong turbulence. ($C_N^2 \cong 2 \times 10^{-14}$ $cm^{-2/3}$). The others were obtained inside the lab.

To the right of and below each R_I = a constant line, glints may move around or vary the I/R ratio without causing glint hopping. To the left of and above each of these lines glint hopping will occur. Performance improvement is marked by R_G becoming smaller. The closer that the intruder glint may be moved to the reference without causing interference, the better the system performs.

The glint discrimination capabilities shown in Figure 36 are quite impressive. For example, in low turbulence an intruder that is 1000 times (30 dB) stronger than the reference may be effectively locked out for glint spacings as small as ~ 2.5 beam radii with the use of R_I = 0.25 or 0.50 IMPACT stops. In strong turbulence ($C_N^2 \cong 2 \times 10^{-14}$ $cm^{-2/3}$), an intruder that is 100 times (20 dB) stronger than the reference may be locked out, for spacings as small as 4 beam radii, with the use of an R_I = 1.0 IMPACT stop.

The performance improvement due to the IMPACT stop may be expressed in two ways. With the first technique we compare how much closer two glints of a given I/R may be moved as we decrease the IMPACT stop size. In the second method we determine how the I/R ratio that may be effectively locked out increases with decreasing stop size for a fixed glint spacing. Both of these characterizations may be determined from the data of Figure 36.

Using the first approach, if we choose I/R = 100 we see that with the stop fully open (R_I = 3.4) the guarding action is effective down to spacings of only 5 beam radii. For R_I = 1.0, 0.5 and 0.25 the guarding action becomes effective down to spacings of 2.3, 1.5 and 1.3 beam radii, respectively. Thus, for example, a 20-dB-stronger glint may approach 5.0/1.3 = 3.9 times closer by changing the stop from full open to nearly closed. Different values for this ratio will be determined for each I/R.

Using the second method, if we choose the spacing to be 3 beam radii, we see from Figure 36 that an I/R ratio of only 2 can be discriminated against with the stop fully open. Closing the stop through

sizes R_I = 1.0, 0.5, and 0.25, increases I/R to 450, 3500, and 6500, respectively. Thus, for example, with a spacing of 3 beam radii an improvement in I/R of 6500/2 = 3250 (35 dB) is obtained by closing the stop from fully open to nearly closed. An interesting point to note is that since this is a semi-log plot and the R_I = constant lines are roughly parallel, the improvement in I/R due to changing the IMPACT stop by a fixed amount is roughly the same for all spacings.

The degradation due to turbulence can be found from Figure 36 by comparing the two R_I = 1.0 curves that were determined during low- and high-turbulence conditions. The lines are roughly parallel. The reduction in I/R due to an increase in turbulence from $C_N^2 < 10^{-17}$ $cm^{-2/3}$ to $C_N^2 \cong 2 \times 10^{-14}$ $cm^{-2/3}$ for a fixed glint spacing is roughly a factor of 100 for the range of glint spacing studied. This reduction is quite large, and is due primarily to the glint images being degraded by the turbulence. The turbulence tends to smear out the images and cause the intruder glint diffraction pattern to have a larger spatial extent. Light return from the intruder (particularly side-lobe structure) can thus more easily leak through the IMPACT stop and cause interference. In a system which corrects the return wave (such as Shared Aperture IMPACT), the degradation observed here would not be as great.

The glint discrimination data for the Shared Aperture IMPACT system are shown in Figure 37. Due to the lower light-gathering capability of the experimental setup used here, the range of the I/R values that could be studied was more limited than in Figure 36. (Recall that I/R is varied by decreasing the return signal from the reference.) Two low-turbulence curves were obtained for R_I = 1.0 and 3.4, and one data point for $C_N^2 \cong 2 \times 10^{-14}$ $cm^{-2/3}$ was also determined for R_I = 4 beam radii.

The high-turbulence data point was obtained using corner cube reflectors with 2-mm apertures as the glints. The cats-eye glints did not provide sufficient S/N (> 30) required for a good lock-on. Unfortunately the corner cubes could not be moved closer than 4 beam radii due to their size, and above I/R = 4 the S/N fell below 20. Therefore we obtained only one data point.

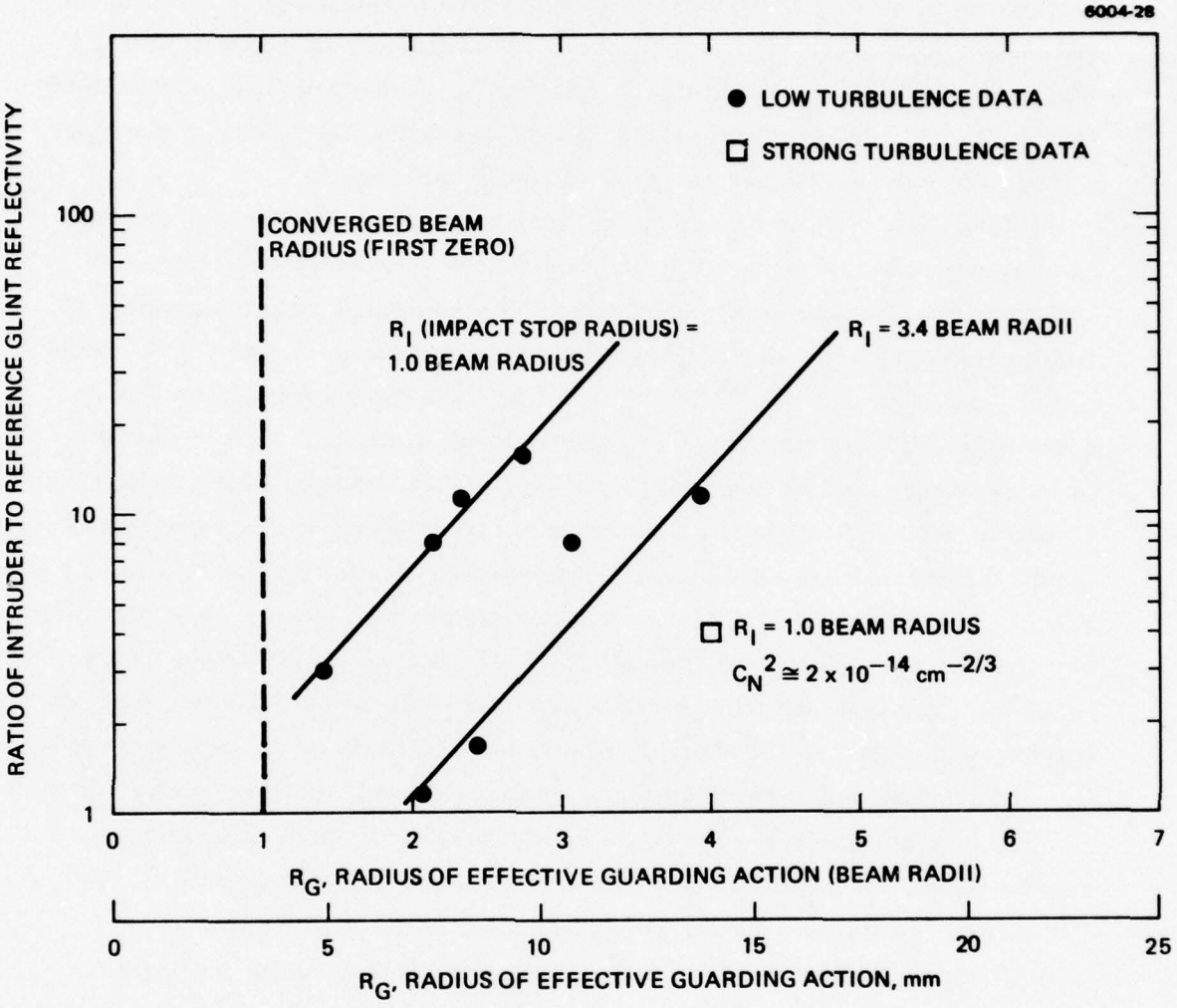

Figure 37. Glint discrimination capabilities of Shared Aperture IMPACT.

The data in Figure 37 show that the glint discrimination performance of the Shared Aperture IMPACT system is also quite good. For example, in low turbulence an intruder that is ~25 times (14 dB) stronger than the reference can be discriminated against for spacings as small as ~3 beam radii by using an $R_I = 1.0$ IMPACT stop. In strong turbulence, an I/R ratio of 4 (6 dB) can be discriminated against down to glint spacings of 4 beam radii. Holding I/R = 10, we see that by closing the IMPACT stop from fully open ($R_I = 3.4$) to $R_I = 1.0$, the intruder may be more than a factor of ($R_G = 3.75$) ÷ ($R_G = 2.3$) = 1.6 times closer to the intruder before interference occurs (This ratio changes depending upon the value of I/R chosen). For a fixed glint spacing, the I/R ratio is seen to improve by a factor of ~6 (8 dB) by closing the IMPACT stop from fully open ($R_I = 3.4$) to $R_I = 1.0$.

The degradation due to turbulence can be estimated by extending the $R_I = 1.0$ curve out to $R_G = 4$. This produces I/R = 80 at $R_G = 4$. Comparing this with the high turbulence data point we see that the turbulence has degraded the I/R ratio that can be discriminated against by a factor of 80/4 = 20. This is less of a degradation than the factor of ~100 seen in the Annular Aperture IMPACT system.

The smaller degradation in I/R with turbulence seen with Shared Aperture IMPACT is probably due to the corrected image this system provides. However, due to the limited data available a firm conclusion is not possible. The most we can say with confidence is that the data tend to support the contention.

In absolute terms the glint discrimination capabilities of Annular Aperture IMPACT appear from Figures 36 , and 37 to be superior to Shared Aperture IMPACT. This is not unexpected since, due to the way our optics are set up, the Annular Aperture system has a 3.6 times better resolution than the Shared Aperture configuration (The annular receiver mirror is 7.2 cm in diameter, the Shared Aperture IMPACT receiver is 2.0 cm in diameter).

The role of resolution in helping to determine glint discrimination performance is illustrated schematically in Figure 38. The top figure shows the intruder glint image produced by an optical receiver of diameter D. The central lobe of the diffraction pattern is fairly small and the sidelobes fall off in intensity to very low values by the time the position of the reference glint is reached. Very little energy from the intruder glint will find its way through the IMPACT stop to the detector.

The lower figure shows the intruder glint image produced by a receiver with a 3.6 times lower resolution. The central lobe as well as sidelobes are spread out farther than before. The energy from the intruder that passes through the IMPACT stop is much greater in this case.

Due to the larger spatial intent of the image, the poorer resolution system will thus exhibit a greater tendency to be confused by the intruder. We believe this is what is occurring in Figures 36 and 37. A meaningful theoretical analysis of the problem would require a fairly detailed model of the sidelobe structure of the intruder glint image, receiver optics aberrations, and the power distribution in the argon laser beam at the target. Such an analysis is beyond the scope of the present study.

C. ROTATING TARGETS

1. Use of IMPACT to Eliminate Glint Hopping

In this experiment, Annular Aperture IMPACT was employed to lock out an intruder glint that was 10 times stronger than the reference. Both glints were placed on a disc that could be rotated at from 0 to 1.5 Hz. The target geometry is shown in Figure 39. Scotchlite glints with area ratios of 10:1 were used. Insufficient signal return was obtained to carry out this experiment with the Shared Aperture IMPACT system.

The experimental results are shown in Figure 40. The photos show the peak irradiance on the reference glint for several center-to-center glint spacings. The rotation speed here is 1 Hz. In the left

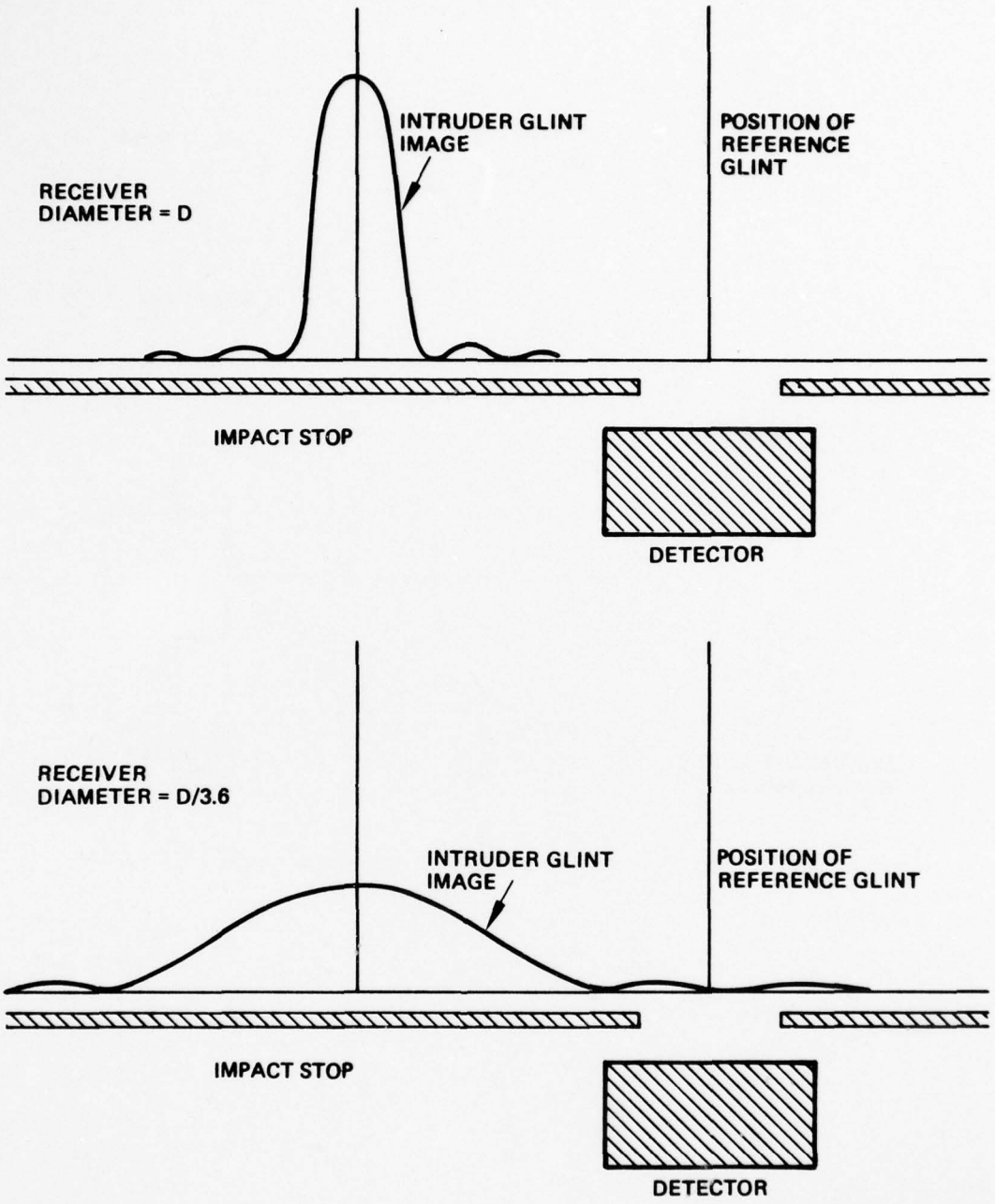

Figure 38. Effect of receiver resolution on intruder glint image.

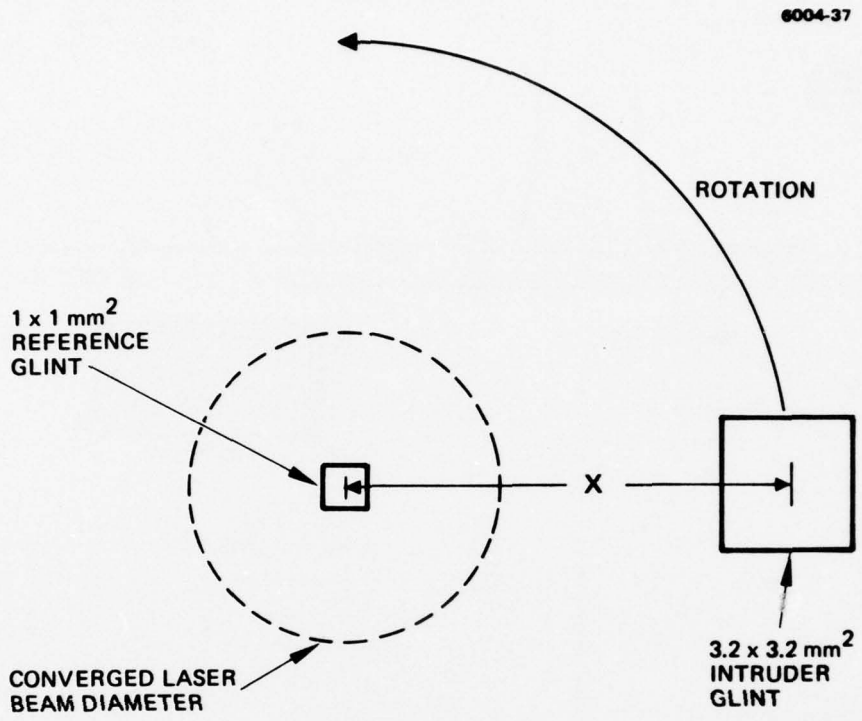

Figure 39. Target geometry for the rotating glint experiment.

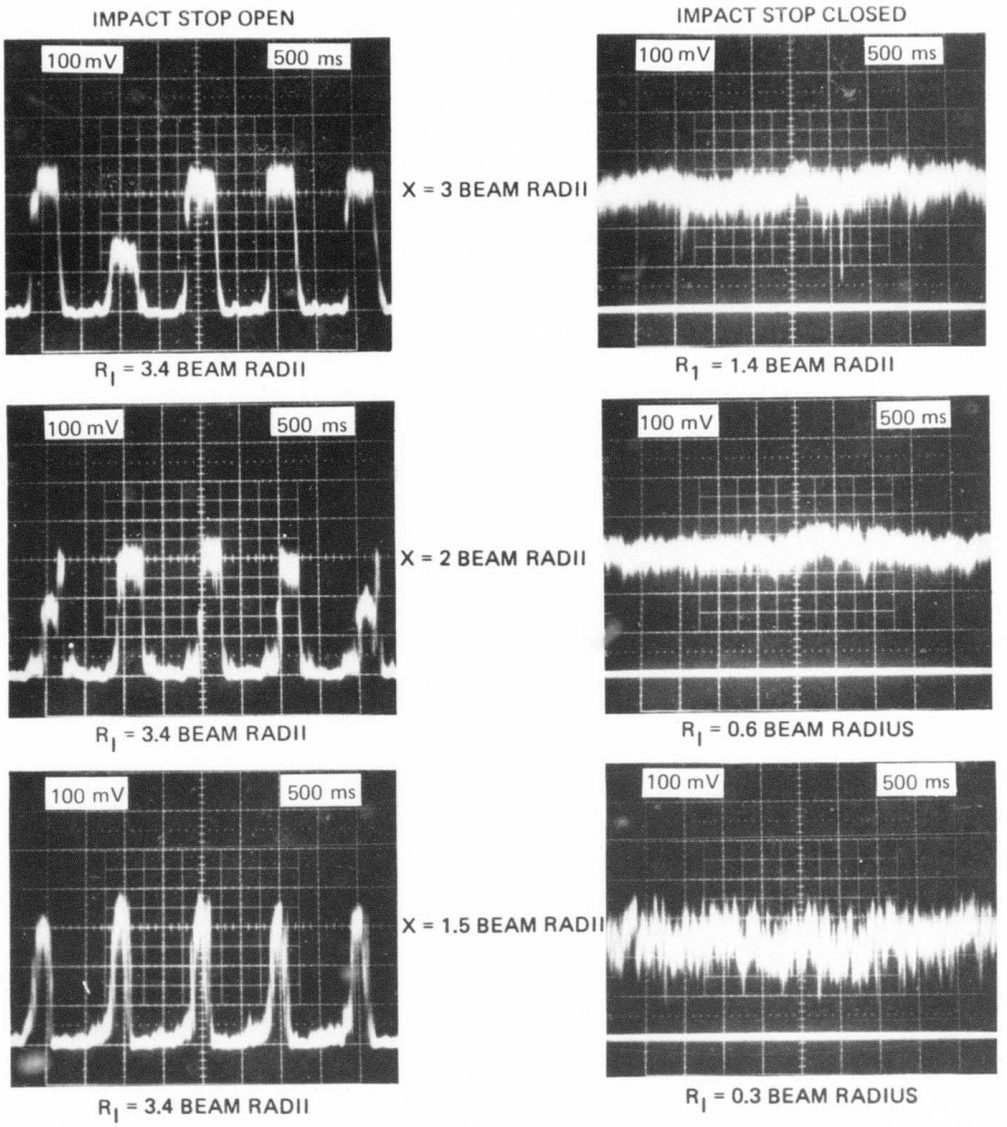

Figure 40. Peak irradiance on reference glint stabilized with use of IMPACT stop.

column the IMPACT stop is fully open. The power on the reference glint is observed to fall to zero each time the intruder reaches a certain angular position and causes the COAT system to converge on it. This angular sensitivity to glint hopping was encouraged by steering the COAT off laser boresight slightly to one side of the reference glint. When the intruder approached this side, the beam would hop over and then track the intruder for ~1/2 to ~3/4 of the way around.

As the photos indicate, this behavior was readily eliminated by closing down the IMPACT stop to the values shown. Beam stability nearly equal to that obtained for a non-rotating reference glint was observed. The beam instability seen in the lower right photo is due primarily to the IMPACT stop partially obscuring the reference glint image. The signal was reduced and an unfavorable S/N resulted.

Similar results were obtained over the entire rotation range 0 to 1.5 Hz. Speckle return was observed, but was not a dominant part of the received signal. Undoubtedly the relatively large-diameter annular mirror employed here helped in averaging out the speckle modulations.[11,12]

2. Convergence on a Rotating Spherical Target

In this experiment Annular Aperture IMPACT is used in the glint mode to converge on the near-edge highlight of a rotating ball. The ball was roughly spherical (a silver Christmas tree ornament) with a diameter of 6.7 cm. Scaling this to the 4 km, 3.8 μm scenario of Section 2.D, this would correspond to a target diameter of 1.10 meters. The rotation rate could be varied over the range of 0 to 1.5 Hz. System performance was investigated in both low and high turbulence. The low turbulence behavior is shown in Figure 41 for both a stationary (left) and rotating (right) target. The rotation rate used here was 1 Hz. Performance at other rotation rates was substantially the same. Beam profiles and convergence times are unaffected by the rotation. The beam stability is affected somewhat.

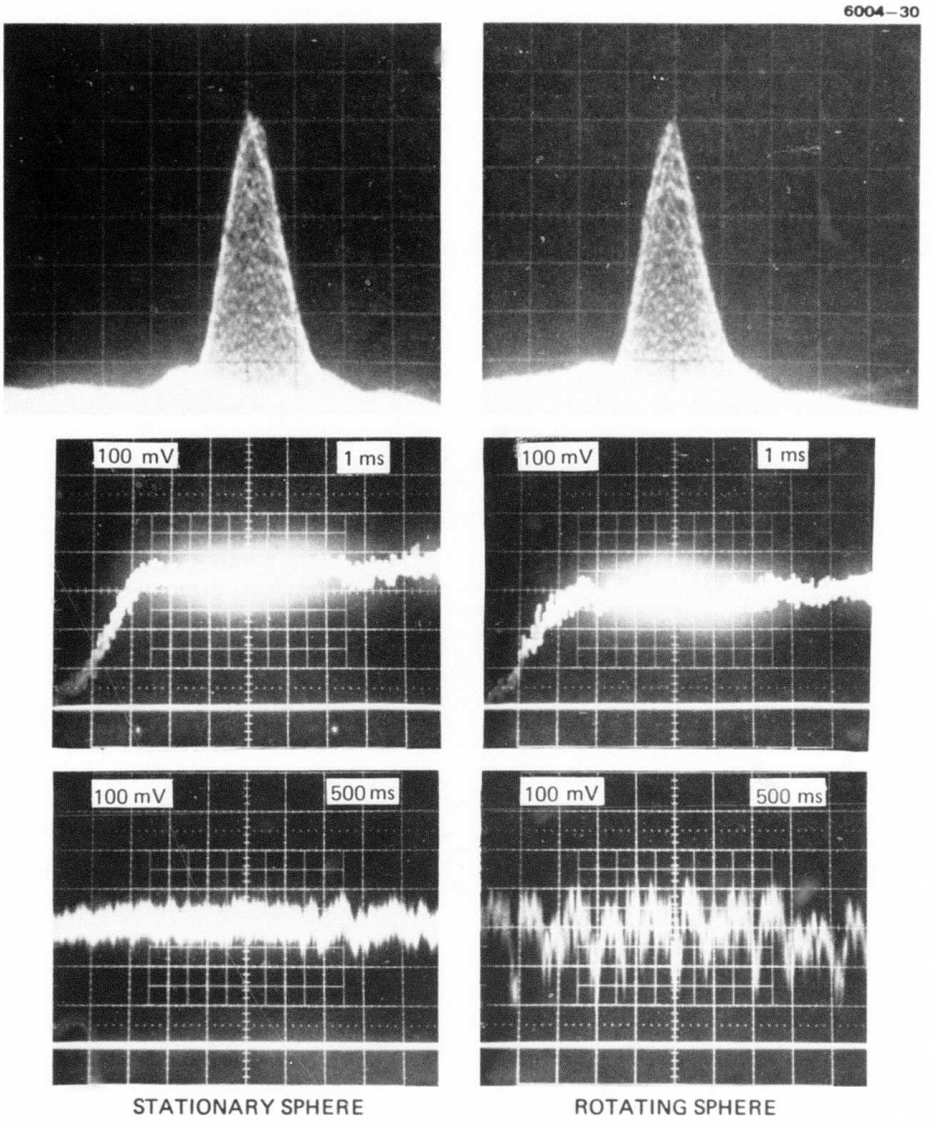

Figure 41. Convergence of Annular Aperture IMPACT on spherical target in low turbulence. Top: Beam profile; center: convergence time; bottom: beam stability.

In the lower right photo of Figure 41 a large part of the beam instability is due to the target not being perfectly spherical. Due to the slightly irregular surface, the position of the near-edge highlight shifts from side to side slightly as the ball rotates. The beam follows the highlight and also shifts around. Since the beam irradiance is measured by a stationary detector with a small entrance aperture (see Figure 13), the peak of the beam is not always centered on the detector. The larger fluctuations that have a period of ~1 sec are due to this effect. The smaller fluctuations are result of dither signal modulations and perhaps a slight amount of instability due to speckle return. A very small speckle return signal was observed, but its spectrum was not measured. As in the previous experiment, the large annular mirror employed here served to average out much of the speckle modulations.[11,12]

Performance in strong turbulence ($C_N^2 \cong 1.0 \times 10^{-14}$ $cm^{-2/3}$) is shown in Figure 42. The beam stability and convergence time are unaffected by the target rotation. As was the case in Figure 41, the performance achieved by this system using a rotating sphere for a target is essentially the same as that obtained in Section 3 using a simple stationary glint.

D. GLINT SIZE AND CONTRAST RATIO EFFECTS

1. Strehl Ratio as a Function of Glint Size

The Annular Aperture IMPACT system operating in the glint mode is used here to determine how the peak beam irradiance varies as the size of the glint is increased. The experiment was performed indoors under low-turbulence conditions. The target was a large piece of Scotchlite with a variable-diameter iris placed in front of it. The COAT off dc signal return level was maintained constant at 50 mV (S/N ≅ 30) during the glint diameter variations by placing various netural-density filters in front of the PMT. As in previous indoor experiments the transmitter optics were defocused to give the COAT system an error to correct.

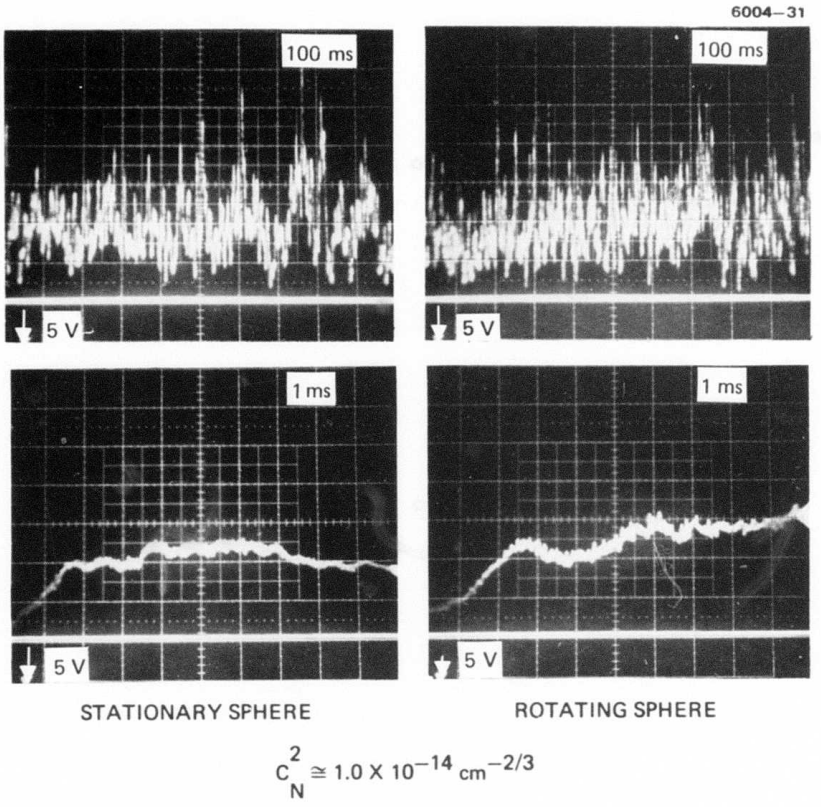

Figure 42. Convergence of Annular Aperture IMPACT on spherical target in high turbulence. Top: beam stability; bottom: convergence time.

Figure 43 shows the effects of glint size upon the power incident upon the center of the glint. The fully converged beam diameter is 7 mm. For glint diameters up to 5 mm (70% of beam diameter) there is no change in power at the glint center. For glint diameters larger than this, the power decreases fairly rapidly, falling to 65% convergence when the glint diameter is 7 mm. Although insufficient return was obtained from this target to repeat the experiment with the Shared Aperture IMPACT system, we would expect behavior to be similar.

2. Performance as a Function of Glint to Background Contrast Ratio

Here we investigate how bright a glint must be with respect to its surroundings in order to be recognized as a glint by the COAT system. The target configuration used is shown in Figure 44. A Scotchlite glint of dimensions 3 x 3 mm^2 is glued to the center of a neutral density filter (approximately 5 x 5 cm^2). By using different neutral density filters, the effective reflectivity of the background Scotchlite can be varied. The filter-glint combination is then placed in front of a larger piece of Scotchlite and convergence on the small glint is investigated.

The results of such a variation using the Annular Aperture IMPACT system indoors are shown in Figure 45. The background and glint return signals were measured with COAT off. The glint return signal was held constant at the value shown. Numbers beside each data point indicate the ratio of effective glint reflectivity to background reflectivity, calculated from the known attenuation of the neutral density filters.

Convergence of 90% or better is obtained for background to glint returns ratios $\lesssim 6.5$. That is, as long as the return from the glint is greater than $\sim 13\%$ of the total return the COAT system will converge to nearly the full value. For this glint size, 90% convergence occurs when the reflectivity of the glint is roughly nine times the reflectivity of the background. Since the COAT system works on return signal rather than reflectivity, smaller glints would have to be more reflective than this, and vice versa.

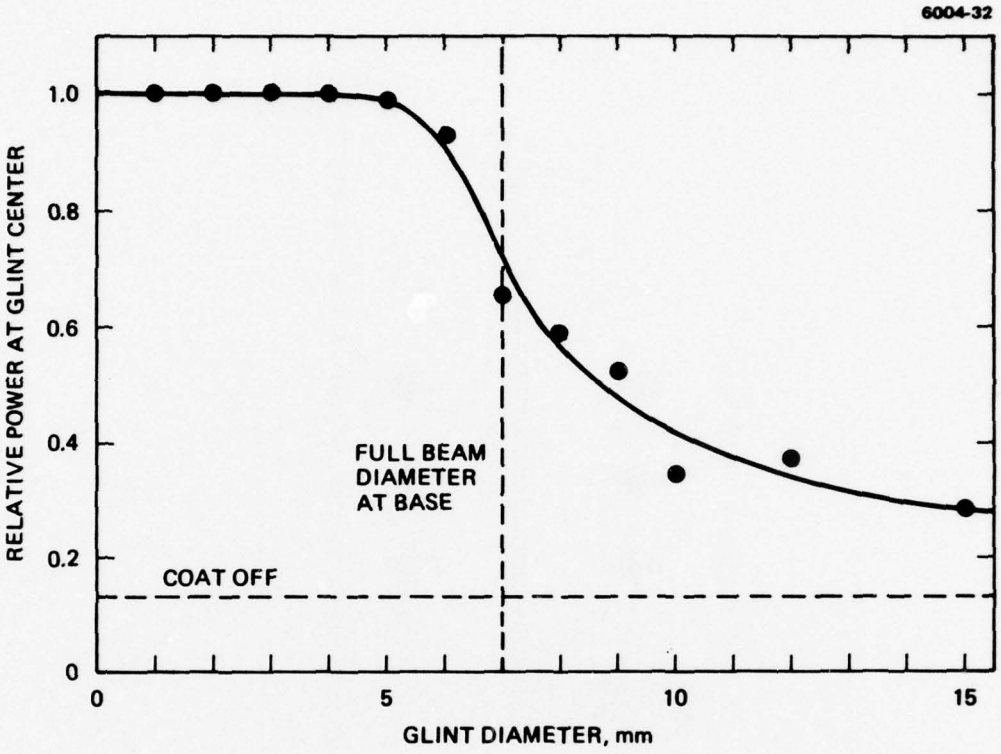

Figure 43. Effect of glint size upon peak irradiance at center of the glint.

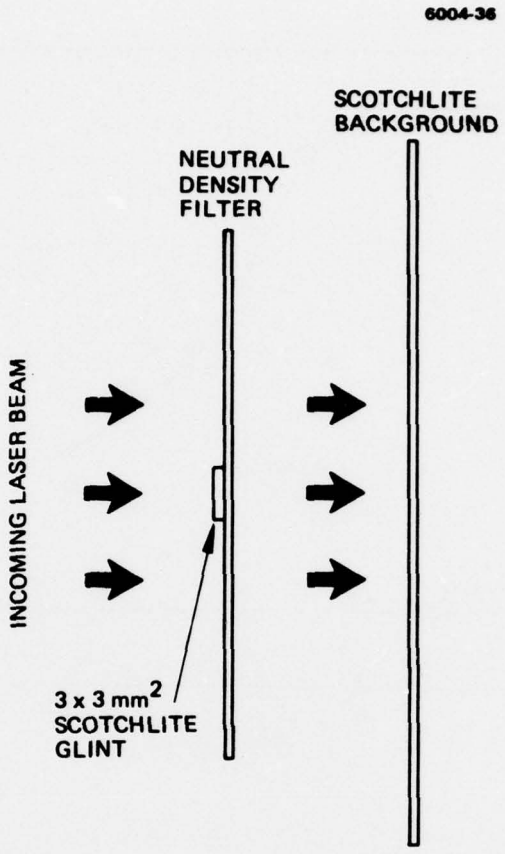

Figure 44. Target configuration for contrast ratio experiments.

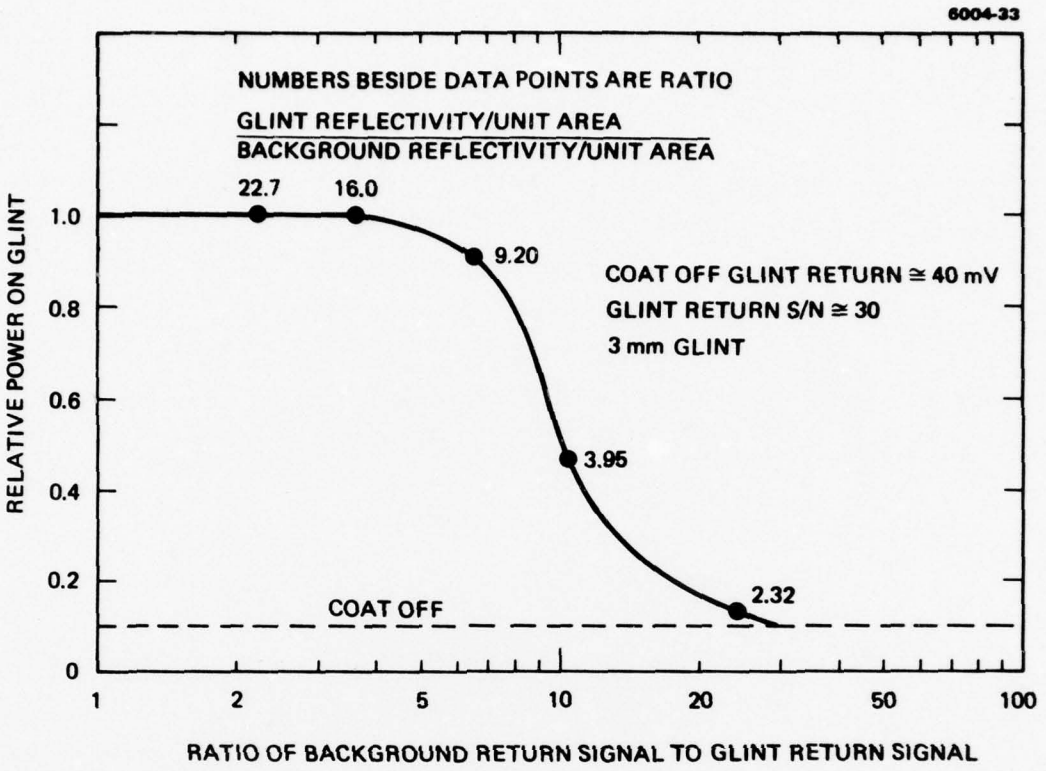

Figure 45. Effect of glint to background contrast ratio upon beam convergence.

SECTION 5

RECOMMENDATIONS FOR FUTURE STUDIES

As noted in Section 3 and 4 there are several areas in which further investigation would prove particularly fruitful. The first of these would be the addition of an auxiliary tracking control to the Annular Aperture IMPACT system so that featureless target operation could be evaluated more meaningfully. The second area involves featureless target operation of the Shared Aperture IMPACT system, which was not demonstrated in the study due to low signal return levels. In order to increase the signal level, a larger receiver could be employed. Backscatter could be reduced by a more comprehensive analysis and a more sophisticated design of the optical system than was possible on this contract.

Beyond these fundamental system demonstrations, there are more sophisticated COAT configurations that show great promise for practical high-power laser applications. One of the most promising is the concept of hot-spot tracking, where the COAT system locks onto the light emitted by the laser-produced plasma. There are important questions to be answered regarding the best method for acquiring the initial target lock-on and then transferring it to the hot-spot tracking mode once the plasma is formed. An experimental investigation of several possible scenarios, including a realistic hot-spot simulation, would be a significant advancement in this area.

APPENDIX A

DETERMINATION OF CONTROL SYSTEM S/N

During all experiments the received signals were monitored at the output of the preamplifier/line driver. This location was chosen since the signal voltages were of readily measurable magnitudes here (amplified by a factor of 20), and since any thermal noise which might be introduced by the preamp could also be observed.

An RCA type 4840 photomultiplier with S-9 response was used in all experiments. It was biased at 600 volts, a value which gave maximum S/N for the range of target return signals obtained in the study. The sensitivity of this PMT was measured with a UDT model 40X "opto-meter" power meter and was found to be $\sim 4 \times 10^{-12}$ watt/mV at 4880 Å and $\sim 6 \times 10^{-12}$ watt/mV at 6328 Å with the normally-used 4880-Å and 6328-Å pass filters in place. The voltages referred to here were measured at the output of the preamp/line driver.

The rms noise (N) at the preamp output as a function of dc return signal voltage (S_o) is shown in the lower curve of Figure A-1. The bandwidth was limited to the range 3 to 30 kHz for these measurements so that the noise values would approximate the noise actually present in the 4- to 20-kHz dither band. The data are plotted as a function of the square root of the dc return signal (x axis is non-linear) and the good straight-line fit indicates that $N \propto S_o^{1/2}$. The system is thus predominantly shot-noise limited at these signal levels.

Due to the design of the COAT servo electronics, only noise within a 400-Hz bandwidth around each dither frequency is actually coupled into the corresponding control channel. Since shot noise has a white-noise frequency spectrum, the noise present in a typical control channel can be calculated by multiplying the measured broad-band (Δf = 27 kHz) noise curve (lower curve Figure A-1) by the ratio 400/27,000. This 400-Hz noise plot is shown in the upper curve in Figure A-1.

The dc component of the return signal is lost upon passage through the AGC/high pass filter and only the ac dither return (S_f) at each dither

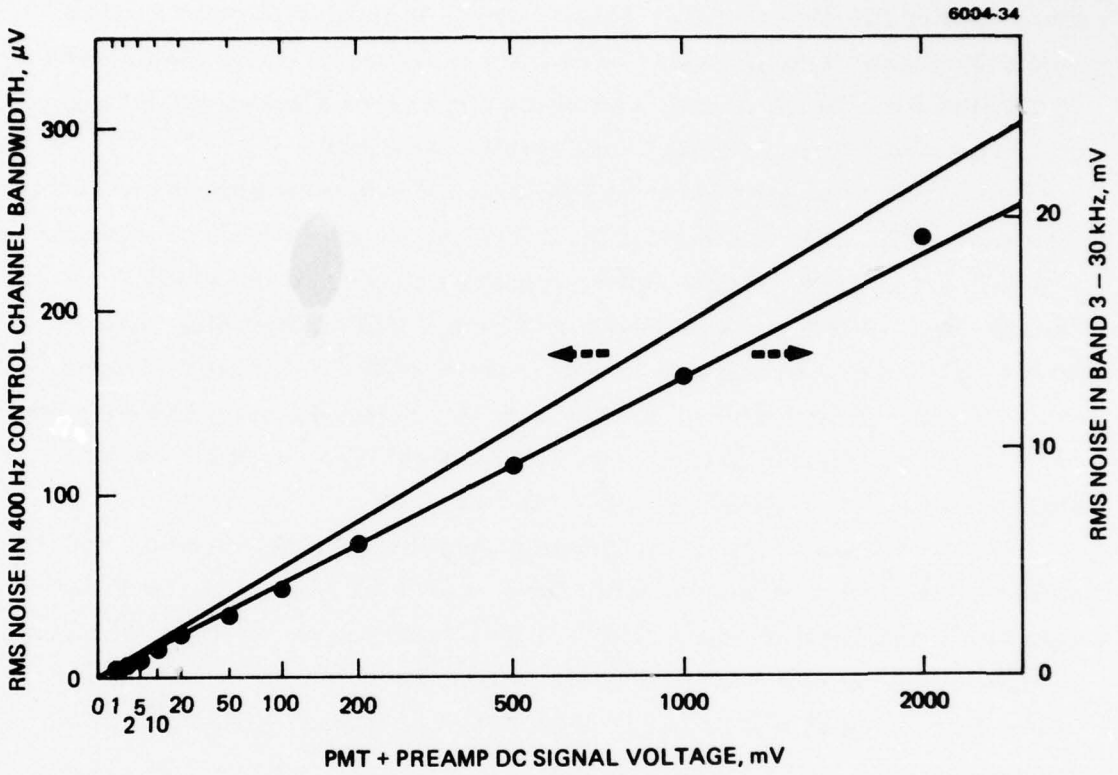

Figure A-1. Receiver noise as function of dc signal return.

frequency is coupled to the control channels. Rather than measuring 18 values of S_f/N each time the operating conditions are changed, it is much more convenient to determine an average dither signal return (call it S) for representative operating conditions and then to relate S to the easily-measured dc signal return S_o. The unconverged (COAT off) state is the most meaningful condition upon which to base a measure of S/N, since this is the starting point for the convergence process.

To make this measurement, the Annular Aperture IMPACT system was employed inside the lab. A silicon photodiode was put in place of the PMT (IMPACT stop open) and a flat mirror (no apertures) was placed at the target position and aligned to reflect the laser light back into the receiver optics. The Ar laser beam was approximately collimated. With the servo loop open, one dither was turned on at a time and the ratio of the rms dither return to dc return was measured for each of the 18 channels. On the average it was found that

$$S_f/S_o = 0.0263 \pm 0.0184$$

where the error is one standard deviation.

We now define $S = 0.0263\ S_o$. If we now divide this expression at each dc signal by the 400-Hz noise curve (upper) of Figure A-1, we obtain an "average" S/N as a function of S_o. This is shown in Figure A-2.

To reiterate, the S/N shown in this figure and referred to throughout this report is defined as the ratio of (the average single channel rms dither return with COAT off) to (the rms noise in a typical 400 Hz control channel bandwidth).

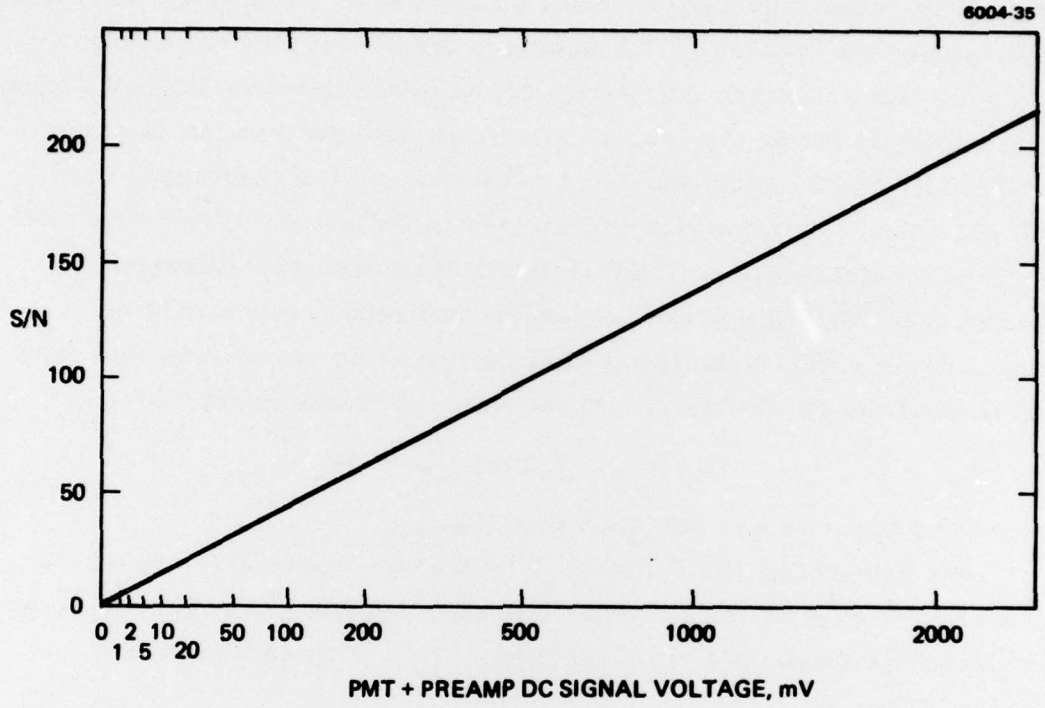

Figure A-2. Signal-to-noise as function of dc signal return.

REFERENCES

1. J.E. Pearson, S. Hansen, and T.R. O'Meara, "Adaptive Control Over Extended Targets," Interim Technical Report on contract N60921-76-C-0050, NSWC/WOL, Sept. 1976.

2. J.E. Pearson and S. Hansen, "Experimental Studies of a Deformable Mirror Multidither COAT System," submitted to J. Opt. Soc. Am., July 1976.

3. J.E. Pearson et al., "COAT," Final Report on Contract F30602-73-C-0248, RADC-TR-75-46.

4. J.E. Pearson, N.B. Bridges, S. Hansen, T.A. Nussmeier, and M.E. Pedinoff, Appl. Opt. 15, 611 (1976).

5. J.E. Pearson, "Comparison of Scintillometer and Microthermometer Measurements of C_N^2," J. Opt. Soc. Am. 65, 938 (1975).

6. D.L. Fried, J. Opt. Soc. Am. 57, 175 (1967).

7. D.L. Fried and J.B. Seidman, J. Opt. Soc. Am. 57, 181 (1967).

8. J.E. Pearson et al., "High Power, Closed Loop, Adaptive System (HICLAS) Study," Final Contract Report, vol 1, contract N60921-76-C-0008, NSWC/WOL, June 1976.

9. T.R. O'Meara, "The $2n\pi$ Problem in Multidither COAT Systems Operating with Zonal Control via Deformable Mirrors," submitted to J. Opt. Soc. Am., July 1976.

10. J.E. Pearson et al., "COAT," Quarterly Technical Report 5, contract F30602-73-C-0248, RADC, Dec 1974.

11. J.E. Pearson, S.A. Kokorowski, and M.E. Pedinoff, "Effects of Speckle in Adaptive Optical Systems," J. Opt. Soc. Am. 66, 1261 (1976).

12. M.E. Pedinoff, S.A. Kokorowski, and J.E. Pearson, "COAT Target Signature Interactions," Technical Report, contract F30602-76-C-0021, June 1976.

Commander
Naval Surface Weapons Center, White Oak
Silver Spring, MD 20910
Attn: Mr. Charles J. Infosino (2)
Dr. Bernard Kessler (1)
Mr. Carl Larson (1)
Library (1)

Massachusetts Institute of Technology
Lincoln Laboratory
P.O. Box 73
Lexington, MA 01273
Attn: Dr. L.C. Marquet (1)

Defense Advanced Research Projects Agency
Strategic Technology Office
1400 Wilson Blvd
Arlington, VA 22209
Attn: Dr. Peter Clark (1)
Mr. John Meson (1)
Lt. Col. R. Oglukian (1)

Director
Naval Research Laboratory
Washington, D.C. 20375
Attn: Dr. Peter Livingston (1)

Air Force Weapons Laboratory
Kirtland Air Force Base
Albuquerque, NM 87117
Attn: Major Larry James (1)

Commander
U.S. Army Missile Command (1)
Redstone Arsenal, AL 35809
Attn: Major Malcolm O'Neil (AMSMI-RX)

Commander
Rock Island Arsenal
Rock Island, IL 61201
Attn: Dr. M. Lavan (1)

Commander
U.S. Army Electronics Command
Ft. Monmouth, NJ 07703
Attn: AMSEL-CT-L(Dr. R.G. Buser) (1)

Rome Air Development Center
Griffiss Air Force Base NY 13441
Attn: OCTM-1 (Mr. R. Ogrodnik) (1)

NASA Lewis Research Center
Cleveland, OH 44135
Attn: Mr. R. Stubbs (1)
M.S. 500-318

Defense Documentation Center (2)
Cameron Station
Alexandria, VA 22314